

NEW DEVELOPMENTS in ENVIRONMENTAL SCIENCE and GEOSCIENCE

**Proceedings of the International Conference on Environmental Science
and Geoscience (ESG 2015)**

**Vienna, Austria
March 15-17, 2015**

NEW DEVELOPMENTS in ENVIRONMENTAL SCIENCE and GEOSCIENCE

**Proceedings of the International Conference on Environmental Science
and Geoscience (ESG 2015)**

**Vienna, Austria
March 15-17, 2015**

Copyright © 2015, by the editors

All the copyright of the present book belongs to the editors. All rights reserved. No part of this publication may be reproduced, stored in a retrieval system, or transmitted in any form or by any means, electronic, mechanical, photocopying, recording, or otherwise, without the prior written permission of the editors.

All papers of the present volume were peer reviewed by no less than two independent reviewers. Acceptance was granted when both reviewers' recommendations were positive.

Series: Energy, Environmental and Structural Engineering Series | 33

ISSN: 2227-4359

ISBN: 978-1-61804-283-5

NEW DEVELOPMENTS in ENVIRONMENTAL SCIENCE and GEOSCIENCE

**Proceedings of the International Conference on Environmental Science
and Geoscience (ESG 2015)**

**Vienna, Austria
March 15-17, 2015**

Organizing Committee

Editors:

Professor Nikos E. Mastorakis, Technical University of Sofia, Bulgaria

Professor Aida Bulucea, University of Craiova, Romania

Program Committee:

Prof. Bharat Doshi, John Hopkins University, Maryland, USA

Prof. Gang Yao, University of Illinois at Urbana - Champaign, USA

Prof. Lu Peng, Louisiana State University, Baton Rouge, LA, USA

Prof. Y. Baudoin, Royal Military Academy, Brussels, Belgium

Prof. F. Rigas, School of Chemical Engineering, National Technical University of Athens, Greece.

Prof. S. Sohrab, Northwestern University, IL, USA

Prof. A. Stamou, National Technical University of Athens, Greece

Prof. A. I. Zouboulis, Dept. of Chemistry, Aristotle University of Thessaloniki, Greece

Prof. Z. A. Vale, ISEP - Instituto Superior de Engenharia do Porto Rua Antonio Bernardino de Almeida, Portugal

Prof. M. Heiermann, Dr., Department of Technology Assessment and Substance Flow, Potsdam, Germany

Prof. I. Kazachkov, National Technical University of Ukraine (NTUU KPI), Kyiv, Ukraine

Prof. A. M.A. Kazim, UAE University, United Arab Emirates

Prof. A. Kurbatskiy, Novosibirsk State University, Department of Physics, Russia

Prof. S. Linderoth, Head of Research on Fuel Cells and Materials Chemistry at Riso National Laboratory, Denmark

Prof. P. Lunghi, Dipartimento di Ingegneria Industriale, University degli Studi di Perugia, Italy

Prof. J. Van Mierlo, Department of Electrotechnical Engineering and Energy Technology (ETEC) Vrije Universiteit Brussel, Belgium

Prof. Pavel Loskot, Swansea University, UK

Prof. N. Afgan, UNESCO Chair Holder, Instituto Superior Tecnico, Lisbon, Portugal

Prof. F. Akgun, Gebze Kocaeli, Turkey

Prof. Fernando Alvarez, Prof. of Economics, University of Chicago, USA

Prof. Mark J. Perry, Prof. of Finance and Business Economics, University of Michigan-Flint, USA

Prof. Biswa Nath Datta, IEEE Fellow, Distinguished Research Prof., Northern Illinois University, USA

Prof. Panos Pardalos, Distinguished Prof. Director, Center for Applied Optimization, University of Florida, USA

Prof. Gamal Elnagar, University of South Carolina Upstate, Spartanburg, SC, USA

Prof. Luis Tavares Rua, Cmte Guyubricht, 119. Conj. Jardim Costa do Sol. Atalaia, Brazil

Prof. Igor Kuzle, Faculty of electrical engineering and computing, Zagreb, Croatia

Prof. Maria do Rosario Alves Calado, University of Beira Interior, Portugal

Prof. Gheorghe-Daniel Andreescu, "Politehnica" University of Timisoara, Romania

Prof. Jiri Strouhal, University of Economics Prague, Czech Republic

Prof. Morris Adelman, Prof. of Economics, Emeritus, MIT, USA

Prof. Germano Lambert-Torres, Itajuba, MG, Brazil

Prof. Jiri Klima, Technical faculty of CZU in Prague, Czech Republic

Prof. Goricanec Darko, University of Maribor, Maribor, Slovenia

Prof. Ze Santos, Rua A, 119. Conj. Jardim Costa do Sol, Brazil

Prof. Ehab Bayoumi, Chalmers University of Technology, Goteborg, Sweden

Prof. Robert L. Bishop, Prof. of Economics, Emeritus, MIT, USA

Prof. Glenn Loury, Prof. of Economics, Brown University, USA

Prof. Patricia Jota, Av. Amazonas 7675, BH, MG, Brazil

Prof. S. Ozdogan, Marmara University, Goztepe Campus, Kuyubasi, Kadikoy, Istanbul, Turkey

Prof. Prof. Jian Wang, Los Alamos National Laboratory, Los Alamos, NM, USA

Prof. Bruno Capaccioni, Universita di Bologna, Bologna, Italy

Prof. Ernst D. Schmitter, University of Applied Sciences Osnabrueck, Germany

Prof. Corina Carranca, University of Algarve, Portugal

Prof. Hing-Ho Tsang, Swinburne University of Technology, Melbourne, Australia
Prof. Paolo Budetta, University of Naples Federico II, Naples, Italy
Prof. Rui Pedro Juliao, Universidade Nova De Lisboa, Lisboa, Portugal
Prof. Victor M. Castano, Universidad Nacional Autonoma de Mexico, Mexioco City, Mexico
Prof. S. V. Dinesh, Siddaganga Institute of Technology, Tumkur, India
Prof. C. C. Sorrell, University of New South Wales, Sydney, Australia
Prof. Efthimios Karymbalis, Harokopio University, Athens, Greece
Prof. Belkheir Hammouti, Mohammed Premier University, Oujda, Morocco
Prof. Ismail Rakip Karas, Karabuk University, Turkey

Additional Reviewers

Jose Flores	The University of South Dakota, SD, USA
Abelha Antonio	Universidade do Minho, Portugal
Lesley Farmer	California State University Long Beach, CA, USA
Takuya Yamano	Kanagawa University, Japan
Miguel Carriegos	Universidad de Leon, Spain
Francesco Zirilli	Sapienza Universita di Roma, Italy
George Barreto	Pontificia Universidad Javeriana, Colombia
Eleazar Jimenez Serrano	Kyushu University, Japan
Tetsuya Yoshida	Hokkaido University, Japan
Philippe Dondon	Institut polytechnique de Bordeaux, France
Genqi Xu	Tianjin University, China
M. Javed Khan	Tuskegee University, AL, USA
Xiang Bai	Huazhong University of Science and Technology, China
Dmitrijs Serdjuks	Riga Technical University, Latvia
Hessam Ghasemnejad	Kingston University London, UK
José Carlos Metrôlho	Instituto Politecnico de Castelo Branco, Portugal
João Bastos	Instituto Superior de Engenharia do Porto, Portugal
Tetsuya Shimamura	Saitama University, Japan
Imre Rudas	Obuda University, Budapest, Hungary
Konstantin Volkov	Kingston University London, UK
Frederic Kuznik	National Institute of Applied Sciences, Lyon, France
James Vance	The University of Virginia's College at Wise, VA, USA
Angel F. Tenorio	Universidad Pablo de Olavide, Spain
Sorinel Oprisan	College of Charleston, CA, USA
Santoso Wibowo	CQ University, Australia
Jon Burley	Michigan State University, MI, USA
Kazuhiko Natori	Toho University, Japan
Shinji Osada	Gifu University School of Medicine, Japan
Francesco Rotondo	Polytechnic of Bari University, Italy
Deolinda Rasteiro	Coimbra Institute of Engineering, Portugal
Alejandro Fuentes-Penna	Universidad Autónoma del Estado de Hidalgo, Mexico
Moran Wang	Tsinghua University, China
Bazil Taha Ahmed	Universidad Autonoma de Madrid, Spain
Andrey Dmitriev	Russian Academy of Sciences, Russia
Masaji Tanaka	Okayama University of Science, Japan
Matthias Buyle	Artesis Hogeschool Antwerpen, Belgium
Kei Eguchi	Fukuoka Institute of Technology, Japan
Zhong-Jie Han	Tianjin University, China
Valeri Mladenov	Technical University of Sofia, Bulgaria
Ole Christian Boe	Norwegian Military Academy, Norway
Yamagishi Hiromitsu	Ehime University, Japan
Stavros Ponis	National Technical University of Athens, Greece
Minhui Yan	Shanghai Maritime University, China

Table of Contents

Environmental Impact Test in Thermal Power Plants; Experimental and CFD Evaluation of Burning Alternative Fuels	11
<i>Jesús M. Blanco, Lakhdar Remaki, Francisco Peña</i>	
Urban Planner – Model for Land Use Suitability Assessment	19
<i>Jaroslav Burian, Jan Brus, Stanislav Stastny</i>	
Safety of Critical Facilities	27
<i>Dana Prochazkova</i>	
Flash Flood on July 21, 2014 in the Vratna Valley	34
<i>P. Pekarova, V. Bacova Mitkova, P. Miklanek</i>	
Development of Land Use in the Morava River Floodplain During the Past 175 Years	39
<i>Vilém Pechanec, Ivo Machar, Helena Kilianová</i>	
Model Parameters Estimation in Two River Basins in Slovakia and Korea	43
<i>Pavol Miklanek, Hyosang Lee, Pavla Pekárová, Michal Danko</i>	
Measuring Devices for Visualization of WJM and AWJM Technologies Physical Factors	47
<i>Peter Poor, Michal Simon, Lýdia Sobotová, Monika Karkova</i>	
The Water Temperature Simulation in the Morava River Basin Watercourses	53
<i>Dana Halmova, Pavla Pekarova, Jan Pekar, Katarina Kucarova</i>	
Measurement Results of Longitudinal Dispersion Coefficient in Urban Sewer Networks under Dry Weather Conditions	57
<i>Marek Sokáč, Yvetta Velísková</i>	
Grey Water System Application – Water Savings and Use in the Hotel Building	61
<i>Martina Rysulová, Daniela Káposztássová, Zuzana Vranayová</i>	
Infiltration Efficiency of Percolation Facility for its Safety Operation	65
<i>Gabriel Markovič, Daniela Káposztássová, Zuzana Vranayová</i>	
Migration of Travel Time in a Common-Shot Gather by Structural Similarity	70
<i>Hernando Castañeda M., José Luciano Maldonado, Rómulo Sandoval F.</i>	
Taking Account of Covariance Estimation Uncertainty in Spatial Sampling Design for Prediction with Trans-Gaussian Random Fields	79
<i>Gunter Spöck, Jürgen Pilz</i>	
Authors Index	99

Environmental impact test in thermal power plants; Experimental and CFD evaluation of burning alternative fuels

Jesús M. Blanco, Lakhdar Remaki and Francisco Peña

Abstract—Alternative fuels are being considered in gas turbines given the scarcity and costs of conventional fossil fuels but also due to climate change concerns. This paper is focused on a comparative study of performance and emissions between fossil and alternative fuels. First of all, a complete theoretical evaluation of the global efficiency associated to a power plant of reference depending on the fuel burned has been performed and improved significantly with the proper determination of the so called “difficult evaluation losses term”, showing no significant differences for the fuels tested. Secondly, a fully CFD model was built as a result of the full CHEMKIN® implementation, based on the results provided by a scaled experimental facility, fully monitored and ready for burning both fossil and alternative fuels such as natural gas and a gas derived from biomass respectively. It is demonstrated a good agreement between the experimental data and CFD results, which validates the computational model and justify its use for further characterizations of other fuels prior to a big scale implementation in a thermal power plant.

Keywords— Alternative fuels, bio gas, CFD, efficiency, natural gas.

I. INTRODUCTION

Fossil fuels stocks are limited and are considered non-renewable sources. From the decade of the 90’s, the possibility of converting fuel oil (FO) fired power plant into natural gas (NG) has been raised [1], due mainly to the significant increasing in the global concern about the “greenhouse effect”.

Natural gas expectations as fuel replacement in some sectors are suffering a substantial increase but the most important fact is that recent increases in crude oil prices have brought

alternative fuels into the energy scenario. General Electric, Pratt & Whitney, and other gas turbine manufacturers, have been testing these fuels in their machines for a long time [2], [3]. Today, bio-fuels have an additional attraction as they are considered “renewable sources” which is a strong argument for the success of their implementation [4], [5]. Note that special attention has to be paid to technical and operational challenges have to be taken into account regarding any fuel replacement issues.

Gas derived from biomass (BG) obtained in fluidized beds has been revealed as a credible option. There is an important source of biomass called “Miscanthus giganteus” for the production of energy either for direct combustion or through cellulosic ethanol as has been treated here. The gas matrix contains high traces of ashes [6], which are crucial to be eliminated, otherwise the gas would not be suitable for burning in gas turbines due to the enormous abrasive action of the exhaust gases caused by the high temperature (around 800°C) combined with a high speed around the blades as described in [7].

Key driving factors for bio-fuels are the monetary incentives built into particular regulations of each estate which makes it difficult to evaluate and compare among different countries. Too many questions arise in order to make a clear decision at least in the near future as these alternative fuels are still not available in sufficient volume all over the world for supporting the current power generation [8].

There is also another significant challenge as conventional power plants have been gradually replaced by combined cycles around the world. The most commonly fuel burned in conventional cycles has been the fuel oil (FO); the so called “N^{er}2” and the low sulphur index fuel (LSI) have been traditionally used in the main thermal power plants in Spain. Their substitution for NG has been widely proposed because its basic component methane (CH₄), contributes to the greenhouse effect by about 18 % while SO₂ emissions are almost annulled [9], [10]. The advantages of burning some of these fuels have been demonstrated through this paper in terms of efficiency, with data from a power plant of reference.

Finally a complete CFD (Computational Fluid Dynamics) model was built and validated later on through the measurements obtained from an experimental facility designed and built ready for burning different fuels instead of burning

This work was supported in part by the University of the Basque Country under special project OPCOFLUID 2012-2015.

J. M. Blanco is with the Department of Nuclear Engineering and Fluid Mechanics, School of Engineering, University of the Basque Country, Bilbao, SPAIN (corresponding author phone: +34946014250; fax: +34946014043; e-mail: jesusmaria.blanco@ehu.es).

L. Remaki, is with BCAM, Basque Center for Applied Mathematics, Bilbao, SPAIN (e-mail: lremaki@bcamath.org).

F. Peña is collaborating with the Department of Nuclear Engineering and Fluid Mechanics, School of engineering, University of the Basque Country, Bilbao, SPAIN (e-mail: fpfbg@telefonica.net).

them directly in the fossil-fuelled thermal power plant. Two different fuels were tested in this paper such as natural gas and a gas derived from biomass, in order to compare both performance and emissions issues

II. AIMS AND METHODOLOGY

The aim of the present work is to show the overall effect of the gradual replacement of fossil fuel consumption for natural gas or other alternative fuels such as bio-fuels in terms of emissions ensuring combustion quality.

It is crucial to point out that the global efficiency in a thermal power plant on the base of the LCV is about 39 % in case of conventional cycles, while nowadays for combined cycles this value reaches around 58 % [11], so the assessment of this particular situation of burning different fuels is another relevant objective. This paper aims also to compare efficiencies when burning such a different fuels.

First of all, the boiler and global efficiencies for conventional cycles burning fossil and alternative fuels will be determined based on both their gross and lower calorific values on a thermal power plant of reference.

Finally, the advantages of burning some of these fuels will be demonstrated through a CFD (Computational Fluid Dynamics) model, validated by the measurements obtained in an experimental scaled combustion chamber, which will be fully described later, ready for burning different fuels.

III. DETERMINATION OF THE GLOBAL EFFICIENCY

A. Procedure

The global efficiency of the power plant can be calculated according to (1).

$$\eta_G = \eta_c \times \eta_b \quad (1)$$

Whereas the cycle efficiency reaches a constant value of 0.41 regardless of the fuel type burned, the global efficiency can be directly obtained through the boiler efficiency which can be associated to the low or gross calorific values of the fuel burned according to (2 and 3) respectively.

$$\eta_{b(GCV)} = \frac{(GCV + \sum fCr) - \sum_{GCV} P}{GCV + \sum fCr} \quad (2)$$

$$\eta_{b(LCV)} = \frac{(LCV + \sum fCr) - \left(\sum_{GCV} P - Q_{v(H_2O)} \right)}{LCV + \sum fCr} \quad (3)$$

The losses and the credit factor summations can be split into several terms, according to (4 and 5).

$$\sum_{GCV} P = P_{dg} + P_{wf} + P_{H2} + P_{wa} + P_{CO} + P_{CR} + P_{DE} \quad (4)$$

$$\sum fCr = fCr_a + fCr_b \quad (5)$$

Special treatment will be given to the last term, so called "Difficult evaluation losses term" (P_{DE}). This is in fact the sum of a set of minor entity losses such as, ashes radiation heat, sensitive heat of slags, latent heat of fusion of slags, unburned hydrocarbons, and formation of free radicals and species dissociation.

Due to their special nature, the direct and rigorous evaluation of the three first terms turns to be really complex whereas the evaluation of the last two ones is simply impossible, given that the combustion is reached inside great boilers with burners in turbulent flow regime.

For the evaluation of these losses, a value of $DE = 1 \%$ (kJ per kilogram of fuel burned over the GCV) is commonly applied. Here nevertheless a value of 1.078 % will be applied with the exception of 1.92 % for the biomass derived fuel and bio-oil respectively [12].

B. Considerations

The next considerations must be taken into account for this particular approach:

- A full load electrical consumption of the pumps: $E_p = 985$ kWh has been considered.
- The percentage of carbon that gets transformed to CO, admitting a good operative practice of the boiler together with a suitable design of this one, provides values between 4 and 20 mg/Nm³. These values correspond to averaged real full load measurements in real thermal power plants, which have a permanent CO analyzer.
- The specific losses associated with convection and radiations (kJ/hm²) respectively were proposed by ASTM Committee C-8, Subcommittee on heat transfer, 1937 (revised on 1947).
- The total boiler wall area ($A_{bw} = 3,370$ m²) has been divided into $N = 56$ walls according to their temperature distribution so an average temperature (T_{bwi}) was assigned to each one of these parts.
- The boiler inlet temperature is assumed to be a constant value ($T_b = 46$ °C).
- The credit factor associated to the boiler recirculation pumps (kJ per kilogram of fuel burned) considers that only 50% of the energy supplied by the boiler pumps is transferred to heat the water inside the boiler.

In short, a breakdown of the different losses and credit factors previously defined are shown in Table 1 for both traditional and alternative fuels.

Table 1. Losses and credit factors for different fuels

(kJ/kg)	FO "N 2"	FO "LSI"	NG	BG
P_{de}	1,937.64	1,937.64	2,163.65	811.63
P_{wf}	12.12	0.00	0.00	0.00
P_{H2}	2,498.09	2,498.09	5,858.56	1,518.84
P_{wa}	30.76	30.76	36.11	2.96
P_{CO}	1.08	1.08	1.08	0.58
P_{CR}	61.44	61.44	61.44	24.53
P_{DE}	1,393.69	1,145.44	556.82	325.87
fCr_a	383.51	383.51	380.04	151.52
fCr_b	20.56	20.56	20.56	8.19

And finally the boiler efficiency can be calculated associated to the low and gross calorific values of the fuel burned, as has been shown previously in (2 and 3), while the global efficiency can be determined according to (1). These outputs are then summarised in Figure 1 for all the fuels considered here.

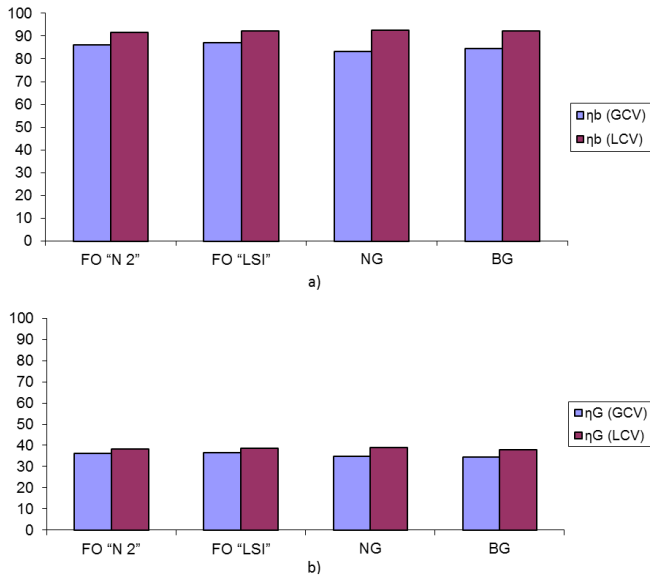


Fig. 1 Comparative test of efficiency, a) Boiler; b) Global

The most important conclusion is that boiler and global efficiencies present comparable values for all the fuels so alternative fuels could be considered an efficient option in thermal power plants regarding their least emissions.

IV. EXPERIMENTAL WORK

Experimental results have been achieved through direct measurements over a 465 kW thermal power experimental installation which is basically composed of a 4 m length combustion chamber whose walls are fully protected with glass fibre of 70 mm. thickness and equipped with a control board composed by two thermostats, a clock of temperature and pressure and a safety thermostat. It is semiautomatic, where, by means of a hydraulic system, it is able to regulate required air for every level of power requested.

The chamber consists of three parts: fuel supply unit, adapted burner, and finally the boiler. The air is supplied by a centrifugal fan and passes outside through 12 uniformly-placed nozzles, where the fuel is finally injected, producing the required air-fuel mixture while the initiating spark produces the flame.

The measurement process was considered as a decisive part of the design and hence carefully designed. Four reference areas were carefully studied inside the chamber such as, chimney, combustion chamber, water and fuel respectively. These outcomes will provide enough information to define properly the boundary conditions but also to validate the CFD model that will be fully described later. Fig. 2, shows the burner and redefined combustion chamber.



Fig. 2 Picture of the prototype chamber

For each one of these areas, several physical quantities were measured in order to guarantee that the information further needed for the CFD model would be precise enough. A 20 channels data-logger with complex software ready to get the average value for each one of the measurements was used. The instrumentation used is briefly described below:

- **Temperature:** Ambient temperature is mostly measured using a platinum thermostat while flue gas temperature was measured at several points by a thermocouple. The following equipments were used for the measurement of the maximum temperature of the flame and of the walls of the combustion chamber: a wet-bulb thermometer, a resistance thermometer, thermocouples, and a portable colorimetric pyrometer, model QL2500, with analogical 4-20 mA.
- **Pressure:** Bourdon gauge of graduated mask, pressure differential cut-out and differential gauges.
- **Barometric pressure:** Standard aneroid barometer.
- **Flow:** Perforated plate (certified), for measuring the water flow, a differential gauge of 4-20 mA. exit, for measuring the pressure drop, and a digital flow meter, model RMC205 for measuring the gas flow.
- **Emissions:** Gas analyzer RS232C that provides a clear display values for carbon monoxide, carbon dioxide, oxygen, NO and sulphur dioxide gas volume concentration but also flue gas and ambient temperatures.

These outcomes provide enough information to define properly the boundary conditions and the validation of the CFD model.

V. CFD MODEL

A. Domain and computational mesh

A CFD model was built in order to predict the exhaust gases in the combustion chamber from various fuels and validated through the experimental results previously described. This data were implemented in the compressible parallel finite volume-element solver ANSYS-FLUENT, which is able to

handle hybrid grids to simulate the whole combustion process. In a previous design process of an experimental dual burner [13] a preliminary model was built over a similar combustion chamber, but in this study, the full CHEMKIN[®] reaction solver [14] has been implemented. The geometry was created using a powerful pre/processor code ICEM CFD, and then the domain is discretized using hexahedral elements that guarantee better numerical results [15]. Once the discretization of the geometric volume was completed, the mesh is exported, into the main code (processor), where the boundary conditions would be set to complete the numerical model. The mesh size is around 4,000,000 cells.

In Fig. 3, the computational outline domain including part of the burner and redefined combustion chamber are depicted. The outlet of the chamber can be clearly seen on the roof and the fuel nozzles are depicted inside the burner.

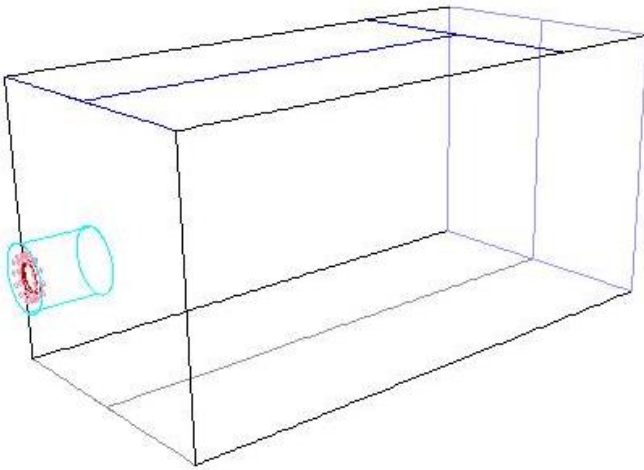


Fig. 3 Full model outlined domain including the burner

B. Boundary conditions

The boundary condition “mass flow inlet”, for the fuel was selected because the corresponding value of the flow was available. Thus, the consumption of air was obtained by calculating the ratio “kg air/kg fuel” for combustion with an excess air of 10 %.

The condition of “outflow” for the outlet of the combustion chamber was adopted. It is appropriate where the exit flow is close to a fully developed condition, as the outflow boundary condition assumes a zero, normal gradient for all flow variables, except pressure [16].

The external walls of the burner were considered to be adiabatic, considering that the gas nozzle was inside the refractory of the fireplace [17]. With the optical pyrometer, the maximum temperature that was reached on the lateral walls was measured.

To evaluate correctly the temperature of the walls, an average temperature was considered and two criteria were used. For the first criterion, the temperature of the exhaust gases was determined from the combustion chamber. This temperature depends on the power of heat given out by the burner and the heat exchange across the walls in the fireplace. For the second criterion, the heat across the walls for the

thermal calculation was given by the manufacturer. To fit this value, modelling was carried out several times, imposing a temperature to the walls verifying always the values of the average temperature for the CEG and the flow of total heat evacuated through the walls.

C. Turbulence closure

The realizable k - ε model in FLUENT has been finally adopted for this study, since the standard model was used as initial guess. The realizable k - ε models provide better results than the standard k - ε model, thanks to their modifications for adverse pressure gradient flows. The word “Realizable” actually implies that the model satisfies specific constraints on the Reynolds’ stresses that make the model more consistent with the physics of turbulent flows and hence more accurate than the standard k - ε model.

This model makes the eddy-viscosity coefficient, C_v , dependent on the mean flow and turbulence parameters. The notion of variable C_v has been suggested by many authors and is well substantiated by experimental evidence. Note that in the realizable model, C_v can be shown to recover this standard value of 0.09 for simple equilibrium flows [18]. Transport equations for k and ε respectively are as follows:

$$\frac{\partial}{\partial t}(\rho k) = \frac{\partial}{\partial x_j} \left[\left(\mu + \frac{\mu_t}{\sigma_k} \right) \frac{\partial k}{\partial x_j} \right] + G_k - \rho \varepsilon \quad (6)$$

$$\frac{\partial}{\partial t}(\rho \varepsilon) = \frac{\partial}{\partial x_j} \left[\left(\mu + \frac{\mu_t}{\sigma_\varepsilon} \right) \frac{\partial \varepsilon}{\partial x_j} \right] + C_{g1} \cdot \frac{\varepsilon}{k} \cdot G_k - \rho \cdot C_{g2} \cdot \frac{\varepsilon^2}{k}$$

D. Radiation closure

Radiative heat transfer was included because the radiant heat flux was high compared to the heat transfer rate due to convection or conduction. The radiative transfer equation adopted for an absorbing, emitting, and scattering medium at position \vec{r} in the direction \vec{s} , is:

$$\frac{dI(\vec{r}, \vec{s})}{ds} + (a + \sigma_s) \cdot I(\vec{r}, \vec{s}) = a \cdot n^2 \cdot \frac{\sigma \cdot T^4}{\pi} + \frac{\sigma_s}{4\pi} \int_0^{4\pi} I(\vec{r}, \vec{s}') \cdot \Phi(\vec{s}, \vec{s}') d\Omega \quad (7)$$

The net radiative heat flux at flow inlets and outlets is computed in the same manner as at the walls, as described above. It has been assumed that the emissivity of all flow inlets and outlets is 1.0 (black body absorption).

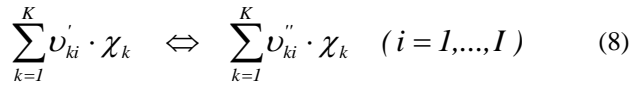
E. Combustion closure

The temperature-dependent portion of the rate expression contains an exponential, which is computationally expensive to evaluate. To facilitate a more computationally efficient solution algorithm, CHEMKIN[®] provides additional subroutines that either provide the temperature-dependent rate coefficients or, given these rate coefficients, return the species’ net rates of production.

In addition to chemically reacting flow applications, it includes an Equilibrium Reactor model. This model allows

users to determine the chemical state of a mixture under equilibrium conditions. It can be used to determine phase equilibrium, between gas and condensed phases, as well as chemical equilibrium.

Gas-phase reactions describe interactions and conversions between gas-phase species. Each species in a reaction must be associated with thermodynamic data which are used to calculate equilibrium constants and reverse-rate coefficients for the reaction [19]. Consider elementary reversible (or irreversible) reactions involving the chemical species that can be represented in the general form:



The production rate of the k th species can be written as a summation of the rate-of-progress variables for all reactions involving the k th species:

$$\dot{\omega}_k = \sum_{i=1}^I \nu_{ki} \cdot q_i \quad (k = 1, \dots, K) \quad (9)$$

The “third body” is required for the reaction to proceed; this is often the case in dissociation or recombination reactions. The concentration of the effective third body must appear in the expression for the rate-of-progress variable as:

$$q_i = \left(\sum_{k=1}^K (a_{ki}) \cdot [X_k] \right) \cdot \left(k_{fi} \prod_{k=1}^K [X_k]^{\nu'_{ki}} - k_{ri} \prod_{k=1}^K [X_k]^{\nu''_{ki}} \right) \quad (10)$$

VI. RESULTS AND DISCUSSION

A. Experimental results from the combustion chamber

The boiler was loaded about one hour before the starting of the tests in order to ensure stability, especially for several parameters such as: pressure, temperature, and flow of both gases and water. The different instruments were checked in order to verify the stability of the process [20]. The parameters were considered to be steady when the variation between them did not exceed a range of 5 % in every measurement process. Once stability was achieved, the input of data commenced [21].

All the tests and measurements were carried out with the experimental burner in automatic mode (working conditions of the burner were defined automatically, according to heat consumption) as well as manual alternative selection of low and high flame process monitoring respectively.

Our portable gas analyser, model IMR3000, whose main characteristics are summarised in Table 2, is a microprocessor-based gas analyser. It has a totally automatic microprocessor-based operation including auto start-up, auto-calibration, auto-range, internal parameter monitoring and alarms. A large multifunction 5” LCD monitor provides a clear display. The unit features a paramagnetic oxygen measurement.

Table 2. Main specifications for the gas analyser.

Response Time	5 s
Accuracy	+/- 1.0 %
Linearity	0.5 %
Max. Temp.	1,500 °C
Voltage	230 V / 50Hz, 110 V / 60Hz
Battery	12 VDC (6h autonomy)
Interface	RS 232 C
Memory	10,485 measurements
Monitor	5” LCD
Units	ppm, mg/Nm ³
Emissions	CO, CO ₂ , SO ₂ , O ₂ , NO, NO ₂ , H ₂ S
Dimensions	510 x 180 x 430 mm
Weight	Aprox. 16 kg

Results obtained in the combustion of NG and BG respectively is summarized in Table 3. The combustor performance with both fuels is similar, being obtained with comparable values of temperature rise, combustion efficiency and CO emissions.

Table 3. Measured values in the combustion chamber

	NG	BG
ENVIRONMENT:		
Dry bulb temperature (K).	296	297
Barometric pressure (Pa).	101,329	101,330
Relative humidity (%).	78	79
CHIMNEY:		
CO (ppm)	3.60	4.36
CO ₂ (%)	10.9	14.9
O ₂ (%)	2.0	1.0
Outlet temperature (K)	512	505
CHAMBER:		
CO ₂ (%)	10.6	14.6
O ₂ (%)	2.1	2.4
Outlet temperature (K).	1,352	1,343
Máx. Combustion temperature (K).	2,138	2,150
WATER:		
Flow (kg/s).	12.2	12.2
Inlet temperature (K).	388.2	389.1
Outlet temperature (K)	417	419
Total pressure (Pa).	1,084.1	1,088.2
FUEL:		
Flow (kg/s)	0.0352	0.0352
Inlet temperature (K).	295	295
Relative pressure (Pa).	6,754.1	6,758.2

B. Validation

The experimental values measured with the previously mentioned facility and the results obtained with the CFD model can be seen summarised in Table 4 for natural gas and bio-gas respectively which seem to be the best options. A significant agreement is achieved between CFD and experimental results showing that the procedure can be considered fully acceptable.

A small difference in the maximum combustion temperature was expected, because it is well known that the combustion model tends to over-predict such values of temperature. As a consequence, the temperature of the combustion exhaust gases

from the combustion chamber is obviously slightly lower than this given value.

Table 4. Validation of the CFD model.

	NG		BG	
	Exp	CFD	Exp	CFD
Q_b (W)	(*) 545,221	544,970	(*) 555,546	554,908
T_{avg} (K)	1,352.00	1,360.41	1,343.00	1,350.32
T_{max} (K)	2,138.00	2,169.00	2,159.00	2,180.00
CO (ppm)	3.60	3.63	4.36	4.69

(*) Calculations based on data provided by direct temperature measurements over the walls.

Fig. 4 up shows the average temperature along the centerline of the combustion chamber in a comparative test for experimental values and CFD outcomes for NG, showing a relevant coincidence both in values and distribution, whereas in Fig. 4 down the same are depicted for BG, showing in both cases a good agreement.

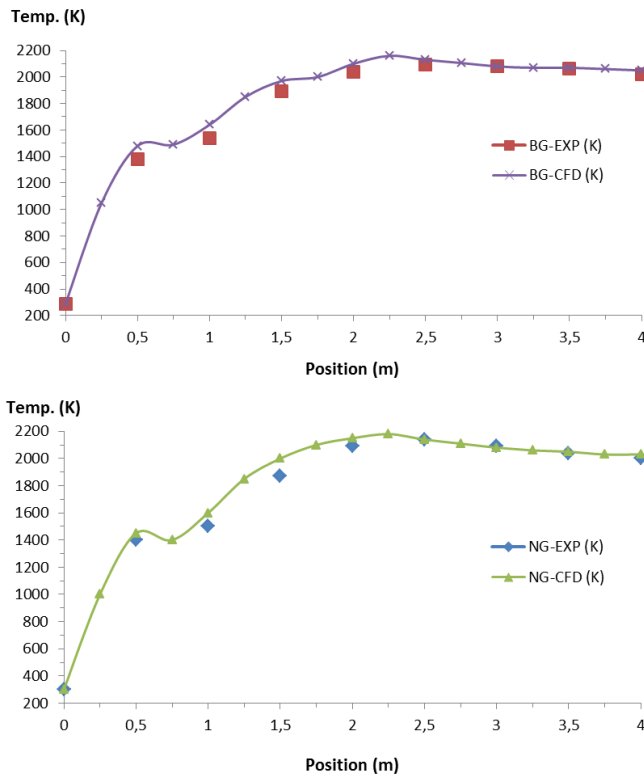


Fig. 4. Temperature (K) along the centreline of the chamber up NG; down BG.

C. CFD outcomes

Fig. 5 shows the contours of CO (ppm) over the symmetry plane of the combustion chamber for two different fuels such as NG and BG, addressing the quality of the combustion.

Contours of CO are revealed following the flame shape, as expected, especially at the end of the chamber where finally it almost becomes exhausted especially for the natural gas. A higher amount of CO traces has revealed anyway in the case of

BG as expected from the experimental values measured at the exit of the chamber.

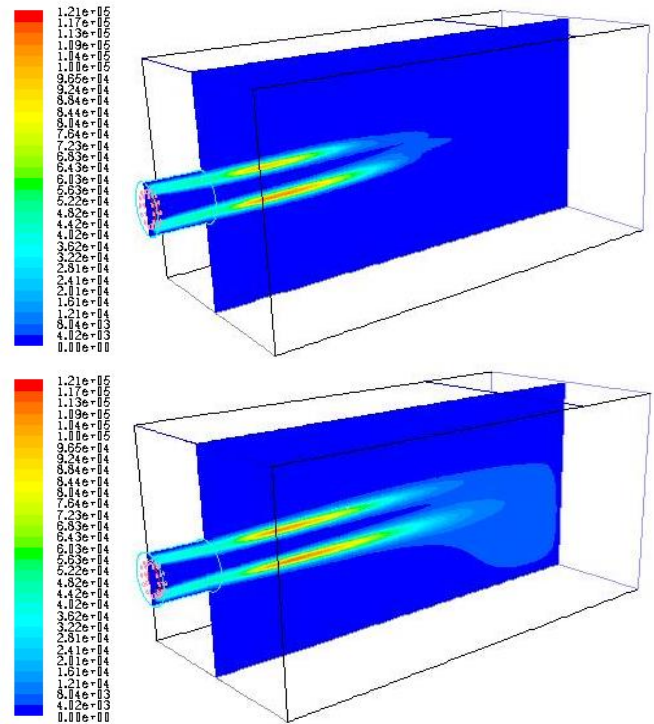


Figure 5. CO (ppm) inside the chamber, up NG; down BG.

Fig. 6 shows the contours of CO₂ (ppm) over the symmetry plane of the combustion chamber for the same two fuels. Differences in combustion between the two fuels are evident as CO₂ concentrations are distributed in a different way.

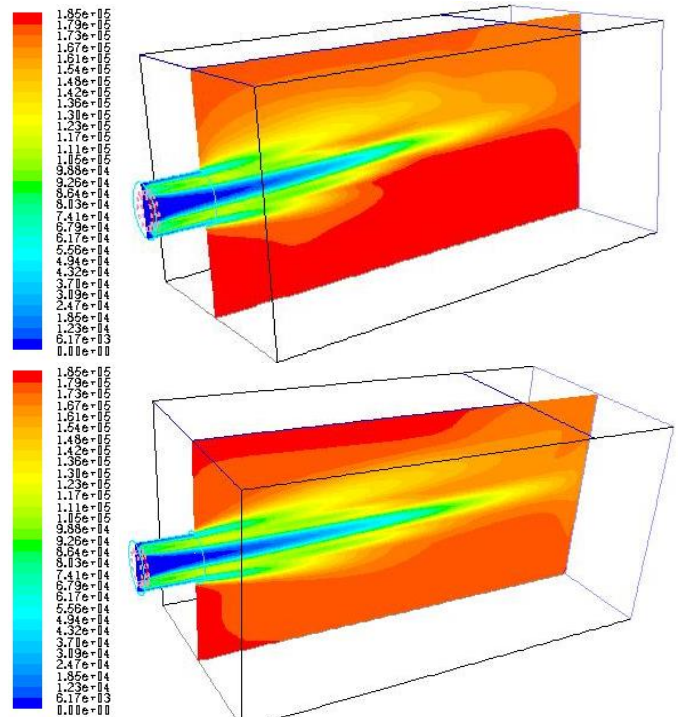


Figure 6. CO₂ (ppm) inside the chamber, up NG; down BG.

Fig. 7 shows the contours of surface temperature over the walls. The effect of the heat transfer process from the CEG to the walls over the whole combustion chamber is appreciated.

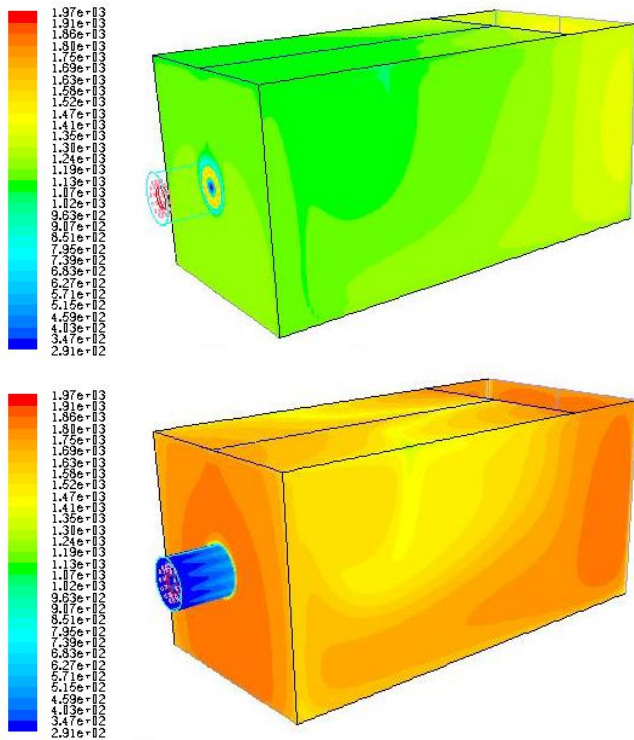


Figure 7. Surface temp. (K) inside the chamber, up NG; down BG

VII. CONCLUSION

The complete methodology for the evaluation of the boiler and global efficiencies associated to the burning of NG and BG (regarding both Gross and Lower Calorific Values) including an exhaustive definition of the “losses and credit factor terms” with a innovative improvement on the definition of the “difficult evaluation losses term” has also been carried out here, obtaining for the Bio Gas and Bio Oil values really close to the ones referred to the Natural Gas (such as 92 % and 39 % for boiler and global efficiency respectively both referred to LCV). Anyway, the considerable amount of ashes present in the matrix of the two alternative fuels would represent a decreasing on their respective real thermal efficiencies comparing with the theoretical values calculated here.

Computational Fluid Dynamics has been revealed as a powerful tool for the characterization of fuels in terms of pollution and performance. The improved models fully implement the CHEMKIN[®] code and have been widely validated throughout a fully monitored experimental facility showing a significant agreement with the CFD outcomes. This means a considerable improvement in relation to previous similar results obtained in the past, only for the natural gas combustion, due on the one hand to the implementation of the great number of equations fully solved now in the combustion process, and on the other hand, to the use of improved User

Defined Functions (UDF) defining faithfully the behavior of fluids properties involved.

Detailed information about the axial flame temperature was obtained now by performing several thermocouple traverse measurements on the experimental facility which has been useful for the characterization and further validation of the heat transfer across the walls for the different fuels, carried out through CFD.

In general, the range of efficient operation of the combustor burning biogas (equivalence ratio) decreases compared with the operation with standard fuels.

This study brings the possibility of analyzing and testing other fuels of interest in the future in a small scale over this controlled combustion chamber which could provide valuable comparative information and further insight.

ACKNOWLEDGMENT

Authors deeply thank the control staff of the thermal power plant of reference for their help, support and assistance on the test experiments and also for their suggestions in the elaboration of this manuscript.

NOMENCLATURE

BG	Gas derived from biomass (Bio-Gas).
CEG	Combustion exhausts gases.
CFD	Computational Fluid Dynamics.
CO ₂	Carbon dioxide.
DE	Difficult evaluation losses term (%).
E _p	Full load electrical consumption of the pumps (kJ/h).
\vec{F}	External body forces.
fCr	Credit factor (kJ/kg fuel).
GCV	Gross calorific value (kJ/kg fuel).
G _{k,m}	Production of turbulence kinetic energy.
G _{b,m}	Production of turbulence kinetic energy due to buoyancy.
k	Kinetic energy term.
LCV	Lower calorific value (kJ/kg fuel).
\dot{m}	Mass flow (kg/h).
NG	Natural gas.
P	Losses (kJ/kg fuel).
ppm	Particles per million.
PFBC	Pressurized Fluidized Bed Combustion.
q _i	Rate of progress of the i th reaction (mol/cm ² s).
Q _b	Total heat power supplied by the boiler (W).
Q _{v(H₂O)}	Water vaporization heat (kJ).
r	Latent heat of vaporisation for the water (kJ/kg).
\vec{s}	Direction vector.
\vec{s}'	Scattering direction vector.
T _k	Temperature of the k th species (K).
T _{avg}	Averaged temperature inside the chamber (K).
u'	Ratio of the root-mean-square of the velocity fluctuations.
UDF	User defined function.
\vec{v}	Velocity (m s ⁻¹).
[X _k]	Molar concentration of the k th species (mol/cm ³).

Greek symbols

ρ	Density.
υ _k	Thermal Diffusion velocity of the k th species (cm/s).
η _G	Global efficiency.
η _b	Boiler efficiency.
η _c	Cycle efficiency.
ε	Boiler external walls emisivity (0.95)
Φ	Phase function.
τ	Stress tensor.
ρg	Gravitational body force.

μ	Dynamic viscosity.
μ_t	Turbulent viscosity.
κ	Von Kármán constant (0.4187).
σ	Stefan-Boltzman constant ($5.672 \cdot 10^{-8} \text{ W m}^{-2} \text{ K}^{-4}$).
σ_s	Scattering coefficient.

REFERENCES

- [1] J.M. Beér, Combustion technology developments in power generation in response to environmental challenges, *Prog. Energy Combust. Sci.*, 26, 2001, pp. 301-327.
- [2] I. Gökalp, E. Lebas, Alternative fuels for industrial gas turbines (AFTUR), *Appl. Therm. Eng.*, 24, 2004, pp. 1655-1663.
- [3] M. Molière, E. Panarotto, M. Aboujaib, Gas Turbines in Alternative Fuel Applications: Biodiesel Field Test, *ASME Turbo Expo'07*, Montreal, Canada, 2007, pp. 1235-1239.
- [4] A. Tolón-Becerra, X. Lastra-Bravo, F. Bienvenido-Bárcena, Proposal for territorial distribution of the EU 2020 political renewable energy goal, *Renew. Energy*, 36/8, 2011, pp. 2067-2077.
- [5] Y. Huang, D. McIlveen-Wright, S. Rezvani, Y.D. Wang, N. Hewitt, B.C. Williams, Biomass co-firing in a pressurized fluidized bed combustion (PFBC) combined cycle power plant: A techno-environmental assessment based on computational simulations, *Fuel Procc. Technol.*, 87/10, 2006, pp. 927-934.
- [6] M. Acaro, D. Aksoy, The cultivation and energy balance of *Miscanthus giganteus* production in Turkey, *Biomass and bioenergy*, 29/1, 2005, pp. 42-48.
- [7] J.M. Blanco, F. Peña, Analytical study of the effects of the clogging of a mechanical precipitator unit in air preheaters in a high-performance thermoelectric power plant based on available data. *ASME J. Eng. for Gas Turbines and Power*, 130(2), 2008, pp. 22001-22007.
- [8] M. Molière, Expanding fuel flexibility of gas turbines, *Journal of Power and Energy*, 219/2, 2005, pp. 109-119.
- [9] J.M. Blanco, F. Mendía, F. Peña, Comparative analysis of CO₂ and SO₂ emissions between combined and conventional cycles with natural gas and fuel oil consumption over the Spanish thermal power plants, *Fuel*, 85, 2006, pp. 1280-1285.
- [10] J. Matthew, R. De Kam, M. Vance, D.G. Tiffany, Biomass Integrated Gasification Combined Cycle for heat and power at ethanol plants, *Energy Convers. Management*, 50/7, 2009, pp. 1682-1690.
- [11] S.X. Zhou, Z.P. Song, On evaluation reference of energy utilizations, *Journal Eng. Thermophysics*, 29/8, 2008, pp. 1267-1271.
- [12] J.M. Blanco, F. Peña, Obtención del valor real de las pérdidas de difícil evaluación aplicables al cálculo de rendimiento de calderas, *Inf. Tecnol*, 17/3, 2006, pp. 123-128.
- [13] J. Chacón, J.M. Sala, J.M. Blanco, Investigation on the Design and Optimization of a Low NO_x-CO Emission Burner both experimentally and through CFD simulations, *Energy and Fuels*, 21, 2006, pp. 42-58.
- [14] R.J. Kee, F.M. Rupley, J.A. Miller, M.E. Coltrin, J.F. Grcar, E. Meeks, et al, *CHEMKIN v. 4.0*, Technical Report San Diego, CA, Reaction Design, Inc., 2004.
- [15] M.S. El-Azab, K.M. Abdelgaber, Finite element solution of nonlinear diffusion problems, *Applied Mathematics and Computation*, 217/13, 2011, pp. 6198-6205.
- [16] B.E. Launder, Second-Moment Closure and Its Use in Modeling Turbulent Industrial Flows. *International Journal for Numerical Methods in Fluids*, 9, 1989, pp. 963-985.
- [17] B. Spinewine, V. Guinot, S. Soares-Frazão, Y. Zech, Solution properties and approximate Riemann solvers for two-layer shallow flow models, *Computers and Fluids*, 44/1, 2011, pp. 202-220.
- [18] F. Hamba, Analysis of filtered Navier-Stokes equation for hybrid RANS/LES simulation, *Physics of Fluids*, 23/1, 2011, pp.123-131.
- [19] S.C. Kong, R.D. Reitz, Application of detailed chemistry and CFD for predicting direct injection HCCI engine combustion and emissions, *Proc. Combust. Inst.*, 29, 2002, pp. 663-669.
- [20] J.M. Blanco, L. Vazquez, F. Peña, Investigation on a new methodology for thermal power plant assessment through live diagnosis monitoring of selected process parameters; application to a case study, *Energy*, 42, 2012, pp. 170-180.
- [21] J.M. Blanco, L. Vazquez, F. Peña, D. Diaz, New Investigation on Diagnosing Steam Production Systems from Multivariate Time Series

Applied to Thermal Power Plants, *Appl. Energy*, 101, 2013, pp. 589-599.

Jesus M. Blanco, Ph D, is Assistant Professor at the University of the Basque Country, School of Engineering, Fluids Engineering Department from 1993 and tutoring assistant lecturer at the Open University since 1997. This author became industrial engineer in 1992, (School of Engineering, University of the Basque Country), Doctor in industrial engineering in 1998 (School of Engineering, University of Navarre) and MSc by Research in 2009 (School of Engineering, Cranfield University, UK). Responsible of a Doctorate course since 1999 focused on computational fluid dynamics (CFD) and assistant lecturer in this later University from 2008 where he has been doing several research stays. Now is supervising three PhD theses in this field.

He has published more than 20 papers both in international journals and 30 in conferences in the field of thermal engineering optimization and CFD. Is author of several laboratory practical worksheets and has leaded numerous Research Projects. Current research interests are focused on industrial optimization projects, environmental protection and CFD.

Dr. Blanco is member of the Technical Association for Air Conditioning and Cooling (ASHRAE) since 1998, member of the editorial board and habitual Referee of several international journals such as *Applied Thermal Engineering* since 2004, member of the scientific committee of the Spanish Society for Numerical Methods in Engineering since 2008. He was awarded by the Open University in Spain for research projects in the field of minimization of the environmental impact associated to industrial processes in 2005.

Lakhdar Remaki, Ph D, is a Research professor at BCAM: Basque Centre for Applied Mathematics (Bilbao), from 2012. This author became B.S.c in Mathematics in 1991 at the USTHB University, Algiers, specialization: Partial differential equations, Master in Applied Mathematics (1992) Specialization: Numerical analysis, partial differential equations and computational methods and finally doctor in Applied Mathematics in 1997, both in Claude Bernard University, Lyon, France, Specialization: Numerical analysis, partial differential equations and computational methods. He was Postdoctoral Fellow at the School of Engineering (E.T.S) and Polytechnic School at Montreal 1998-2001, Research associate at Computational Fluid Dynamics Laboratory, McGill University 2002-2007, Research officer at Civil and Computational Engineering Centre, School of Engineering, Swansea University, UK 2008-20011, Researcher at CTA: Centre of Advanced Technologies BRP (Bombardier), Sherbrooke University 2012.

He has leaded numerous Research Projects and published several papers both in international journals and conferences in the field of CFD, gas particles modeling, mesh adaptation, aeroacoustics and turbomachinery, PDE's and numerical methods in engineering.

Dr. Remaki research interests are focused on Computational Fluid Dynamics, Gas-Particles modeling, Mesh Adaptation, Delaunay Mesh Generation, Turbomachinery, Partial Differential Equations (PDEs) and Numerical Analysis

Francisco Peña, Ph D, became naval engineer in 1972, (School of Naval Engineering, University of the Basque Country) and doctor in industrial engineering in 1998 (School of Engineering, University of the Basque Country). He has been working for IBERDROLA generation corporation for more than twenty years doing relevant research progress in the field of thermal design optimization, being responsible of the operational and starting procedures of a nuclear power plant from 1975 till 1980. He became senior engineer and chief inspector of Thermal Power Plants from 1998 till 2007 and assistant lecturer from 2001 at the School of Engineering, University of the Basque Country, teaching power plants in a master's degree focused on sustainability.

He is co-author of several papers in international journals and conferences in the field of thermal energy and efficiency improvement but also in the educational innovation context. Recently published a chapter entitled: "Optimizing preliminary design of industrial equipment involving different thermal engineering calculation procedures over a power plant" at the Thermal engineering research developments edited collection, NOVA Science Publishers and a book "Ampliación de Tecnología Energética" for the School of Engineering, University of the Basque Country.

Dr. Peña worked for a Committee based on teaching innovation procedures for power plant technicians in the field of thermal efficiency from 1980 till 1987 in several thermal power plants in Spain.

Urban Planner – model for land use suitability assessment

Jaroslav Burian, Jan Brus, Stanislav Stastny

Abstract— The paper describes model Urban Planner (released as an analytic extension for Esri ArcGIS for Desktop) designed to evaluate the land suitability and to detect the most suitable areas for spatial development. The model uses a multi-criteria analysis and respects the principles of sustainable development. The core of the model focuses on the evaluation of land suitability according to input data, its values, and weights. Land suitability is analyzed for selected categories of land use (housing/residential, recreation, public facilities, industry and agricultural production).

Keywords—ArcGIS, land use, modelling, urban planner

I. INTRODUCTION

MANY authors deal with the topic of land suitability assessment Baran-Zglobicka [1], Kenderessy [2], Picher and Romero [3], Kolejka [4, 5], Sklenička [6] and Růžička [7]. All of them used GIS technologies on very limited levels and the capacity of GIS analysis, modelling and simulation is not fulfilled.

On the other hand, the current advances in spatial planning and modelling have induced the development of many different computer models and applications (e.g. Burian et al. [8], Pechanec et al. [9], Paszto et al. [10], Pechanec et al. [11]. Brail and Klosterman [12] describe in their book several programmes (METROPILUS, INDEX, TRANUS, CUF I, CUF II or CURBA) that are commonly used for the purposes of regional planning, primarily in the USA but also in other countries. Klosterman, in his numerous publications (e.g., Klosterman [13]), describes his software solution for creating scenarios – the tool “What if?” – Which belongs to a group of planning support systems (PSS) and is an extension of the Esri products.

Several models and software are described by many authors: LADSS [14], Geogacom 5W [15], SUDSS [16], UrbanSIM [17]. Burian [18] describe detailed comparison.

This paper was supported by the project nr. CZ.1.07/2.3.00/20.0170 co-financed by the European Social Fund and the national budget of the Czech Republic.

Jaroslav Burian is with the Department of Geoinformatics, Palacký University, Olomouc, 779 00, 17. listopadu 50 Czech Republic (corresponding author provide e-mail: jaroslav.burian@gmail.com)

Jan Brus is with the Department of Geoinformatics, Palacký University, Olomouc, 779 00, 17. listopadu 50 Czech Republic (e-mail: jan.brus@upol.cz)

Stanislav Stastny is with the Department of Geoinformatics, Palacký University, Olomouc, 779 00, 17. listopadu 50 Czech Republic (e-mail: stastny.stan@gmail.com)

These models can create highly advanced results (especially UrbanSIM microsimulation sub-models). Suitable data (e.g., detailed data about income and traffic data) are needed to utilize them in the Czech Republic. These data are very concrete and missing on a detailed level. These situations make all the mentioned models virtually unusable, and this was the main reason to develop new model/extension which would be fully applicable in Czech Republic.

The model was created based on the study of Czech and foreign approaches to the assessment of land suitability [4, 5, 7, 13, 19], finding conflicting areas and proposals for optimal land use.

In comparison with existing models, Urban Planner is much more applicable not only as a new methodological approach but also as a practical tool for urban planning processes [20].

II. LAND SUITABILITY CALCULATION

The core of the model focuses on the evaluation of land suitability according to input data, its values and weights. Land suitability is analyzed in three levels (pillars, factors, and layers) for the 6 predefined categories of land use:

- 1) Housing/Residential - smaller areas used mainly for housing purposes or mixed residential areas with services of local importance.
- 2) Recreation - areas used primarily for recreation (holiday houses, cottages) usually limited by height limits.
- 3) Commercial/Public Services - larger areas used primarily for commercial public services - administrative centres, larger retail areas, entertainment centres, exhibit centres, mostly with high transport demands.
- 4) Heavy Industry - larger production areas of heavy industry with potential negative influence on the landscape and healthy lifestyle, usually with protection zone.
- 5) Light Industry and Warehousing - production areas of light industry and warehousing without production activities with negative influence on the landscape. If negative aspects exist, their influence is limited only to the area of activity.
- 6) Agricultural production - areas for building used for livestock, agricultural equipment and storage of crop production.

Beyond these categories, the user can set a custom category or edit selected categories.

The total land suitability is calculated according to setting of the weights between the three classes (the three pillars): ecological, social, economic. Weight can acquire values from 0 to 100; the sum of the weights of all three pillars must be equal to 100. Extension allows the user to select from the predefined options, or set your own. By different weights settings, it is possible to create several scenarios of land suitability.

SCENARIO	Ecological	Social	Economical	SCENARIO	Ecological	Social	Economical
Sustainable	33%	33%	33%	Ecological pillar priority	60%	20%	20%
Acceptable	40%	40%	20%	Social pillar priority	20%	60%	20%
Viable	40%	20%	40%	Economical pillar priority	20%	20%	60%
Fair	20%	40%	40%	Custom	? %	? %	? %

Fig. 1 Scenario variants

Each of the three pillars (classes) consists of factors. Factors are divided into 3 groups - positive, negative and limits. Positive factors increase the value of land suitability, the negative factor decrease this value and the limits eliminate the value of land suitability. In some individual cases, the limits determine the purpose, method, borders and the conditions of land use. As in the case of pillars the combination of factors is based on weighted overlay method.

The most detailed level of settings are parameters that are described as properties of factors. They are represented by specific layers (shapefiles) and their attributes. Factors' weights can be set up in the range of scales 0-10. From a technical perspective, the most of calculations are based on raster weighted overlay. The results of this part of the model are raster layers of land suitability.

Parameters of the layer considered as the limits have to be set very carefully. If the layer is a hard limit eliminating any activity in the area, it is recommended to set its value to "NoData" (excluded land suitability). If the layer is a soft limit which only reduces the activity in the area, it is recommended to set its value to a higher value (starting from 1 to the higher values).

If any parameter of the layer within the selected factor is set to "NoData", the land suitability in this location will be excluded and non-other layers (even those with the highest land suitability) will affect total land suitability.

If any parameter of the layer within the selected factor is set to 0, the land suitability is inappropriate in this location (0 value), but other layers can increase total land suitability in this place.

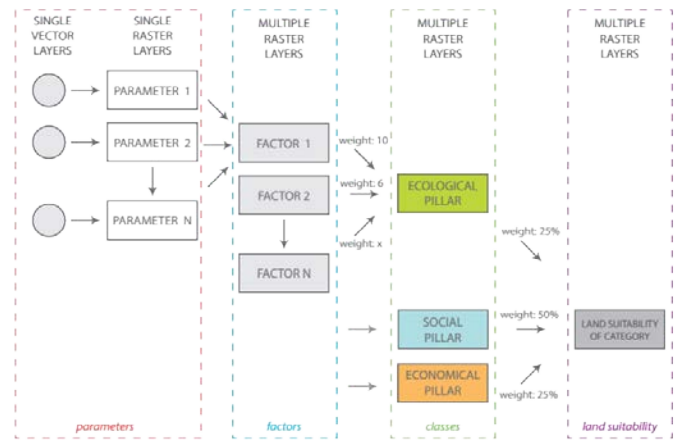


Fig. 2 Land Use calculation

III. OPTIMAL LAND USE CALCULATION

The second part of the methodology is designed to identify areas suitable for optimal allocation (optimal land use). Cadastral map (parcel units) can be used for allocation process, but due to spatial variability of land suitability in one parcel is recommended to use more regular units (hexagonal grid covering the studied area). It is possible to exclude build-up areas and non-buildable areas from the calculation. Each category of land suitability (housing, industry, recreation, etc.) has to be evaluated individually. The main variables, which affect the allocation, are the total area of allocation and minimum area of allocation.

The following procedure performs the allocation process. The whole area is covered with vector hexagonal network; the built-up areas are eliminated. It is recommended to use hexagonal network, which describes the spatial variability in more detail. The width of the hexagon is necessary to choose with respect to the grid size. Recommended size of one edge of the hexagon is 50 m. Smaller size of hexagon is not recommended because of the computation troubles. The larger size of the hexagon loses information value. By using zonal statistics the average value of the land suitability is calculated for every hexagonal unit. One percent of units with the highest value of land suitability are selected and combined into contiguous areas. If the conditions of minimum and total allocated area are fulfilled, the calculation is done. If the conditions are not fulfilled, the process of units selections is repeated (2 % of units with the highest value of land suitability are selected).

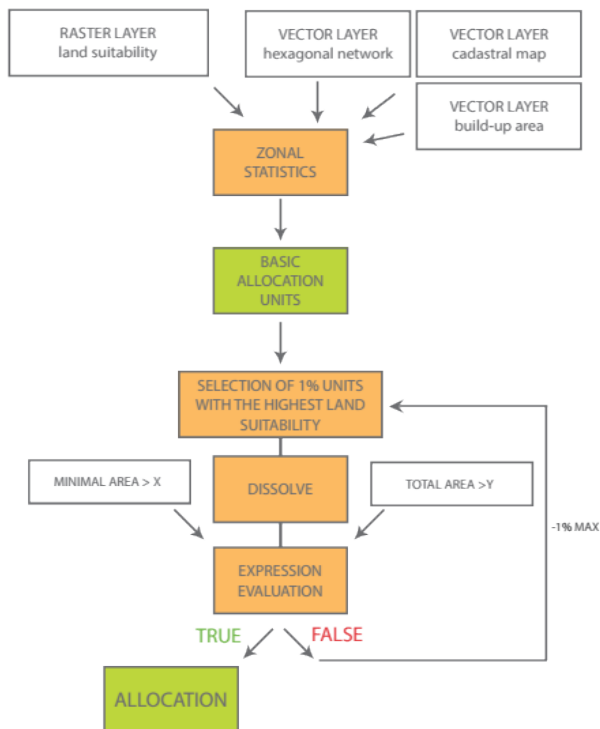


Fig. 3 Identification of optimal land use

IV. APPLICATION INTERFACE

Urban Planner is released as ArcGIS for Desktop plugin (Add-In). For full functionality, ArcGIS for Desktop Basic license and Spatial Analyst extension is needed. The extension requires .NET Framework version 3.5 or higher.

The main extension toolbar is divided into four main sections (Land Suitability, Land Use, Data Manager and Settings). Land suitability component offers two sub-sections: Pillar Suitability and Land Suitability. Land suitability cannot be calculated without previous partial calculations of pillar suitability. Land Use component also contains two sub-sections: Suitability Transfer and Allocation, which must also be run sequentially.

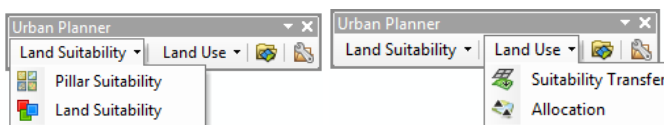


Fig. 4. Urban Planner Toolbar

A. Application settings

Basic settings are used to define the main inputs used across applications in all calculations. All settings are stored in profiles that can repeatedly be run. All settings are stored automatically in Access database connected with current mxd project and can be exported or imported. This functionality can be used in case of multiple users or different scenarios. Profiles can be added, deleted or modified.

In the settings window is necessary to set up the area border, directory for analysis outputs and resolution of the output rasters. Especially raster resolution has to be set up according to the total area and according to the computational capacity of

the computer (CPU and memory). It is recommended to work with the more detailed grid (about 10 m / pixel). Users are advised to test the performance of the calculation for one sub-analysis and according to the speed adjust the input resolution value. All outputs are stored in UrbanPlanner.gdb that is created automatically.

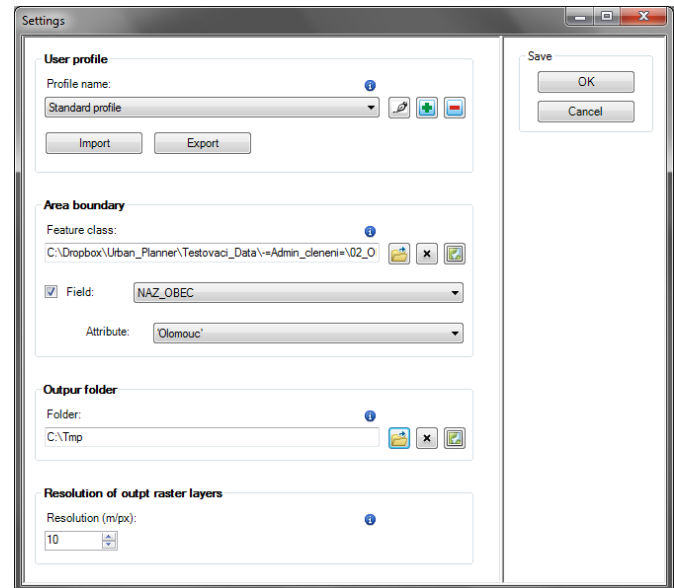


Fig. 5. Input Parameters Settings

B. Input parameters settings

In the case of Czech data of planning analytical material, the Data Manager can be used for automatic data import. In all other cases, the paths to all single layers have to be set up manually for all factors. If the user has its data model, application can be modified, and automatic data import can work too.

C. Land suitability

Land suitability analysis consists of two sub-parts. First of all is necessary to calculate land suitability of pillars (environmental, economic and social). Also, the category of land use (residential, recreational, commercial, industrial or agricultural), for which land suitability is calculated, has to be selected. These categories can be deleted, and new categories can be set up by user.

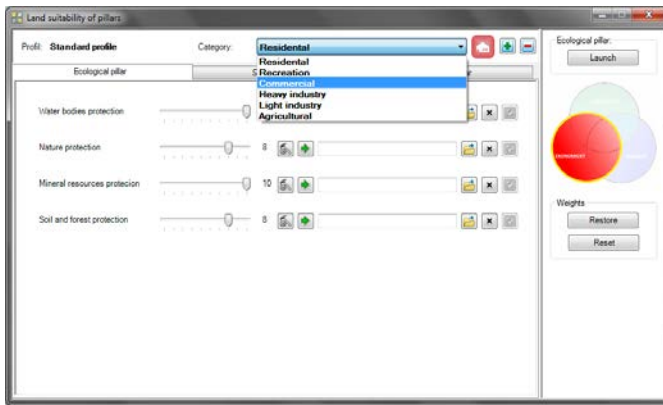


Fig. 6. Selection of the Category for Land Suitability Calculation of Selected Pillar

For each pillar is necessary to choose, what factors will enter into the calculation and what will be their weights. Default factors and their weights were calculated using the Saaty method [21] by several experts. According to the specific conditions of the territory, it is possible to change the factor's weights. Factors can be deleted or added, and there is no requirement concerning number of factors in each pillar.

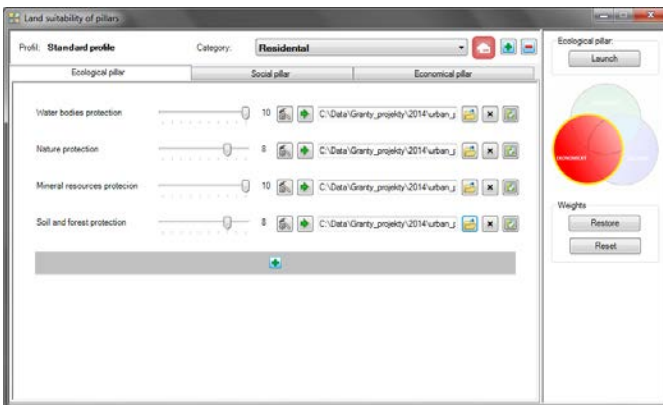


Fig. 7. Calculation of Land Suitability for Pillar

For each factor, it is necessary to check the settings for parameters that describe all factors. Each factor is composed of several sub-layers, where it is needed to set the path to the input data (possibly also choose a field attribute), and then specify the settings (values). If the user always uses the same data model, Urban Planner can be modified, and paths to the data can be uploaded automatically.

The parameters and weights for all layers already set, the user can change them in scale from the excluded potential (NODATA value) through inappropriate potential (value 0) to the optimum potential (value 10). There are two types of data: ordinal and interval. For ordinal data, the weight is assigned to the whole phenomenon, for interval data the weights (0-10) are divided into all range of values (such as gradients, distances).

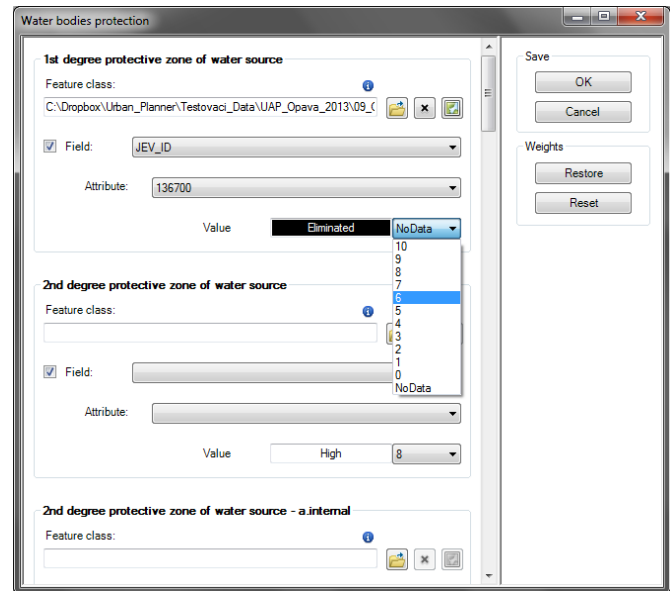


Fig. 8. Detailed Settings for Selected Layer

Each pillar must be run separately by using Start button in the upper right part of the window analysis. The user is informed about analysis results in a new window. After completing the calculation output, raster layers are loaded into ArcMap environment, and the path to the output layer is set up in the analysis window.

After the calculation of all three pillars, the total land suitability has to be calculated. If the previous calculations were correct, the path of each raster layer is set up automatically. Alternatively, they can be selected manually. The essential step during total land suitability calculation is selection of predefined scenarios of development. Several scenarios are predefined; user values can be set up too.

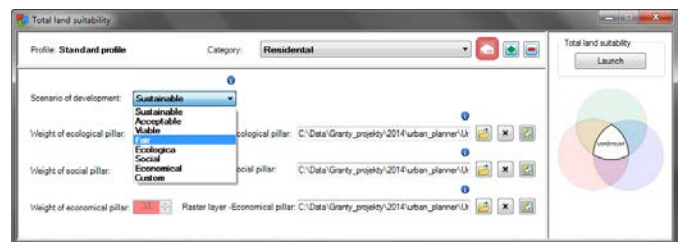


Fig. 9. Selection of Scenario of Development

The final output of Land suitability calculation is raster layer of land suitability for the selected category according to the selected scenario development. For the calculation of the other categories, it is necessary to repeat all the steps described above. For the calculation of different scenarios, it is sufficient to repeat only the final step of the analysis. During all calculations, many raster layers are created. Therefore, all outputs are named according to predefined abbreviations that are described in the extension manual.

D. Land use

The second component Land use allows to search (allocate) areas suitable for development on the basis of the previous

total land suitability calculation. Land suitability is converted to the selected polygonal units. For each vector unit, average value of land suitability is calculated. As the polygonal unit typically cadastral map can be used. In the case of large parcels, land suitability can be very variable, so use of regular vector network is recommended (hexagonal grid). The hexagonal grid can be created by Repeating shapes extension [22] or by the tool Generate Pattern of Repeating Shapes. Unit size should be selected larger than the pixel size. Optional setting is layer of non-buildable area (usually the same as built-up area). If the layer is set up land suitability in this area is calculated as 0 values.

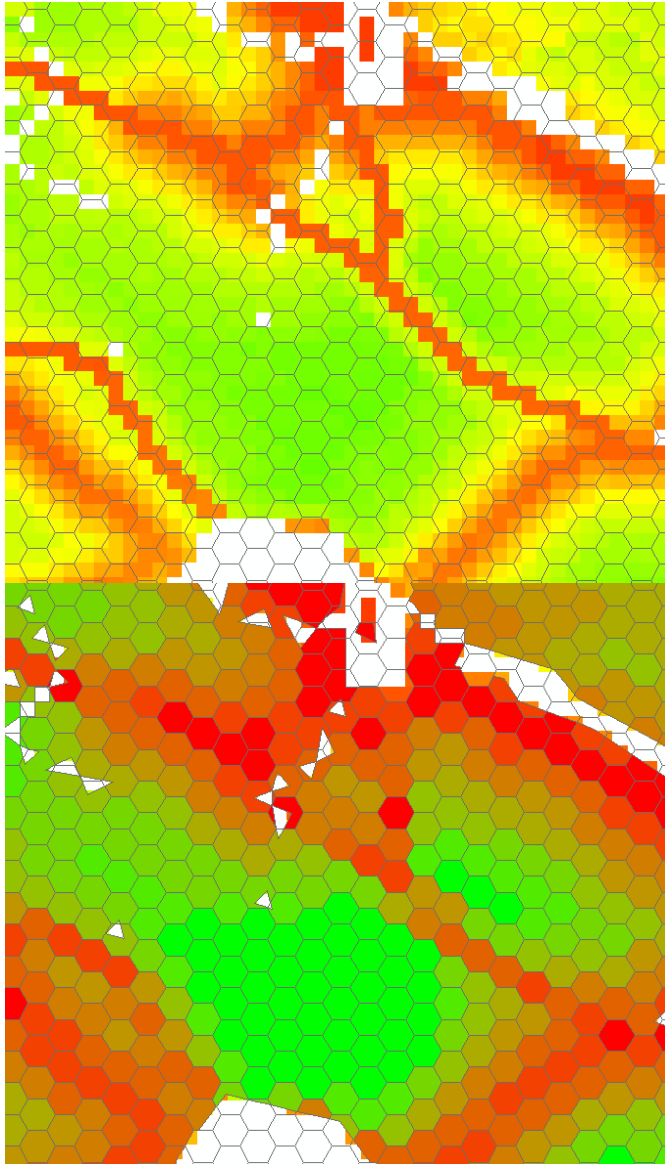


Fig. 10. Raster layer of land suitability covered by hexagonal network of basic allocation units (upper figure), Hexagonal network of basic allocation units with values of land suitability in attribute table (lower figure)

The last tool allows finding (allocate) areas with the highest value of land suitability for selected category of land use. Raster layer of total land suitability and the basic allocation

units are the input layers. The most significant input values are the minimum size of the allocated area, which defines the minimum allowed size of areas intended for allocation and then the total allocated area. The result of the analysis is a vector layer showing areas with the highest value of land suitability for selected category of land use with regard to the total and minimal area of allocation.

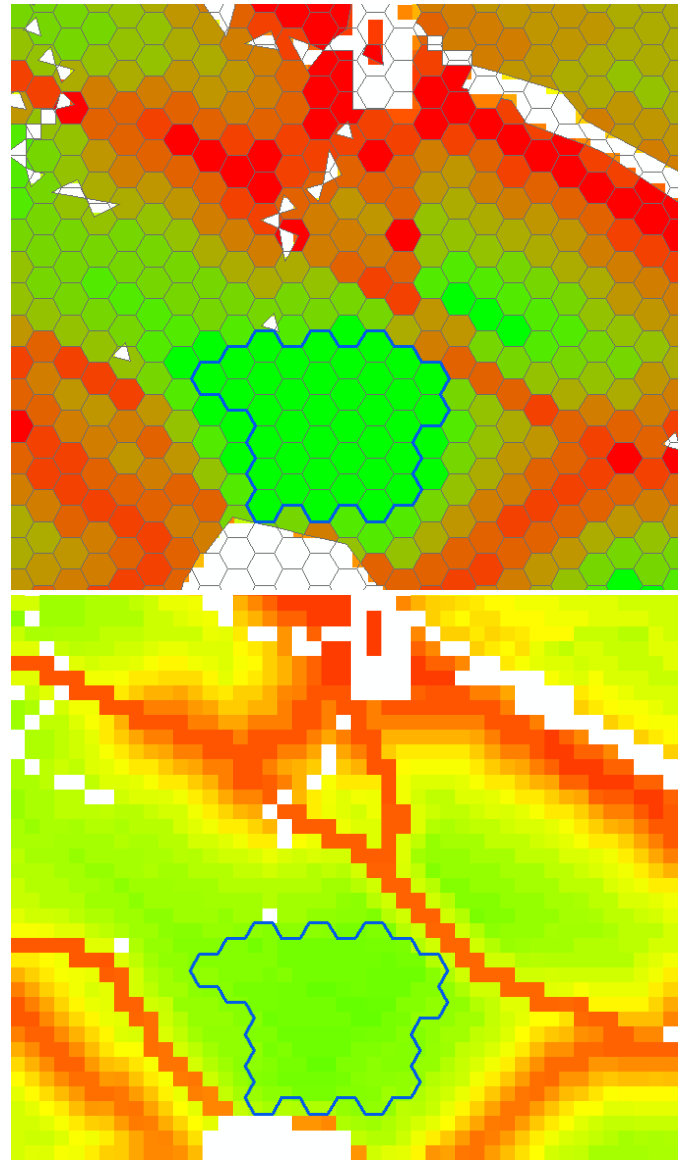


Fig. 11. Total allocated area with highest values of land suitability - conditions of the minimal and the total allocation fulfilled (upper figure shows this with basic allocation units, the lower figure shows this with raster layer of land suitability)

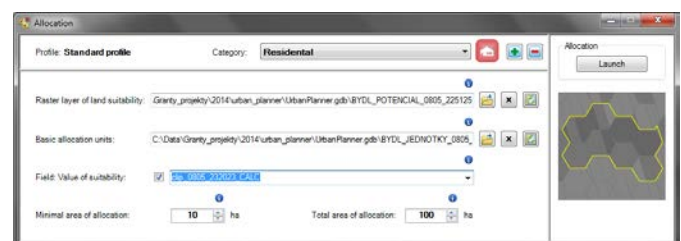


Fig. 12. Allocation Settings

V. URBAN PLANNER OUTPUTS

A. *Outputs description*

The outputs of the components Land Suitability Analysis are mainly raster layer showing the potential of individual factors, the potential of the three pillars (A) and the total land suitability (B) for selected category of land use. These raster layers can be used for verification of existing or planned activities. The final analysis (calculation of the total land suitability) can be calculated in several variants (scenarios), which can be compared and evaluated. This type of analysis may be used for comparison of possible variants of land development.

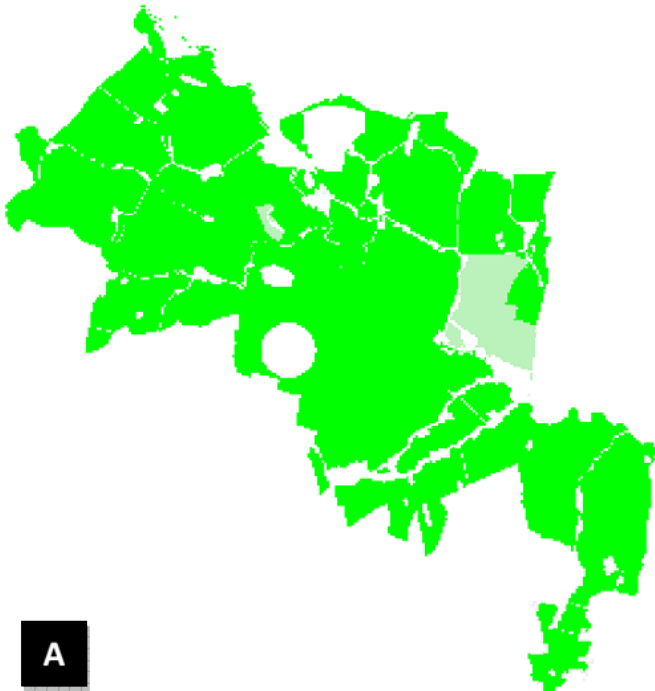


Fig. 13. Raster layer of land suitability of economic pillar (A)

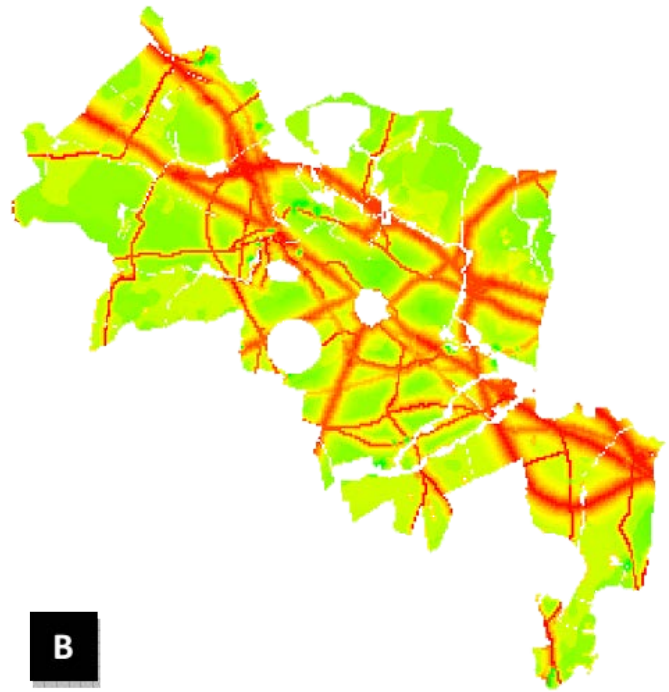


Fig 14 Raster layer of total land suitability (B)

The outputs of the second component (Land Use) are primarily vector layers (C, D) that show the total suitability shown in the polygon layer (the basic allocation unit) and the final areas suitable for allocation. If a vector layer polygon units used e.g. Layer municipal boundaries, basic settlement units, boroughs, etc., the total suitability can be easily recalculated for different polygon units (municipalities, district, basic settlement units, etc.) as the average value.



Fig. 15. Basic settlement units with land suitability values in vector format (C)

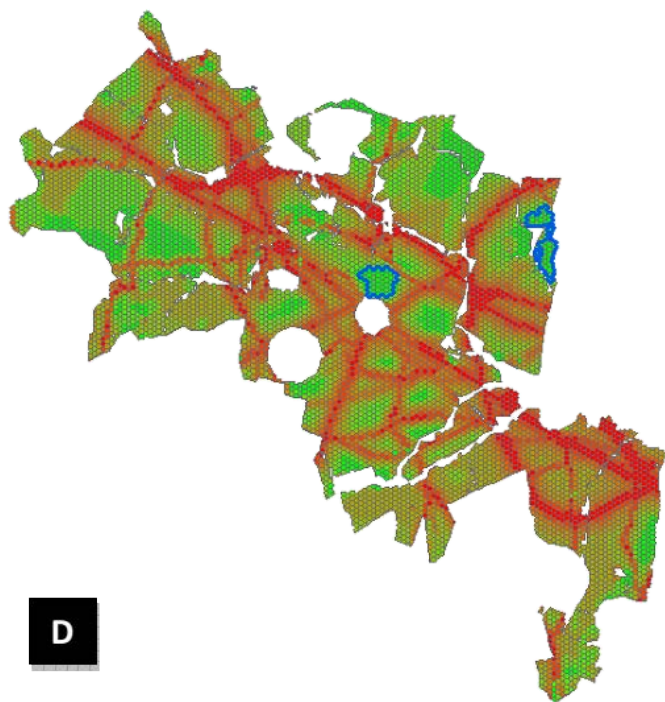


Fig. 16 Basic settlement units with land suitability values in vector format with final areas suitable for allocation (D)

Each category of land use is calculated separately and can cause overlapping of allocated space. This fact must be taken into account by expert estimate or integration of the input data.

B. Use of outputs

Urban Planner has high potential for use in all planning processes. First of all, can be used as a comprehensive tool to evaluate the land suitability and main principles of sustainable development. Result "Scenarios of sustainable development" can verify if current or proposed activities correspond to the areas with the highest land suitability. Based on the similarities and differences it is possible to determine what factors were omitted during urban plan creation and what should be improved. Overall it is possible to create six scenarios used in the scenario modelling and many others according to user settings. With this analysis, the user can determine which scenario has the highest potential in the chosen location.

The outputs from the second component can be used to detect areas with the highest land suitability for the selected category of land use. These areas can be searched according defined parameters (minimum area of allocation a total area of allocation) by using "Allocation tool" and can be used especially in cases when searching for the optimal development areas.

VI. CONCLUSION

This paper describes the extension "Urban Planner", which is the first software product of its type in the Czech Republic. In comparison with existing models, Urban Planner is much more applicable not only as a new methodological approach but also as a practical tool for urban planning processes. A strong connection (and the development of a connection) with

the data used in Czech urban planning is one of the largest advantages.

The functionality of Urban Planner was tested in two town regions - Hranicko Region and Olomouc Region, located in Moravian part of Czech Republic and Prague region. The extension was developed with strong cooperation with Olomouc local government officials. The scenarios of future development and all particular results (maps, text, and tables) were used in urban planning processes (local urban plan creation).

REFERENCES

- [1] B. Baran-Zglobicka, "Badania krajobrazowe wybranych obszarów lessowych jako podstawa oceny możliwości wykorzystania terenu w procesie planowania przestrzennego," PhD thesis, Maria Curie Skłodowska University, Lublin, 2004.
- [2] P. Kenderessy, "Integrácia GIS do tvorby krajinnokoekologického plánu," *Životné prostredie*, vol. 2003, 2003.
- [3] A. Picher and R. Romero-Calcerrada, "GIS-based spatial decision support system for landscape planning. New system of analysis for decision making," in *CORP 2006 & Geomultimedia06*, Vienna, 2006.
- [4] J. Kolečka, "Geoinformační systémy v aktivním managementu životního prostředí: Data a možnosti hodnocení a modelování rizik," *Životné prostredie*, vol. 2003, 2003.
- [5] J. Kolečka, "Krajinné plánování a využití GIS," in *Česká geografie v období rozvoje informačních technologií*, Olomouc, 2001.
- [6] P. Sklenicka, *Základy krajinného plánování*. Praha: Nadezda Sklenicková, 2002.
- [7] M. Ružička, *Krajinnokoekologické plánovanie-LANDEP: (Systémový prístup v krajinnéj ekológii)*. Bratislava: Združenie Biosféra, 2000.
- [8] J. Burian, J. Brus, and V. Voženílek, "Development of Olomouc city in 1930–2009: based on analysis of functional areas," *Journal of Maps*, vol. 9, pp. 64–67, 2013.
- [9] V. Pechanec, J. Burian, H. Kilianova, and Z. Nemcova, "Geospatial analysis of the spatial conflicts of flood hazard," *Morav. Geogr. Rep. Moravian Geographical Reports*, vol. 19, pp. 41–49, 2011.
- [10] V. Pászto, A. Brychtová, P. Tuček, L. Marek, and J. Burian, "Using a fuzzy inference system to delimit rural and urban municipalities in the Czech republic in 2010," *Journal of Maps*, pp. 1–9, 2014.
- [11] V. Pechanec, J. Burian, and Z. Dobesova, "Integrating neural networks and GIS in modelling landscape changes," *14th SGEM GeoConference on Informatics, Geoinformatics and Remote Sensing*, vol. 1, pp. 651–658 pp, 2014.
- [12] R. K. Brail and R. E. Klosterman, *Planning support systems: integrating geographic information systems, models, and visualization tools*: Esri Press, 2001.
- [13] R. Klosterman, E. "The what if? Collaborative planning support system," *Environment and Planning, B: Planning and Design*, vol. 26, pp. 393–408, 1999.
- [14] K. B. Matthews, A. R. Sibbald, and S. Craw, "Implementation of a spatial decision support system for rural land use planning: integrating geographic information system and environmental models with search and optimisation algorithms," *Computers and electronics in agriculture*, vol. 23, pp. 9–26, 1999.
- [15] V. Bougromenko and M. Zakirov, "Geogacom 5W-expert system for sustainable urban and regional transport development," presented at the *Computers in Urban Planning and Urban Management*, Venice, 1999.
- [16] P. Jankowski and M. Stasik, "Design considerations for space and time distributed collaborative spatial decision making," *Journal of Geographic Information and Decision Analysis*, vol. 1, pp. 1–8, 1997.

- [17] P. Waddell, "UrbanSim: Modeling urban development for land use, transportation, and environmental planning," *Journal of the American Planning Association*, vol. 68, pp. 297-314, 2002.
- [18] J. Burian, "GIS analytical tools for planning and management of urban processes," in *GIS Ostrava 2008*, Ostrava, 2008, p. 13.
- [19] M. H. Carr and P. D. Zwick, *Smart land-use analysis: the lucis model land-use conflict identification strategy*: ESRI, Inc., 2007.
- [20] J. Burian, J. Brus, V. Pechanec, V. Vozenilek, and S. Stastny, "Urban Planner – model for optimal land use scenario modelling," *Geografie - sborník České geografické společnosti*, (to be published), 2015.
- [21] T. L. Saaty, "Priority setting in complex problems," in *Essays and Surveys on Multiple Criteria Decision Making*, P. Hansen, Ed., ed Berlin/Heidelberg/New York: Springer, 1983, pp. 326-336.
- [22] J. Jenness, "Repeating shapes for ArcGIS," ed: Jenness Enterprises, 2012.

Safety of Critical Facilities

DANA PROCHAZKOVA

Department of Security Technologies and Engineering

Czech Technical University in Prague

Konviktska 20, 110 00 Praha 1

CZECH REPUBLIC

prochazkova@fd.cvut.cz <http://www.cvut.cz>

Abstract: - The work deals with critical facilities integral safety. On the basis of principles of strategic safety management in dynamically variable world it gives historical development of work with risks in engineering disciplines and present model of management and trade-off with risks used in critical facilities. It characterizes present process model of critical facility safety management, its processes and programme for critical facility safety upgrading in a context of integral safety directed to existence, security and development of humans.

Key-Words: - Critical facility; risk; safety; safety management model; safety culture.

1 Introduction

The main goal of all human effort is ensuring the human life, i.e. all human needs, interests, and wishes. Human needs, interests and wishes are fulfilled by intangible and material goods that have a utility value. Unfortunately, in the world it is not just a human society, but also other systems, which are not subordinated to the human society. Therefore, conflicts originate: man vs. the environment; technology vs. the environment; man vs. technology; man vs. man, etc. Because the human kind is based on its education, as well as in the present case, it must realize that, in a given situation it must be based on knowledge, which accumulated science and historical experience of life, which shows that there is a limit for the activities of the people, which cannot be exceeded, in order to prevent the destruction of mankind.

The starting point is to accept the need for the co-existence of several systems and search conditions and ways of controlling it. The sustainable development strategy is comparable with other systems of values, which do not have the final form (e.g. the system of human rights and freedoms). It leads to ensure the highest attainable quality of life for the present generation and to create conditions for quality of life of future generations, even knowing that the ideas of the quality of life of future generations can be compared to our different. The man knew during his development, for your life and development needs the nature and a number of other assets. He understood that the most valuable asset is its existence, security and development potential, and that the safe world is disturbed by harmful phenomena (disasters). From the

evaluation of credible data, knowledge and experience, e.g. [1], it follows that the human knowledge and abilities are: small to avert disasters, which are the manifestation of the evolution of the planetary system of the Earth; adequate to mitigate the impact of disasters, which are the manifestation of the evolution of the planetary system of the Earth; and sufficient to prevent disasters that are associated with the activities of humans and with the development of human society.

To use the knowledge and skills the humans consciously create a comprehensive system tool, which is called the *safety management* and also specific targeted tools to deal with emergency and critical situations, which are emergency management and crisis management; in the professional literature can be found, as well as other tools such as disaster management [2]. For qualified management of entities, according to the present knowledge and experience is considered a strategic safety management of entities in the dynamically varying world, which means the skilled management of disasters [2], which is based on the approach of "All Hazard Approach" that was introduced by FEMA in 1996 [3] and it is used by EU and OCHA [1,2]. Having regard to the complexity, many disciplinary and the interdisciplinary nature of the solved problems, understanding of the situation and find solutions for the humans' security and development, the critical installations safety is based on the systems approach, a comprehensive concept of safety and proactive way of safety management, because the environ / space is dyna-

mic, i.e. it is variable in the space and time in particulars and as well as in a whole [1, 4].

On the basis of current knowledge the reasonable human negotiates with the risks so that systematically carries out preventive, mitigating, reactive, and recovery measures and activities in order to avert unacceptable impacts that affect and cause the losses to both, the humans and the public assets that they need to their life. Because of their knowledge, capabilities and possibilities are limited in the subject area, so on the basis of the experience they constantly prepare to cope with the situations, which are caused by an occurrence of a variety of phenomena, with harmful impacts on them and on the vital assets.

The aim of human effort is to construct the technical works that fulfil the prescribed function after specified time period and do not threaten human health and the environment, i.e. are safe. In order to ensure the safety of the technical works they are created since the beginning of the cultural evolution of the human species the legislation, technical standards and norms. There are processed procedures of good practice in cases in which there is not enough data for the standard or norm. At each stage of the development, the legal rules (directives, regulations) of a different legal force reflect the level of knowledge and experience of the company. Norms and standards for the current period reflect the knowledge level at the time of the present.

2 The Development of Management and Trade-off with the Risks

The basis of human effort in creating a safe space is to handle the (tame) risks. The term "*risk*" has its origin in the Middle Ages and our present knowledge about trade-off with the risks has been systematically collected since the 1930s. The acquired knowledge and experiences have been gradually applied in risk management and designated measures and activities have been introduced gradually into the practice by engineering disciplines [5, 6]. In the present work with the risk, the risk is seen as the potential that a given action or activity (including the option of doing nothing) originates loss (the undesirable outcome). In today's practice, it uses the five concepts of risk management and risk engineering, i.e.: a classic risk-management and risk engineering; the classic risk management and risk engineering involving the human factor; management and engineering focused on security (security management and security engineering); management and engineering

focused on safety, i.e. such control and trade-off with risks, that ensure both, the secure system and its safe surroundings; and management and engineering focused on the safety of system of systems (SoS) [5, 6], Figure 1. It is obvious that the more advanced the concept of the use, the higher are the demands on the knowledge, the tools, time,

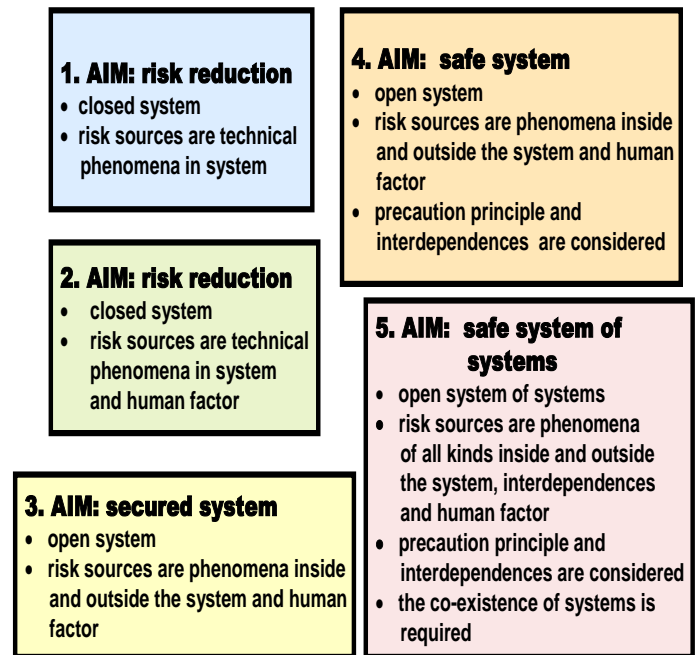


Fig.1 Concepts of management and engineering trade-off with risks and their goals, arranged in chronological order according to the time of their introduction to engineering practice

For each concept, management and engineering was developed by a certain set of standards and norms for its use in practice, [6], which amends and supplements in conjunction with the development of knowledge. Due to different assumptions of concepts the results of their application in practice are not the same. Because the reality that the higher the concept of risk management and risk trade-off is used, the greater the demands are on the resources, forces and means, it is necessary to choose the concept according to the targets in the field of safety [7]. The basis is the awareness of the targets of the work with the risks, i.e. whether the object comprehended as a system to be a secure system or a safe system. Since the accident, the Three Mile Islands in the critical field it is used the target "safe object". Basic terms from safety domain specified for the critical facilities are listed in [1, 2]. On their basis in accordance with the concepts of the UN [8], the OECD [9,10], and the EU [11] it holds: *secured critical facility* is a system that is protected against all disasters, the

sources of which are inside and outside the system, including the human factor; and *safe critical facility* is a system that is protected against all disasters, the sources of which are inside and outside the system and it does not affect their surroundings in its normal, abnormal and critical conditions.

3 Management of Safety of Critical Facilities

The safety is a set of anthropogenic measures and activities, which lead to ensure security and development. Since the world is dynamically changing, so the management of the safety of critical installations is focused on priorities. In the first place, it means the application to access All Hazard Approach [3], determining the hazards posed by individual disasters, and according to the assessment of the size of the threat from real disasters and vulnerabilities of a site and of critical installations against real disaster the separation of disasters into the following groups: the disasters, which cannot have impacts on critical facility; disasters that have only an acceptable impacts on critical facility, for which we use the designation “relevant disaster”; disasters that have on a critical facility only impacts that are manageable at performance of the prepared prevention and mitigation measures, for which we use the designation “specific disaster”; and disasters that have an unacceptable impacts on the critical facility and, therefore, it is necessary to carry out essential preventive measures in the field of technical, organizational, legal and educational and it is necessary to have the possibility to activate all of the resources and the means to cope with their impact and jump-start further development, for which we use the designation “critical disaster”. The disasters have the potential to cause extreme emergency situations and for their defeat it is necessary to use the tools for crisis management.

Problem areas in safety management according to [1, 12] are in 14 different sectors, the list of which is in [1, 12]. The strategy for ensuring the security and sustainable development of the critical facility consists in: the application of the system and pro-active management, which relies on the knowledge and experience obtained for the critical facility from qualified data; a qualified trade-off with the risks in a benefit of security and sustainable development of critical facility; settlement of risks by help of prevention, mitigation, insurance, reserves, preparedness for response and recovery, and compilation of a plan for trade-off with unforeseen situations (with

contingency plan); the application of the correct procedure, in which the interconnected safety management, emergency management and crisis management; building a program to increase the safety in critical facility and in its surroundings; the determination of the assessment the safety rate in sense of effectiveness of the secured system (indicators); the fulfilment of the program by linked interconnected projects + fulfilment projects by linked interconnected processes; directly specified allocation of tasks and responsibilities to all concerned; and the implementation of the relevant activities and measures, that is associated with a qualified and consistent monitoring.

The basic principle is qualified interconnection of technical, organizational, financial, personal, social, knowledge domains; and clear roles and responsibilities of all those involved. The safety management system of critical facility, therefore, covers a number of areas, i.e. technical, military, legislative, financial, economic, social, ecological, educational, research, etc. In the field of safety, in terms of current knowledge and current concepts of sophisticated security systems, the tasks have all participants. The tasks of each participating and their interconnection in various situations are prescribed by the laws, moral and other standards and norms.

In the framework of the strategy for ensuring the security and sustainable development [1] it must be in a critical facility set up: a program for increase the safety of critical installation; rates for the assessment of the level of safety in terms of the efficiency of the security system (indicators); a program to ensure the safety that is filled by interlaced projects; and projects filled with interlaced processes.

The critical facility management tools that ensure the security and the development of a critical facility, i.e. in other words, the conservation and protection and development of the protected assets [1] are: coherent management system involving the management of strategic, tactical and operational, which is based on the qualified data, expert assessments and good methods of deciding; education and training of employees; science, research, and TSO (the professional organization to ensure professional support to the operator of a critical installation and to public administration); specific education to technical and management personnel; technical, medical, environmental, social, cyber and other standards, norms and regulations, i.e. the tools for the control of processes, which can or could lead to the occurrence of (the origination of) a disaster, or to

amplify its impacts; the inspection; a system of cooperation with the public administration, with organizations in the territory and with organizations that use similar technology; units for defeat of emergency situations; components and systems to cope with critical situations (i.e. after all ways ensured continuity management and crisis management); and security, emergency and crisis planning.

That procedure was correct, it is necessary to use the tools competently, i.e.: use the documents obtained on the basis of the qualified data that meet the requirements for representative data files (completeness, valuation and settlement of random uncertainties, settlement of vagueness (epistemic uncertainties) in the data using a specific mathematical approaches) and apply correct methods of decision-making, which are adequate to the problem, which will be decided. **The uncertainty** is related to the scattering of observation and measurements. It can be incorporated into the assessment and prediction using the apparatus of mathematical statistics. **The vagueness (epistemic uncertainty)** is associated with both the lack of knowledge and information, as well as with the natural variability of the processes and events that trigger disasters. **For processing and consideration, the epistemic uncertainty is the device of mathematical statistics insufficient and it is necessary to use a different, more modern mathematical apparatus that provide such as the theory of extreme values, the theory of fuzzy sets, theory of fractals, theory of dynamic chaos, the selected expert methods and suitable heuristics.** Data on epistemic uncertainty follows from the fact that the data are incomplete, non-homogeneous (i.e., their accuracy depends on their size, or on the time of the occurrence) and unsteady. They have considerable variance and are loaded with random and sometimes systematic errors, the distribution functions of which are usually not possible to determine. This means that for: strategic management of the organization that is focused on safety management, it is necessary to **use the verified data files, proven methods for data processing and proven methods for decision making**; medium-term management of the organization, which is aimed at readiness a routed to cope with the problems associated with emergency situations (natural disasters, accidents, etc.) in a critical facility, it is possible to use **less accurate data, data processing method and methods of decision-making** (less accurate process models, software, estimates, etc.), since each emergency situation is unique due to the variable

conditions of its formation and changes in the availability of resources, the forces and capabilities of the organization on the reaction ; and operational management, which decides in the time constraints and at the lack of data (response), it should be **on the basis of acquired knowledge and experience to use targeted learned and trained procedures** (e.g. processed in the form of case studies), because rapid response is desirable.

On the basis of current knowledge summarized in the works [1,4-6] it should be noted that each of the targeted management (goal is security and development or intermediate objectives such as competitiveness or just survival) must be based on high-quality work with risks, Figure 2; qualified cope with risks at the current level is described in work [5].

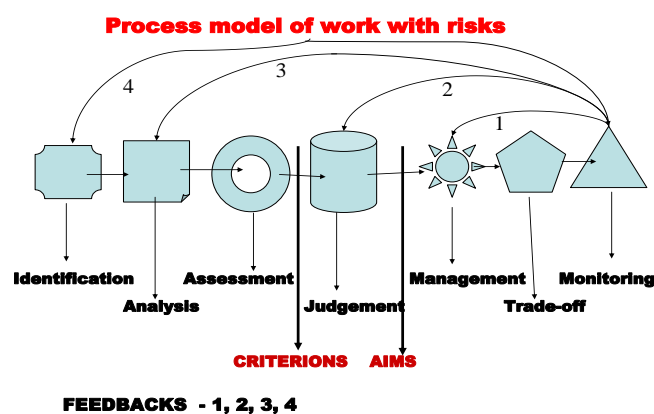


Fig. 2 Basic procedural model showing the work with the risks.

Criteria are conditions which determine when the risk is acceptable, conditionally acceptable or unacceptable. The objectives are the formulations, that denoted: the limit to which we want to reduce the risk; rate of security of a system; or rate of security of a system and its surroundings. Arrows (1, 2, 3 and 4) indicate the feedbacks, which are applied when the risk is unacceptable

From Figure 2 it is obvious, a major role of monitoring. In the event that it is established that the risk is unacceptable, it is necessary to make changes, as indicated on the feedback on Figure 2. Because the changes require resources, forces and means, so on the basis of ensuring the cost-effectiveness firstly it implements feedback 1, and only when it is not desirable, it realizes the feedback 2; after the feedback 3, and when, even after it is not a desirable outcome, so feedback 4. In the case of the occurrence of extreme phenomena with disastrous impacts it is immediately implemented the feedback 4.

The safety and risk together in some way related (in more detail in [1, 4-6] and in the works that are cited in them), it's not about complementary

phenomena. On the basis of current knowledge, summarized in the works [1, 4-6,13], the safety management system (the so-called SMS) of a critical facility is based on the process management and it includes the organizational structure, responsibilities, practices, rules, procedures, and resources for determining and implementing the prevention of disasters, or at least mitigating their unacceptable impact in the territory. Usually refers to a number of questions, inter alia, the organization, workers, the identification and assessment of hazards and risks resulting from them, the management of the organization, the management of changes in the organization, emergency and crisis planning, monitoring the safety, audits and reviews [1, 13]. On the basis of the cited works, the SMS of critical facility consists of processes: 1. Process of concept and management, which is further divided into sub-processes, which ensure: the overall concept; partial safety objectives; leadership / management of safety; the safety management system; the staff, which is further divided into sections: human resources management, training and education, internal communication / awareness, working environment; and review and evaluation of the implementation of the objectives in the safety. 2. Process of administrative procedures, which are further divided into sub-processes, which ensures: identification of hazards from potential disasters and risk assessment; documentation; procedures (including work permits); the changes; safety in conjunction with the contractors; and supervision under safety of products. 3. Process of technical issues, which are further divided into sub-processes, which ensures: research and development; design and assembling; inherently safer technical and technological processes; industry standards; storage of dangerous substances; maintenance of the integrity and maintenance of equipment and buildings. 4. Process for external cooperation, which is further divided into sub-processes, which ensures: cooperation with the administrative authorities; cooperation with the public and other stakeholders (including academic institutions); and cooperation with other enterprises. 5. Process of the emergency preparedness and response, which is further divided into sub-processes, which ensures: planning of internal (on-site) preparedness; facilitating the planning of external (off-site) preparedness (to which the public administration corresponds); the coordination of the activities of the departmental organizations at emergency preparedness and response. 6. Process of reporting and investigation of accidents / accidents almost, which is further

divided into sub-processes, which ensures: reports on accidents, incidents, near-misses and other lessons learned; investigation of near-misses, incidents and accidents; and responses and follow-up after the incidents and accidents, including the application of lessons learned and information sharing. Processes must be coordinated so that they are targeted to the objectives set, i.e. the safe operation of critical facilities.

On the basis of analyses of the existing safety management systems, which are described in the professional literature, for which the data are summarized in the works [1,4-6,13], and in particular the knowledge collected by the OECD [9, 10, 14, 15] the author compiled by the method of analogy to existing safety management models the general process safety management system of real entity and she verified it on the data collected in the archive [16], and by the method of analogy she has transferred to critical facility, Figure 3.

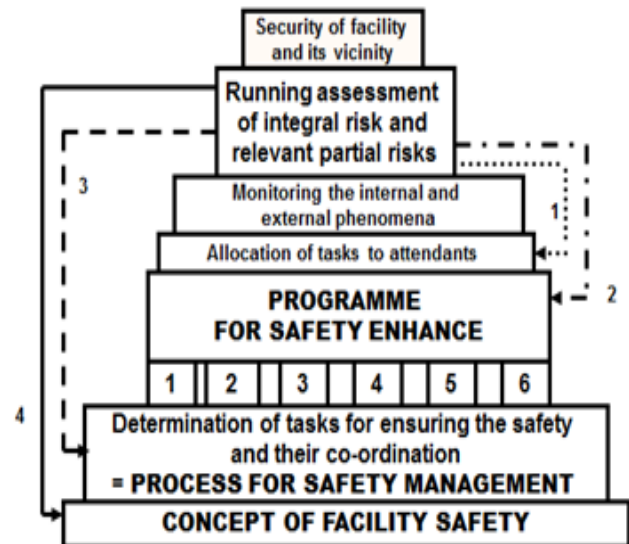


Fig. 3 Process safety management model of a critical facility. Black block specifications the essential processes of the entity; the dotted line — feedback 1, dash-dot line — feedback 2 dashed line-feedback 3, full line — feedback 4

In Figure 3 it is evident basic role of concept of facility safety. It specifies the essential processes of a critical facility, that predispose a safe critical facility, i.e. its existence, safe operation and development. Then there follow the sequential steps aimed at the security and development of the entity. As the entity and its environment dynamically develops it considers with corrections and changes. In case of the need for corrective measures there are indicated the basic feedbacks, by which it is corrected the set of measures and activities; the dotted line — feedback 1, dash-dot line — feedback 2 dashed line-feedback 3, full line —

feedback 3. Because the changes require resources, forces and means, on the basis of ensuring the cost-effectiveness, there is realized in the first the feedback 1, and only when not desirable, it realizes the feedback 2; after the feedback 3, and when, even after it is not a desirable outcome, so feedback 4. In the case of the occurrence of extreme phenomena with disastrous impacts, it is immediately implemented the feedback 4.

The safety management system (SMS) of a critical installation is based on the concept of prevention of disasters, or at least their serious effects [1, 9, 10], which includes the obligation to establish and maintain a management system in which they are taken into account the following issues: roles and responsibilities of persons participating in important hazards management on all organising levels and in ensuring the training; plans for systematic identification of important hazards and risks connected with them that are connected with normal, abnormal and critical conditions, and for assessment of their occurrence probability and severity; plans and procedures for ensuring the safety of all components and functions, namely including the object and facilities maintenance; plans for implementation of changes in territory, objects and facilities; plans for identification of foreseeable emergency situations by systematic analysis including preparation, tests and judgement of emergency plans for response to such emergency situations; plans for continuous evaluation of harmony with targets given in safety concept and in the SMS, and mechanisms for examination and performance of corrective activities in case of failure with aim to reach determined targets; and plans for periodic systematic assessment of safety concept, effectiveness and convenience of the SMS and of criteria for judgement of safety level by top workers group.

The safety of critical facility is a matter for all stakeholders, i.e. the executives, employees, even persons accidentally present. In this context, talking about **the so-called golden rules of all participating** [1, 9, 13], which are: according to their possibilities by application of preventive measures to avert disasters and or at least their unacceptable impacts, to ensure preparedness for capability to defeat the unacceptable impacts on protected assets (the interests) of a critical facility and effective response of the critical facility; to communicate and to cooperate with others interested in all aspects of prevention, preparedness and response of critical facilities; know the hazard from disasters and possible risks in critical facility and in its surroundings; to implement and respect the safety culture,

which is respected and enforced by all stakeholders in all circumstances; to establish the safety management systems, to monitor and if necessary to correct their activities; to use the principles of inherent safety at project, the design and operation of objects and their equipment; carefully drive the changes in critical facilities; be ready to cope with all the disasters that may occur; help others interested at fulfilment of their roles and responsibilities; carry out continuous improvement of safety; to work in conformity with the safety culture, safe practices, and training; to strive constantly for all awareness and provide information, and to provide feedback to managers; to strive for the development, strengthening and constant improvement of the concept of safety, regulations and directives; lead and motivate all other stakeholders in order to fulfil their roles and responsibilities; know the risks within their own sphere of responsibility, appurtenant to plan measures for its proper management; the use of appropriate and coherent policy of planning and follow-up activities; be aware of the risks in critical facility and to know what to do in case of their realization; and to participate in emergency planning and response.

Safety culture means that the man in all his roles (executive, employee, citizen or victim of the disaster) observes the principles of safety, i.e. he behaves so that alone prevented the realization of the potential risks and when it becomes a participant in the realization of the risks, to contribute to an effective response, stabilization of the protected assets (interests) and their recovery and to kick off their further development. An effective safety culture is an essential element of safety. It reflects the concept of safety and is based on the values, opinions and discussions of key management personnel of the organization, and their communication with all stakeholders. It is a clear commitment to actively participate in addressing issues of safety and advocates that all participants did so safely and to comply with the relevant legislation, standards and norms. Rules of safety culture must be incorporated into all activities in a critical facility. Their basis is not the concentration on the punishment of the offenders / originators of errors, but the lessons learned from the mistakes and the introduction of such remedial measures, in order to not repeat mistakes or at least significantly reduced the frequency of their occurrence.

4 Conclusion

Analysis of the current situation shows that we can systematically handle a range of undesirable processes, i.e. defects and failures that we can detect in advance. Sometimes, however, there is a mutual interlocking a series of seemingly unrelated factors, and as a result of non-linearity in the system there are originated very atypical accidents. Analysis of accidents: breaking plateau Alpha in 1988 in the North Sea; the warehouse of aviation kerosene crashes in Buncefield 11. 12.2005; maritime, railway and unexplained air crash in recent years; the accident at the Fuku-shima is 11. 3.2011 (note – it did not respected calculated scenarios of accidents), showed that the number of experts is affected by the operational requirements of the blindness and after fulfilment of the norms and standards to see the remaining risks, or the risks associated with different bindings and couplings with the surroundings. For example, a simple comparison of intervals used in probabilistic assessments shows that: the interval ($\mu - \sigma$, $\mu + \sigma$) covers 68.5% of cases; the interval ($\mu - 2\sigma$, $\mu + 2\sigma$) covers the 85.4% of cases; and the interval ($\mu - 3\sigma$, $\mu + 3\sigma$) covers 99.8% of cases [4].

Therefore, we permit that complex systems to which surely include critical facilities, are for various reasons from time to time in an unstable state and they are formed an organizational accidents, cascade of failures without apparent cause, i.e. we recognize the random and epistemic (knowledge) uncertainties in their behaviour. For the protection reasons we are looking for a solution of response for cases that cannot be revealed by the probabilistic approaches and we build for them, alternative sources of water and energy, specific response systems and specific training of rescuers.

To achieve the desired level of safety it is necessary well manage and properly decide. Good management and good decision making is possible only when we have good data, and we can take advantage of the tools that we have available. The data: must be correct, i.e. it is known their size and accuracy; must have explanatory power for the problem, i.e. they must be validated. The data files must be representative, i.e.: complete; contain the correct data; have a sufficient number of data; the data must be spread homogeneously throughout the reference period and must be validated. In the application of models must be properly considered random and epistemic uncertainties in the data.

It should be noted that in the real world we work at ensuring the safety of critical facilities non-trivial problems, i.e.: there is more protected assets, the objectives of which are conflicting; assets varies in

time and space; and the environ in which the assets are, i.e. the human system, is in dynamic development.

References:

- [1] D. Procházková, *Strategické řízení bezpečnosti území a organizace*. ISBN: 978-80-01-04844-3. Praha: ČVUT 2011, 483p.
- [2] D. Prochazkova, *Study of Disasters and Disaster Management. ČVUT study in frame of FOCUS project*. ISBN: 978-80-01-05246-4. Praha: ČVUT 2013, 207p.
- [3] FEMA, *Guide for All-Hazard Emergency Operations Planning*. State and Local Guide (SLG) 101. FEMA, Washinton 1996.
- [4] D. Procházková, *Principy řízení bezpečnosti kritické infrastruktury*. ISBN: 978-80-01-05245-7. Praha: ČVUT 2013, 225p.
- [5] D. Procházková, *Analýza a řízení rizik*. ISBN: 978-80-01-04841-2. Praha: ČVUT 2011, 405p.
- [6] D. Procházková, *Bezpečnost kritické infrastruktury*. ISBN: 978-80-01-05103-0. Praha: ČVUT 2012, 318p.
- [7] D. Prochazkova, *Validity of Use of Various Concepts of Risk Management and Risk Engineering in Practice*. International Journal of Computer and Information Technology, ISSN: 2279 – 0764, 3 (2014), No 1, pp 21-30.
- [8] UN, *Human Development Report*. New York: UN 1994, www.un.org.
- [9] OECD, *Guidance on Safety Performance Indicators. Guidance for Industry, Public Authorities and Communities for developing SPI Programmes related to Chemical Accident Prevention, Preparedness and Response*. Paris: OECD 2002, 191p.
- [10] OECD, *Guiding Principles on Chemical Accident Prevention, Preparedness and Response*. Paris: OECD 2003, 192p.
- [11] EU, *The Safe Community Concept*. Brussels: EU, 2004, PASR project.
- [12] D. Prochazkova, *Methodology for Estimation of Costs for Renovation of Property in Territories Affected by Natural and Other Disasters*. SPBI SPEKTRUM XI Ostrava 2007, ISBN 978-80-86634-98-2, 251p.
- [13] D. Procházková, *Ochrana osob a majetku*. ISBN: 978-80-01-04843-6. Praha: ČVUT, Praha 2011, 301p.
- [14] OECD, *Environmental Indicators: Overview of Work Programme and Publications*. Group on the State of the Environment. Paris: OECD 1993.
- [15] OECD, *Indicators to measure decoupling of environmental pressure from economic growth*. OECD SG/SD(2002)1/FINAL, 16. 5. 2002.
- [16] D. Procházková, *Archiv vyřešených úloh z oblasti řízení bezpečnosti a krizového řízení*.

Flash flood on July 21, 2014 in the Vratna Valley

P. Pekarova, V. Bacova Mitkova, P. Miklanek

Abstract— A catastrophic flood on July 21, 2014 in the Vratna Valley in the Mala Fatra National Park on the stream of Varinka, and in Terchova village reminded us once again the power of water flow. Since the floods on July 20, 1998 on Mala Svinka stream, there occurred several flash floods in Slovakia, and there are suggestions that their number is growing. Answer to the question, whether the current floodings in our area actually occur more frequently than in the past, has been focused for several years at our institute. By studying historical materials, we came to the conclusion that in the past there also occurred devastating floods in our territory, which had disastrous consequences for the population. For example, in August 2013, 200 years passed since the most destructive floods, which in August 1813 affected the whole Slovakia, northern Moravia, and southern Poland. Neither the 2010 flood withstood the flood of 1813. Economic development in Slovakia after 1813 was slowed for decades.

Keywords — flash flood, Vratna Valley, Slovakia

I. INTRODUCTION

FFLASH floods are defined as strong flows occurring shortly after rainfall [1]. It may be caused by relatively high rain intensity and an intensive watershed response to rainfall. The factors that affect flash flood generation are very complex and mainly include characteristics of the rain (intensity, amount, and time-space distribution), physical and hydrological characteristics of the watershed (area, slopes, shapes, type of soil and land use, vegetation and others) [2]. The type, magnitude and intensity of the hydro-geomorphic response may affect hazard and risk in the downstream channel system and floodplains ([3] and [4]). The sensitivities of runoff generation to rainfall variability and initial wetness conditions were examined for a major flash flood event by Nikolopoulos [5]. Similar problems had been investigated by several authors ([6], [7], [8] and [9]). The hydrogeomorphic response to

extreme rainfall in headwater systems was published in [10]. For example in the last years Smith [11] applied data-based mechanistic (DBM) models to forecast flash floods in a small Alpine catchment. Kjeldsen [12] tested the effect of urban land cover on catchment flood response using a lumped rainfall–runoff model, and compared flood events from selected UK catchments with mixed urban and rural land use.

The occurrence of these extreme events of natural hazards entails acute danger not only for properties but mainly for human lives. Jonkman [13] focused on 13 flood events that happened in Europe and the US in order to improve understanding the circumstances of flood deaths and contribute to prevention strategies. Other studies have also focused on defining and understanding circumstances surrounding flood fatalities for different environments such as Australia [14] and Puerto Rico [15].

The paper is aimed at the description of the catastrophic flood event which occurred on July 21, 2014 in the Vratna Valley in the Mala Fatra National Park (Slovakia) on the stream of Varinka, and in Terchova village. Due to this flood we had done some field measurements on the stream of Varinka in the Vratna Valley on July 29, 2014 and July 30, 2014. These measurements were focused on documenting of the flood development and on measuring of the flood culmination. Subsequently, the measured results were preliminary evaluated.

II. THE FLOOD AREA: MALA FATRA NATIONAL PARK

A. The Mala Fatra National Park

The Mala Fatra National Park (in Slovak: Národný park Malá Fatra) is a national park in the northwest part of the Mala Fatra mountains called Krivanska Mala Fatra. The mountain is covered mainly with mixed beech forests, at higher elevations with fir and spruce. Pine woods and meadows occur at higher altitudes. About 83% of the area is covered by forest. It has an area of 226.3 km² (87.37 mi²) and a 232.62 km² (89.81 mi²) buffer zone. The park was declared in 1988. Between 1967 and 1988 it was a protected landscape area (Fig. 1). The highest peak is the Velky Krivan with altitude of 1709 m. An significant hill is the Velky Rozsutec, which is also the logo of the National Park. Gorges, rocky peaks and an attractive ridge tour are among its attractions too.

This work was supported by the VEGA project under the contract No. 2/0009/15 and it results from the project implementation of the “Centre of excellence for integrated flood protection of land” (ITMS 26240120004) supported by the Research & Development Operational Programme funded by the ERDF.

P. Pekarova is with Institute of Hydrology Slovak Academy of Sciences, Racianska 75, 831 02 Bratislava, Slovakia, (e-mail: pekarova@uh.savba.sk).

V. Bacova Mitkova is with Institute of Hydrology Slovak Academy of Sciences, Racianska 75, 831 02 Bratislava, Slovakia, (e-mail: mitkova@uh.savba.sk).

P. Miklanek is with Institute of Hydrology Slovak Academy of Sciences, Racianska 75, 831 02 Bratislava, Slovakia, (phone: +4212 44259311, Fax: +4212 44259311, e-mail: miklanek@uh.savba.sk).



Fig. 1 The location of the Mala Fatra National Park in Slovakia

B. Some flash flood recorded in the Mala Fatra

The records about historical floods in many towns and villages in Slovakia we can find in some scientific literatures and chronicles. When we go more into the past, the information about floods are rarer and less precise. Let us remember, some of them which occurred in the National Park Mala Fatra.

The publication of Dub [16] describes a catastrophic flood on Vydňanka (tributary of the Biela stream from flysch belt of Javorníky, the catchment area of the central Váh River), and says: “rain was so heavy that it was not seen in ten steps and valley side were all covered with water, which flowed into the river, the effect was devastating. The only longitudinal road was completely destroyed, houses were damaged, shattered and washed away. The coarse river load clogged the original stream bed up to 1-1.5 m, so that the water can create a new bed” This catastrophic flood occurred on June 17, 1939 and culmination of this flood was estimated around the value of $100 \text{ m}^3 \text{ s}^{-1}$ and specific yield around value of $10 \text{ m}^3 \text{ s}^{-1} \text{ km}^{-2}$.

It showed again, that intensive rainfall in a small catchment of flysch belt can cause catastrophic runoff from catchment. The retention capacity of the vegetation cover together with a capacity of shallow soil profile is unable to retain or effectively mitigated the runoff.

Some of significant historical flash floods which occurred in the National Park Mala Fatra were on Lubochnianka stream on May 28, 1925 or on June 25, 1893. Floods destroyed roads, railway and bridges in Lubochnianska Valley and in village Stara Bystrica. According to SHMI archive records the rainfall depth reached value of 193 mm (June 17, 1925) in village Stara Bystrica. Extreme flood occurred in 1958 in the Vratna Valley ([17] and [18]).

And finally, the most interesting and most valuable information about the catastrophic flash flood of 1848 originates from village Terchova on the Varinka / Vratnanka stream. The information was sculpted into the rock in the valley Tiesnavy in year 1948. This mark inform that on June 11, 1848 in village Stefanova died 14 people during the flood

on Varinka stream and shows water level of the flood.

III. VARINKA STREAM

Varinka stream (ID stream 4-21-05-6465) is created from several brooks in the Vratna Valley and Biely Potok (White Brook), near to the community of Terchova. The Varinka stream is the area of European importance. The basin covers an area of 167.307 km^2 and stream length is 24.46 km. The Varinka originates from Krivanska Fatra, the Mala Fatra subunit. Source of the Varinka is located on the northern slope of the mountain section of the ridge between the peaks Chleb (1647 m.a.s.l.) and Hromové (1636 m.a.s.l.). The Varinka stream flows on bottom of the Vratna Valley and flows into the Váh River in Varin village. The Stohovy stream (ID stream: 4-21-05-6748, area is 10.671 km^2 , length is 5.30 km) is one of the tributaries of the Varinka stream. The next tributaries of the Varinka are Biely Potok (ID stream: 4-21-05-6715, area is 17.162 km^2), Struharen stream and Beliansky stream (Fig. 2).

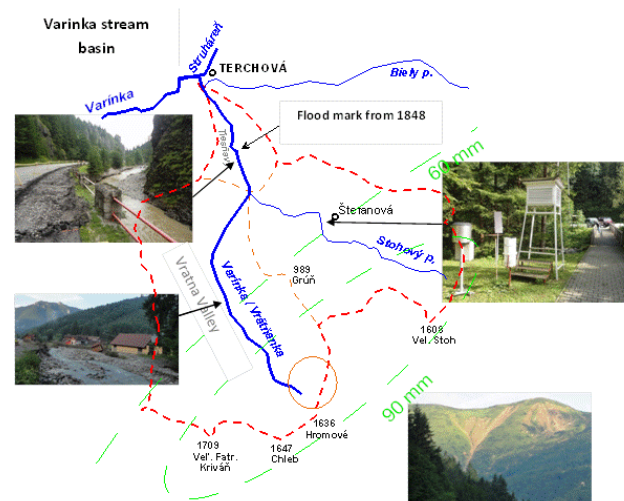


Fig. 2 The basin of Varinka and Stohovy streams in the Vratna Valley to Terchova. Rainfall depth between 4 p.m. – 5 p.m. during the flood on July 21, 2014.

IV. FLOOD ON JULY 21, 2014 ON THE VARINKA STREAM

In contrast to the regional floods from year 2010, which were caused by a several days of heavy rain on the large area, floods of July 21, 2014 had the character of flash floods. These flash floods were created as result of heavy rainfall on July 20, 2014 and July 21, 2014. For example, meteorological station in Vratna village recorded 130 mm of precipitation during two days (Fig. 3a). The rainfalls on July 21, 2014 were characterized by extreme intensity and extreme rainfall totals depth for a very short time (Fig. 3b). Assessment of the meteorological situation in this northwest area of Slovakia was described in [19]. According to data from the Slovak Hydrometeorological Institute (SHMI) from July 21, 2014 the maximum hourly total rainfall depth in the afternoon reached value of 37 mm at the station Vratna Valley (near the mountain rescue cottage), value of 46 mm in village Lubochna and value of 48 mm in town Zilina. Extreme precipitation reached value

of 50 mm per 45 minutes and was recorded near village Stefanova. These rainfall depths are above the average even if dropped during 24 hours. In calculating the average rainfall for the basin Varinka to Terchova, we additionally take into account the high altitudes in the catchment area and the fact that due to rising-altitudes the rainfall totals generally grow (an average of 5 to 10% of the 100 meters with above-sea level). SHMI rain gauge station is located in the valley below Stefanova at altitude below 632 m. On the windward side of the mountain Hromove in altitude of 1450 m rainfall might reach 100 mm during one hour (Fig. 3).

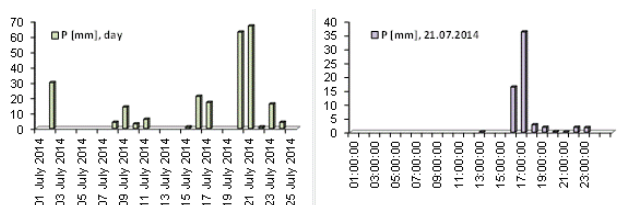


Fig. 3 a - left) Daily rainfall depths in the Vratna Valley station on July 2014.

b - right) Hourly rain-fall depths in the Vratna Valley station on July 21, 2014 (Central European Summer Time).

Such rainfall total depth added the flood in 2014 on Varinka stream to the floods which occurred on July 7, 2011 in the Male Karpaty mountains in village Pila on the Gidra stream and on the Parna stream above the water reservoir Horne Oresany. There we estimated rainfall depth around 95 mm for 3.5 hours. Higher daily rainfall total depths were recorded in the past in Slovakia, e.g.: on June 7, 1873 in Trencin - 267 mm, on July 12, 1957 in Salka - 231 mm, on July 16, 1934 in Zuberec, Zverovka - 220 mm, on June 17, 1929 in Stara Bystrica - 193 mm, on August 14, 1944 in Mutne - 190 mm, on June 29, 1958 on Skalnaté Pleso - 170 mm.

A. Measuring of the culmination flow of the flood on 21.07.2014

All small mountain basins where occur extreme floods cannot be provided with measuring technique. Therefore staff of the Slovak Hydrometeorological Institute (SHMI) performed the hydrological exploration in the basin and measured river profiles after each major flood to estimate the culmination. One of the hydrological problems solved at Institute of Hydrology Slovak Academy of Sciences (IH SAS), are flash floods that occur on basins with the area of 25-35 km². For example we present here some extreme flash floods in Pila on Gidra stream (southwest Slovakia) and Mala Svinka stream in Jarovnice (east Slovakia). These floods were analyzed and evaluated by IH SAS. A flood event on June 7, 2011 on Gidra stream was caused by 3.5-hours rainfall (95 mm) and the specific yield reached value of 1.36 m³s⁻¹km⁻² and maximum discharge reached value of 44 m³s⁻¹. A flood event on July 20, 1998 on Gidra stream was caused by 1.5-hours rainfall (80 mm) and the specific flow reached value of 5.19 m³s⁻¹km⁻² and maximum discharge reached value of 178 m³s⁻¹ (SHMI measured 230 m³s⁻¹). Results show that the most

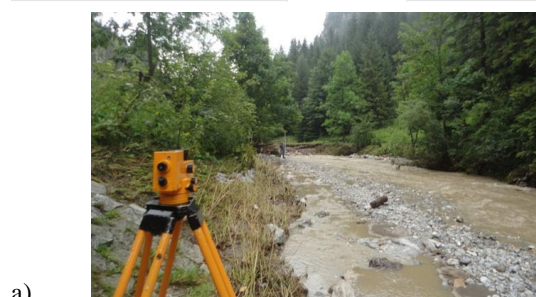
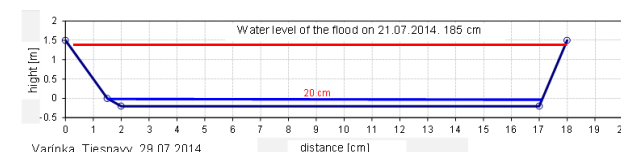
extreme flood was on Mala Svinka ([20] and [21]).

During the experimental measurements on July 29 and July 30, 2014 we were measuring characteristics of stream needed to the calculate culmination discharges at three profiles:

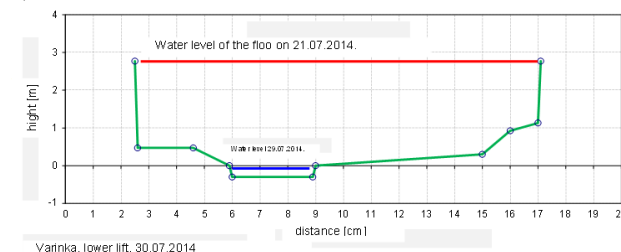
- a) on the Varinka stream in valley Tiesnavy (Fig. 4a);
- b) on the Vrinka stream at lower lift station (Fig. 4b);
- c) on the Stohovy stream near the mountain rescue cottage in Stefanova (Fig. 4c).

According to our measurements after the flash flood on Varinka in the Vratna Valley the peak discharge reached at least value of 56 m³s⁻¹ and specific flow reached value of 2 m³s⁻¹km⁻² (on the Varinka stream in valley Tiesnavy, catchment area is 28.05 km²).

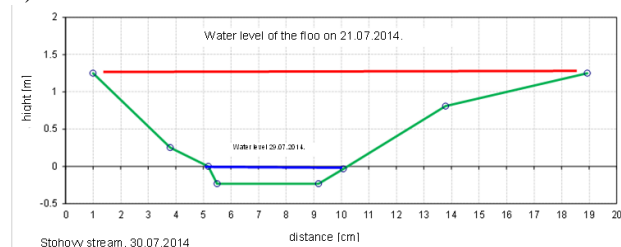
Peak discharge reached value of 57 m³s⁻¹ and specific yield reached value of 4.4 m³s⁻¹km⁻² (with respect to smaller basin area) on the Varinka stream at lower lift station. Peak discharge reached value of 6.7 m³s⁻¹ on the Stohovy stream.



a)



b)





c)

Fig. 4. a-c. Fixation of the cross sections on Varinka and Stohovy streams according to flood tracks of the flood on July 21, 2014.

V. DISCUSSION AND CONCLUSIONS

The lower photo (Photo 1b) shows water level in 2014. Comparison of the photo 1b with photo 1a (flood in 2012) shows 60 cm brighter layer of rock. Flow of the Varinka stream in this narrow profile took away almost all of the bottom sediments and revealed the bedrock.



a)



b)

Photo 1. a) Flood mark situation in 2012, b) Detail of flood mark with indicated water level in 1848 and flood water level in 2014 fixed after the flood with the stream bed nicked by 60 cm approximately (white rock above the water). (Photos by Pekarova, 13.07. 2012 and 30.07. 2014).

Similarly, Photo 2 a)-b) shows riverbed of the Varinka stream in Tiesnavy with two years delay. Photo 3 shows catastrophic mud flows in the Malá Fatra Mountains due to extreme rainfalls on July 21, 2014.



a) valley Tiesnavy 13.07.2012



b) valley Tiesnavy 29.07.2014

Photo 2. a) - b) Original status of the stream channel in 2012 and the stream channel raked out by the flood on July 21, 2014. (Photos by Pekarova 2012 and 2014).



Photo 3. Catastrophic mud flows in the Malá Fatra Mountains due to extreme rainfalls on on July 21, 2014 (Photo by Miklanek, 2014).

Whether the next flood occurs in the future, the history does not tell us, however, suggests that its occurrence in the country is real. Therefore, it would be desirable to build the flood marks after each flood on buildings, bridges, water gauge. Old flood marks, up to 1000 years, we can also to find in Italy or Austria. Human life is short and unfortunately, human memory

is even shorter. After 100 years this great flood will probably fall into oblivion.

REFERENCES

- [1] E. Gruntfest, C. J. Huber, "Toward a comprehensive national assessment of flash flooding in the United-state." *Episodes* vol. 14, no. 1, pp. 26–35, 1991.
- [2] S. Rozalis, E. Morin, Y. Yar, and C. Price, "Flash flood prediction using an uncalibrated hydrological model and radar rainfall data in a Mediterranean watershed under changing hydrological conditions", *J. Hydrol.*, vol. 394, pp. 245–255, 2010.
- [3] M. Jakob, K. Holm, O. Lange and J. W. Schwab, "Hydrometeorological thresholds for landslide initiation and forest operation shut downs on the north of British Columbia." *Landslide*, vol. 3, no. 3, pp. 228–238, 2006.
- [4] L. Marchi, M. Cavalli, M. Sangati, and M. Borga, "Hydrometeorological controls and erosive response of an extreme alpine debris flow." *Hydrol. Process.*, vol. 23, no. 19, pp. 2714–2727, 2009.
- [5] E. I. Nikolopoulos, E. N. Anagnostou, M. Borga, E. R. Vivoni and A. Papadopoulos, "Sensitivity of a mountain basin flash floods to initial wetness condition and rainfall variability." *J. Hydrol.*, vol. 402, no. 3–4, pp. 165–178, 2011.
- [6] M. Hino, Y. Odaka, K. Nadaoka and A. Sako, "Effect of initial soil moisture content on the vertical infiltration process – a guide to the problem of runoff-ratio and loss." *J. Hydrol.*, vol. 102, , pp. 267–284, 1988.
- [7] S. Yatheendradas, T. Wagener, H. Gupta, C. Unkrich, D. Goodrich, M. Schaffner and A. Stewart, "Understanding uncertainty in distributed flash flood forecasting for semiarid regions." *Water Res. Research*, vol. 44, no 5, p. 17, doi:10.1029/2007WR005940, 2008.
- [8] V. M. Castillo, A. Gomez-Plaza and M. Martinez-Mena, "The role of antecedent soil water content in the runoff response of semiarid catchments: a simulation approach." *J. Hydrol.*, vol. 284, pp. 114–130, 2003.
- [9] J. A. Moody and D. A. Martin, "Post-fire, rainfall intensity–peak discharge relations for three mountainous watersheds in the western USA." *Hydrological Processes, Special Issue: Wildfire and Surficial Processes*, vol. 15, no. 15, pp. 2981–2993, 2001.
- [10] M. Borga, M. Stoffel, L. Marchi, F. Marra and M. Jakob, "Hydrogeomorphic response to extreme rainfall in headwater systems: Flash floods and debris flows." *J. Hydrol*, vol. 518, Part B, pp. 194–205, 2014.
- [11] P. J. Smith, L. Panziera, and K. J. Beven. "Forecasting flash floods using data-based mechanistic models and NORA radar rainfall forecasts". *Hydrol. Sci. J.*, pp. 1–15, Publ. online: Jan 2014, 2014.
- [12] T. R. Kjeldsen, J. D. Miller, and J. C. Packman, "Modelling design flood hydrographs in catchments with mixed urban and rural land cover", *Hydrology Research*, vol 44, no 6, pp 1040–1057, 2013.
- [13] S. N. Jonkman and I. Kelman, "An Analysis of causes and circumstances of flood disaster deaths." *Disasters* vol. 29, no. 1, pp 75–97, 2005.
- [14] L. Coates, "Flood fatalities in Australia 1788–1996. *Aust. Geogr.*, vol. 30, no. 3, pp. 391–408, 1999.
- [15] C. Staes, J. C. Orengo, J. Malilay, J. Rullan and E. Noji, "Deaths due to flash floods in Puerto Rico, January 1992: implications for prevention. *Int. J. Epidemiol.*, vol. 23, no. 5, pp. 968–975, 1994.
- [16] O. Dub, "Regime of high water in small streams." The publication of the State Hydrological and Meteorological Institute in Bratislava, (in Slovak), 1941.
- [17] J. Pacl, "Catastrophic flood in the Tatras area in June, 1958." *Proceedings of the works of the Tatra National Park*, vol. 3, pp. 17–56, 1959.
- [18] P. Pekarova, P. Miklanek, P. Skoda and A. Svoboda, "Analysis of floods on the Danube and Vah." In conference proceedings of Conference Floods 2010: Causes, course and experience, Strbske pleso, High Tatras, Slovakia, Water Research Institute (WRI), pp. 1–10, 2010.
- [19] P. Šťastný, M. Turňa, L. Méri, P. Zaujec, "Meteorological assessment of storm activity in northwestern Slovakia July 21 2014. *Water management reporter*, vol. 57, no. 9–10, pp. 24–25, (in Slovak), 2014.
- [20] A. Svoboda and P. Pekárová, "The catastrophic flood of July 1998 in the Mala Svinka catchment – its simulation." *Journal Hydrol. Hydromech.*, vol. 46, no. 6, pp. 356–365, 1998.
- [21] P. Pekarova, A. Svoboda, P. Miklanek, P. Škoda and D. Halmová, "Estimating flash flood peak discharge in Gidra and Parná basin: case study for the 7–8 June 2011 flood." *J. Hydrol. Hydromech.*, vol. 60, no. 3, pp. 206–216, 2012.

Development of land use in the Morava River floodplain during the past 175 years

Vilém Pechanec, Ivo Machar and Helena Kilianová

Abstract—This paper presents the results of the analysis of land use in the Morava River floodplain, CR from 1836 to the present (1999). Significant changes in land use occurred in the study area over the last 175 years. The most striking trend is the increase in arable land throughout the studied period of time. Dynamic enlargement of fields is reflected also in the spatial structure of the landscape. At the beginning of the studied period (in 1836) the landscape matrix of the Morava River floodplain was formed by meadows and forests. In the 1950' the landscape matrix was composed of a mosaic of alluvial forests, meadows and arable land. Currently, the predominant landscape matrix consists of arable land and isolated forest complexes. The area of settlements has also increased significantly over the studied period. The share of meadows and pastures declined in favor of arable land during the studied period and it is manifested by reduced environmental stability of the area, which is quantified by environmental stability coefficients. Land use changes in the Morava River floodplain are linked with changes in landscape character, landscape structure and biodiversity.

Keywords—development of land use, historical maps, floodplain, River Morava

I. INTRODUCTION

Research on the changes of land use is a basis for the studies of cultural landscape. The results of the research can be used e.g. for landscape and spatial planning and in the case of floodplains for the optimization of flood control measures. The study of changes in alluvial landscape is particularly timely in the context of the increasing frequency of flood events in alluvial plains of central European rivers. The Morava River floodplain in the present status is an example of cultural landscape in which most ecosystems are affected by socio-economic activities of the human society. This paper gives an overview of the evolution of the Morava River floodplain during the past 170 years assessed through land use

analyses performed using GIS (geographic information systems).

II. MATERIALS AND METHODS

Land use analysis on the scale of 1: 25 000 was used to evaluate land use changes in the Morava River floodplain. To assess the changes in the landscape, digital maps of the Morava River floodplain on the scale of 1: 25 000 were created for the time period from 1836 to 1840, from 1876 to 1880 and around 1953 (hereinafter referred to as "digital historical maps"). The maps were digitized and processed to vector layers using ArcGIS. Map sheets from the 2nd military mapping (1836 - 1840) and the 3rd military mapping (1876 - 1878) and State maps on the scale of 1: 5000 derived from the period around 1953 formed a cartographic basis for the digital historical maps.

The cartographic contents of the digital historical maps were compared with a digital map of the current land use of the Morava River floodplain and thus the information on the representation of all mapped land use categories in different time periods was obtained. This information was organized into a data system that allows analyzing changes in the evolution of the landscape and individual landscape elements in the studied period of time.

The digitization was followed by the processing of a detailed network of digitized lines. Each spot was assigned coordinates and an identifier to which additional descriptive information was linked. Using post-editation, each spot was then assigned information from the table of codes expressing the use of the area. Finally, the names of towns, forest units and water courses were created in the ArcGIS attribute table. After further necessary topological adjustments a digital map was created, which could be then statistically analyzed using traditional GIS tools. Obtained statistical data (number of individual spots, their size, sum, length of water courses, etc.) were processed into tables and graphs that allowed interpretation of results.

III. STUDY AREA

Studied area represents the alluvial landscape of the Morava River in the Czech Republic. The length of the Morava from its source to the confluence with the Dyje River at the border of the Czech Republic is about 270 km. The Morava River

This work was supported by a grant from Technology Agency of the Czech Republic number TA04020888.

V. Pechanec Palacký University in Olomouc, Dept. of Geoinformatics, 17. listopadu 50, 771 46 Olomouc, Czech Republic (corresponding author phone: +420-585-63-4579; e-mail: vilem.pechanec@upol.cz).

I. Machar Palacký University in Olomouc, Dept. of Biology, Žžkovo nám. 5, 771 46 Olomouc, Czech Republic (e-mail: ivo.machar@upol.cz).

H. Kilianová Palacký University in Olomouc, Dept. of Geoinformatics, 17. listopadu 50, 771 46 Olomouc, Czech Republic (e-mail: helena.kilianova@upol.cz).

floodplain is only a few meters wide in the upper reaches and widens gradually towards the south along the river up to the width of several kilometers. The boundary of the studied area was formed by the boundary of the Quaternary fluvial sediments of the Morava River according to a geological map. The surface area of the studied floodplain was 635.7 km², the elevation ranged from 900 m a.s.l. (narrow floodplain of the Morava in the Králický Sněžník Mts.) to 151 m a.s.l. (confluence of the Morava and Dyje rivers).

IV. RESULTS

A. Development of land use in the the Morava River floodplain

In 1836, the Morava River floodplain was relatively well preserved from the ecological point of view. Most of the surface area was formed by meadows, pastures and forests. Arable land prevailed in the Morava River floodplain in the second half of the 20th century. A trend of a growing area of human settlements within the floodplain is discernible over the whole time period.

Changes of land use in the Morava River floodplain from 1836 till present are expressed by numbers in Table 1.

Table I. Land use in the Morava River floodplain

	1836		1877		1953		1999	
	km ²	%	km ²	%	km ²	%	km ²	%
Forests	177,2 7	27,89	168,9 7	26,58	159,9 2	25,16	162,2 3	25,52
Meadows	273,5 2	43,03	222,6 1	35,02	179,2 6	28,20	53,86	8,47
Pastures	28,7	4,51	21,92	3,45	6,95	1,1	0	0,0
Arable land	136,6 5	21,5	196,7 8	30,95	235,9 4	37,11	329,2 8	51,8
Gardens and orchards	0,85	0,13	4,4	0,69	12,53	1,97	0,47	0,07
Towns	16,3	2,56	19,36	3,05	38,24	6,01	66,16	10,41
Transport areas	0,39	0,06	0,85	0,13	2,06	0,32	2,24	0,35
Water surface	2,02	0,32	0,81	0,13	0,8	0,13	21,46	3,38
Total	635,7	100	635,7	100	635,7	100	635,7	100

own source

The table shows that spatial changes of different land use categories in the Morava River floodplain in different time periods are rather significant. Forests represent the most stable areas. The maximum decrease of their surface area by 17.35 km² (i.e. 2.73%) was recorded in 1953 as compared to the situation in 1836. At present, forests cover 25.52% of the Morava River floodplain. The area of forests decreased by about 1.4% between the time periods, however, the trend has reversed since 1953. Only one particular forest stand has been identified in the floodplain, which was cut down and has not been renewed (an unnamed forest south of the "Olšový les" near Moravský Písek). In all other cases the area of forest decreased as it was usually replaced by meadows or fields. Three stands are currently larger than at the beginning of the

studied period ("V hájích" near Bohuslavice "Černovířský les" near Olomouc and "Olšový les" near Moravský Písek). Compared to the state in 1836, the number of hedgerows, balks and line forest stands declined slightly (estimated, not measured), however, most of them remain or have been renewed.

Meadows and pastures, which accounted for 273.52 km² (i.e. 43.03%) at the beginning of the studied period, almost disappeared from the alluvial landscape. Over time, their area has declined to only 53.86 km² (i.e. 8.47%). The loss of these important landscape elements in the Morava River floodplain was caused by their conversion to arable land. The area of arable land increased 2.5 times during the studied time period (from 21.5% to 51.8%), which is a very significant increase. Furthermore, a substantial portion of arable land has been added in the last decades. In previous periods, the increase was not so marked.

Huge increase of urban areas (settlements) was recorded. Their size increased from the original 16.3 km² (i.e. 2.56%) to 66.16 km² (i.e. 10.41%). The size of urban areas within the floodplain has increased sharply since the turn of the 19th and 20th century and especially in the second half of the 20th century. It can be explained by the development of industry, whose production facilities were located in the floodplain. Since the fifties, when large-scale agriculture originated and agriculture cooperatives were founded, the area of settlements has been enlarged by these economically and agriculturally used areas. Residential areas of towns and cities have expanded too, which is related to population growth and migration of people into towns and cities.

Traffic areas (railway stations and their adjacent transshipment and manipulation areas) were mapped within the built-up areas. Some railway stations, which were located outside of town in the 19th century, are now part of the urban area. New rail lines have been built during the studied period. The surface area of transport infrastructure has therefore increased from the original 0.06% (in 1836) to the current 0.35% of the floodplain area.

B. Comparison of the development of land use in the CR and the Morava River floodplain

The development of land use in the studied area has been influenced by natural processes and conditions specific to the floodplain, as well as social and economic conditions. These factors represent a possible cause of differences in the development of land use in the Czech Republic and in the studied area.

The first difference in the land use structure (Table 2) is very high percentage of meadows in the Morava River floodplain, which already in 1836/1845 exceeded Czech average by 33.73%. It can be explained by natural conditions – the floodplain with its high ground water level and frequent floods did not allow other uses. Waterlogged meadows provided fodder but it was not necessary, and probably not even technically possible, to cultivate (i.e. plow) them. This

also explains low representation of arable land and its location in acceptable parts of the floodplain. The initial low share of forests in the floodplain is surprising and also the following development tendency is opposite if compared to the CR. Within the studied time period, the share of forests increased by 4.6% in the Czech Republic but decreased by 2.73% in the Morava River floodplain (status in 1953).

It is worth noting the fact that the share of built-up areas in the floodplain greatly exceeds their average share in the CR. It is five times higher even though some settlements are only partly situated within the floodplain. This fact can be explained by the location of ancient human dwellings and settlements in the proximity of rivers that were providing water and livelihood. The settlement structure is therefore denser in the floodplain and its neighbourhood if compared to the rest of the territory.

Table II. Comparison (in %) of the development of land use in the Morava River floodplain (MRF) and Czech Republic (CR)

	MRF 1836	CR 1845	MRF 1877	CR 1897	MRF 1953	CR 1948	MRF 1999	CR 1999
Forests	27,89	28,8	26,58	28,9	25,16	30,2	25,52	33,4
Meadows	43,03	9,3	35,02	8,9	28,20	9,1	8,47	7,9
Pastures	4,51	8,3	3,45	5,3	1,1	3,8	0	3,4
Arable land	21,5	48,2	30,95	51,6	37,11	49,9	51,8	39,3
Gardens and orchards	0,13	1,1	0,69	1,5	1,97	1,9	0,07	3,0
Urban areas	2,62	0,6	3,18	0,7	6,33	1,1	10,76	1,96
Water surface	0,32	0,9	0,13	0,5	0,13	0,6	3,38	1,99
Other	0	2,8	0	3	0	3,4	0	9,05
Total	100	100	100	100	100	100	100	100

own source

There are different trends in the development of individual forms of land use in the CR and the floodplain in the studied period. Significant loss of meadows and pastures in the Morava River floodplain and dramatic increase of the area of arable land, which currently exceeds the average share in the CR by 12.5%, indicate strong pressure of highly productive land use in recent decades. The area of arable land in the floodplain increased to 241% of the original area (status in 1836). In contrast, in the CR it decreased to 81.5% of the original area (status in 1845). Meadows and pastures represent very dynamic land use categories in the Morava River floodplain. Their area decreased to 17.8% of the original size, while the most significant decrease was recorded in the second half of the 20th century. The reduction of the area of forests, which were also transformed to arable land, has increased the difference in the share of forests in the floodplain and the CR. The trend of decreasing area of forests was reversed in the mid-19th century in the CR, the same cannot be said for the Morava River floodplain, where this trend had not reversed before 1953.

There is a gradual upward trend in the size of built-up areas in the CR, the size of built-up areas has increased to 326.5%. In the floodplain is has increased to 410%, while up to 1953

the area increased only to 240%. The significant jump in the area of settlements in the floodplain is dated in the last decades, when there was a significant development of industry, large-scale agriculture and housing construction. Flood risk was underestimated probably due to drier climatic conditions in the 20th century and the awareness of the water management paradigm. However, floods are a natural factor in the development of floodplains and their vegetation cover.

It is interesting to monitor the development of water bodies. In the CR, the area of lakes, reservoirs and ponds has increased to 221%, whereas in the Morava River floodplain they represent the most dynamic land use category. Their size has increased to 1056%. This huge increase is linked to the formation of water reservoirs in the areas of extracted fluvial sand and gravel, which were established in the floodplain in relation to the development of construction industry in recent decades.

V. DISCUSSION

The result of the analysis of the study area does not contradict the general trends of the landscape changes in the Czech Republic in the course of the 20th century [1]. According to, the ecological stability of the Morava River floodplain landscape decreased significantly over the course of the 20th century. However, the results of the analysis concern the landscape of the entire the Morava River floodplain which is predominantly deforested. The same applies to [2], who found a significant decrease in the landscape heterogeneity and shortening of the total length of permanent landscape structure edges (which he considers an important landscape characteristics for assessment of changes in ecological stability of the landscape) in the landscape of north Bohemia (in the Ohře riverbasin) which is subject to intensive agricultural cultivation.

When we compare the results of this study to the general developmental trends of the cultivated rural landscape in the Czech Republic, we can see that the overall landscape heterogeneity and ecological stability increased during the 20th century [3]. The change in the observed landscape attributes within the study area in the first half of the 20th century was triggered by the transition from the coppice with standards forest type to that of a high production forest [4]. The intensive and centuries-old forest management processes in the floodplain forests of the Morava River is a conditionally natural state of the floodplain forest geobiocenoses with unusually high biodiversity [5].

Fragmentation is especially challenging for European floodplain forests because they are endangered ecosystems with unusually high biodiversity [6], which at the same time are significantly anthropogenically conditioned [7]. The development dynamics of Central European floodplains is very quick [8], from which follows a very dynamic ecological stability in the floodplain themselves. This was described by Buček and Lacina [9] as the “dynamic fluvial seral section of floodplain biotopes” [10].

VI. CONCLUSION

Land use changes in the Morava River floodplain affected the overall appearance of the landscape significantly. During the last 175 years the Morava River floodplain has changed from extensively used agricultural landscape with prevailing permanent grassland to intensively used agricultural landscape dominated by arable land. The trend of increasing size of built-up areas is also significant. By contrast, no fundamental changes in the share of forests were recorded in the Morava River floodplain throughout the studied period of time. The area of forests has been relatively stable over the last 150 years.

REFERENCES

- [1] Czech Statistical Office, 1999. Statistical Yearbook of Czech Republic. Scientia, Praha: 712.
- [2] P. Sklenička, "Temporal changes in pattern of one agricultural Bohemian landscape during the period 1938–1998," *Ekológia*, vol. 21-2, pp. 181-191.
- [3] Z. Lipský, "The changing face of the Czech rural landscape," *Landscape and Urban Planning*, vol. 31, pp. 39-45.
- [4] I. Machar., 2008. Floodplain forests of Litovelské Pomoraví and their management. *Journal of Forest Science*, 54: 355-369.
- [5] P. Maděra, J. Vukelič, A. Buček, D. Baričević, "Floodplain forest plant communities," In: KLIMO E., HAGER H., KULHAVÝ J. (eds.), *Floodplain forests of the temperate zone of Europe*. Kostelec nad Černými lesy, Lesnická práce: 102-159.
- [6] E. Klimo, H. Hager, "The floodplain forests in Europe : current situation and perspectives," *European Forest Institute research report*. Leiden, Koninklijke Brill NV: 267.
- [7] V. Pechanec, "Analyses of evolution of floodplain forests landscape structure" in. Machar I. (ed): *Biodiversity and target management of floodplain forests in the Morava river basin*. Universita Palackého v Olomouci, Olomouc, 2010 pp. 30-39.
- [8] O. Štěrba, J. Měkotová, V. Benář, B. Šarapatka, M. Rychnovská, F. Kubíček, V. Řehořek. "River landscape and its ecosystems (in Czech)," Univerzita Palackého, Olomouc, 2008..
- [9] A. Buček, J. Lacina, "Biogeography situation (in Czech)," In: *Aspects for revitalization of floodplain River Dyje near Nové Mlýny – confluence with River Morava*. Institute of Geoniche Academy of Science of Czech republic, Brno: 28 – 50.
- [10] I. Machar, V. Pechanec, "Application of geoeological concept of the alluvial landscape in the creation of nature reserve (case study from the Czech Republic)," *Acta Universitatis Agriculturae et Silviculturae Mendelinae Brunensis*, vol. 16 (3), pp. 123-133.

Vilém Pechanec was born in Hodonín, 5.9. 1977. Educational background is Mgr. - Department of Ecology, Palacký University in Olomouc, Ph.D. - Department of Geoinformation Technologies Mendel University of Agriculture and Forestry in Brno and RNDr - Department of Ecology, Palacký University Olomouc, 2007 and habilitation in the field of Landscape management - Mendel University, 2013.

He work in the Administration of PLA The White Carpathians as GIS Specialist (2001-2005) and teacher in Department of Geoinformatics, Palacký University Olomouc (2005-present).

Assoc. Prof. Pechanec is member of IALE and EUROGI and their national office.

Ivo Machar was born in Olomouc, 6.8.1968. Educational background is Ing - Faculty of Forestry Brno University of Agriculture, Department of Forest Engineering 1990, Ph.D. - Mendel University of Agriculture and Forestry Brno, doctoral degree in Ecology 2001 and habilitation in the field of Forest Ecology - Mendel University of Agriculture and Forestry Brno – 2010.

He work in the South Moravian state forests as Forest Techniques (1990-1991), Primary military service (1991), Czech Institute for Nature Conservation (name changes after transformation: PLA Czech Nature Conservation) function: Head of protected area management Litovelské Pomoraví (1992–2005), National Heritage Institute (2005) and Department

of Biology Faculty of Education, Palacký University in Olomouc, as teacher (2006 – present).

Assoc. Prof Machar is member of Society for Conservation Biology (Washington) and IALE and their national office.

Helena Kilianová was born in Rychnov nad Kněžnou, 28. 2 1966. Educational background is 1988 – Agricultural University in Prague – specialisation: agronomy (Ing.), 2001 - Mendel University in Brno – Ph.D. degree at the Faculty of Agriculture

Employment: Palacký University In Olomouc, Department of Geoinformatics of Faculty of Sciences (researcher and project manager) and Department of Biology of Faculty of Education (lecturer and project manager).

She is member of Czech Geography Society.

Model parameters estimation in two river basins in Slovakia and Korea

Pavol Miklanek, Hyosang Lee, Pavla Pekárová, Michal Danko

Abstract—The rainfall-runoff modelling is an important tool for analysis of different hydrological and water management problems, such as assessment of the water resources, simulation of the hydrological processes, forecasting of the runoff changes, particularly the floods and droughts. The paper checks the applicability of a simple rainfall-runoff model HBV-light in different geographical and environmental conditions of the Central Europe (Slovakia) and in the Eastern Asia (Korea). The study catchments are the Bela River in Slovakia and the Bukil catchment in Korea. Model parameters estimation is performed for both catchments. The simulation results are satisfactory.

Keywords—HBV model, runoff simulation, Bela, Bukil.

I. INTRODUCTION

THE rainfall-runoff modelling is an important tool for analysis of different hydrological and water management problems, such as assessment of the water resources, simulation of the hydrological processes, forecasting of the runoff changes, particularly the floods and droughts.

There exist plenty of different mathematical hydrological models for different purposes and with different input data requirements. For many purposes it is more useful to use simple tools, because the data availability is limited in many areas. Very important topic for the proper use of hydrological models is the assessment of model parameters included in the algorithms.

The aim of the paper is to check the applicability of a simple rainfall-runoff model HBV-light in different geographical and environmental conditions of the Central Europe (Slovakia) and in the Eastern Asia (Korea). The HBV-

light model has been used in many applications practically all around the world. In Slovakia the model was successfully tested in several studies, e.g. [1]–[2]. Major issue for proper model application is the calibration of the model and its parameters in different conditions and analysis of the ways how to relate them to extreme runoff formation [3]–[4].

II. STUDY CATCHMENTS

For the purpose of this study the model was applied in two river basins with middle size area and similar rainfall depths. Taking this condition into account, we selected the Bela river basin in Slovakia and the Bukil river basin in Korea.

The Bela River starts with confluence of the Tichy and Koprovy creeks at 976.8 m a.s.l. The Bela River basin area is 244.303 km². The Bela River flows into the Vah River at Liptovský Hradok at an altitude of 629 m a.s.l. and it is its significant right tributary [5].

The Bela River is the major stream of the Tatras in Slovakia and is considered to be a typical river of the highest part of the Carpathians. The vegetation of the Bela basin up to Podbanske water gauge consists by 40% of dwarf pine, 13% cover coniferous forests, 30% is woodland shrub, 16% are natural meadows and the rest are water areas and built-up areas.

Both hydrological and meteorological data for the basin were provided by the Slovak Hydrometeorological Institute.

The Bukil catchment is subcatchment of Miho catchment which is itself a subcatchment located in the headwaters of the Guem River basin draining the central part of the Korean peninsula. The study area has a temperate-continental climate region with distinct dry season and wet seasons. On average 80% of the annual rainfall (1200 mm) falls between June and September.

The area of the catchment is 906.59 km², the average of the altitude in the catchment is 130.3 m, and the average annual rainfall is 1244 mm.

The hydrological data were obtained from the Water Management Information System (WAMIS, <http://www.wamis.go.kr>) held by the Ministry of Land, Transportation, and Marine Affairs (MLTM) and from the Meteorological Administration in Korea [6].

III. DESCRIPTION OF THE HBV-LIGHT MODEL

The HBV model, developed by the SMHI (Swedish Meteorological and Hydrological Institute), has become

This work was supported in part by the VEGA project under the contract No. 2/0009/15, by the KORANET2- 052 project, and it results from the project implementation of the “Centre of excellence for integrated flood protection of land” (ITMS 26240120004) supported by the Research & Development Operational Programme funded by the ERDF.

Pavol Miklanek is with Institute of Hydrology Slovak Academy of Sciences, Raciarska 75, 831 02 Bratislava, Slovakia, (phone: +4212 44259311, Fax: +4212 44259311, e-mail: miklanek@uh.savba.sk).

Hyosang Lee is with School of Civil Engineering, 102, E8-6, Chungbuk National University, 52 Naesudong-ro, Heungduk-gu, Cheongju, Korea (e-mail: hyosanglee@chungbuk.ac.kr).

Pavla Pekarova is with Institute of Hydrology Slovak Academy of Sciences, Raciarska 75, 831 02 Bratislava, Slovakia, (e-mail: pekarova@uh.savba.sk).

Michal Danko is with Institute of Hydrology Slovak Academy of Sciences, Raciarska 75, 831 02 Bratislava, Slovakia, e-mail: danko@uh.savba.sk).

widely used for runoff simulations in Sweden and other countries round the world during the last 20 years [7]–[8]. After twenty years the model has become a standard tool for runoff simulations and forecasting. Many of the applications abroad can be considered as scientific tests of the model feasibility under specific conditions.

The HBV-light model can be classified as a semi-distributed model. It uses subbasins as primary hydrological units, and within these an area-elevation distribution and rough classification of land use are made. The option of subbasins is usually used in geographically and climatologically heterogeneous basins.

The model simulates daily discharge using daily rainfall, temperature and potential evaporation as input. Precipitation is simulated to be either snow or rain depending on whether the temperature is above or below a threshold temperature. There are usually about 12 free parameters to be found by calibration. The list of the main parameters of the model is in Table 1. The HBV-light model consists of three main components (Fig. 1):

- Subroutine for snow accumulation and melt.
- Subroutine for soil moisture accounting.
- Response and river routing subroutine.

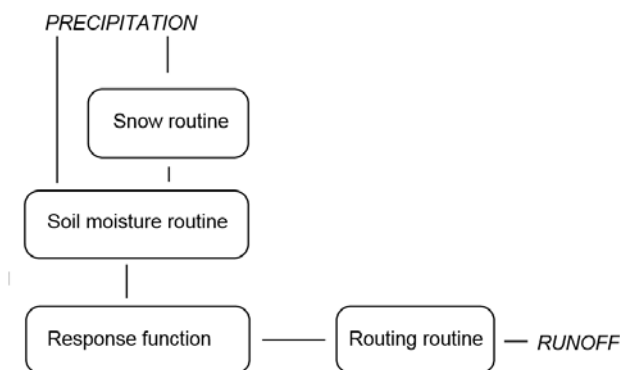


Figure 1. Schematic structure of the HBV model

IV. 1.1 MODEL CALIBRATION

The model input time series consist of daily potential evapotranspiration, rainfall and runoff for different time periods in individual basins. The rainfall and potential evapotranspiration were calculated as areal averages from several meteorological stations. The runoff data series were used from the stations in the closing profiles of the basins.

Fiftyfour-years data series were used for the HBV-light model performance in the Bela River basin (1947/48 – 2000/01), and twelve-years data series were used for the HBV-light model application in the Bukil River basin (2001 – 2012). The time series were divided into calibration and verification periods.

The calibrated parameter values for the Bela and Bukil River basins are in Fig. 2 and Fig. 3, respectively.

Table 1 List of parameters of the HBV-light model

TT [°C]	threshold temperature of snow/rainfall
SFCF [-]	snowfall correction factor
CFMAX [mm °C ⁻¹ day ⁻¹]	degree-day factor
CFR [-]	refreezing coefficient
CWH [-]	water retention coefficient in snowpack
SM [mm]	water content of the soil
FC [mm]	maximum water content of the soil
LP [-]	threshold for actual / potential evaporation
BETA [-]	relative contribution to runoff from rain or snowmelt
SUZ [mm]	upper groundwater box
SLZ [mm]	lower groundwater box
PERC [mm d ⁻¹]	maximum percolation rate
UZL [mm]	threshold value for groundwater content
K _i [d ⁻¹]	recession coefficient for individual boxes
MAXBAS [-]	runoff transformation parameter.

Parameter	
TT [°C]	-2.85
CFMAX [mm/(d °C)]	1.9
SFCF [-]	0.5
CFR [-]	0.05
CWH [-]	0.08
FC [mm]	25
LP [-]	0.99
BETA [-]	3
PERC [mm/d]	1.42
UZL [mm]	85
K0 [1/d]	0.16
K1 [1/d]	0.06
K2 [1/d]	0.00004
MAXBAS [d]	1
Cet [1/°C]	0.005

Simulation		
Start of 'warming-up' period:	Date	No.
461101	471031	365
1	81031	22646

Buttons: Load Parameter, Save Parameter, Model-Run-No: 001, Cancel, OK

Fig. 2 Parameters for the Bela catchment

V. SIMULATION RESULTS

The calibration of the model was done by optimisation. Due to interaction between the model parameters only a few parameters were changed between two consecutive model runs. The calibration of the model consisted of three steps. In the first step, snow parameters were calibrated, which have the influence on simulation of spring snowmelt. Secondly, the parameters of soil moisture were calibrated. They affected summer and autumn flows. In the last step the parameters of runoff response were changed. These parameters influenced the shape of the hydrograph, but didn't affect the volume. The calibration is usually made by trial and error technique.

Parameter

TT [°C]	2	PERC [mm/d]	1.8
CFMAX [mm/(d °C)]	2.472726	UZL [mm]	10
SFCF [-]	0.5327796	K0 [1/d]	0.5
CFR [-]	0.1	K1 [1/d]	0.18
CWH [-]	0.5	K2 [1/d]	0.0001
FC [mm]	160	MAXBAS [d]	2
LP [-]	0.8		
BETA [-]	1.5		

Simulation

Start of 'warming-up' period: Date No.

from 50101 1462 Load Parameter

to 121231 4383 Save Parameter

Model-Run-No 001

Cancel OK

Fig. 3 Parameters for the Bukil catchment

On Fig. 4 and Fig. 5 there are examples of simulation results in the Bela and Bukil River basins, respectively.

On Fig. 6 and Fig. 7 there is the summary information on simulation results in the Bela and Bukil River basins, respectively.

In the rainfall-runoff modelling it is necessary to take into account various sources of model uncertainties influencing the quality of simulated runoff from a catchment. There are three main reasons of uncertainties in the rainfall-runoff modelling: 1) uncertainties related with the parameter estimation, 2) uncertainties resulting from the model structure and simplification of the processes, and 3) uncertainties connected with the input data quality and representativeness. The modelling uncertainties influence the successful application of the model. Therefore a lot of attention was given to proper assessment and reduction of the uncertainties.

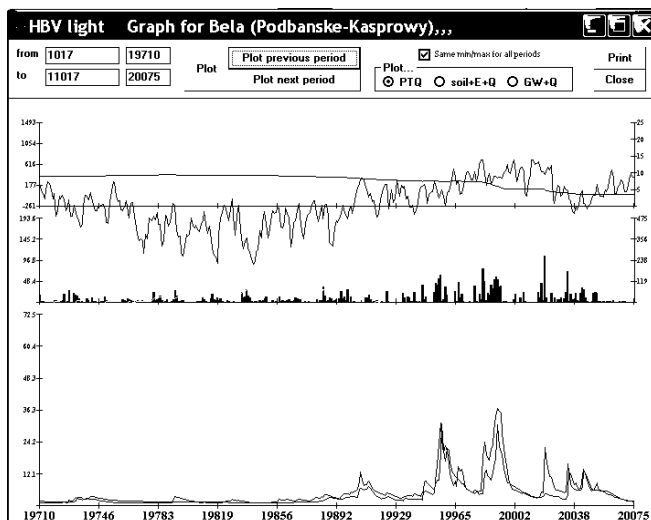


Fig. 4 Model output for the Bela catchment, year 2001

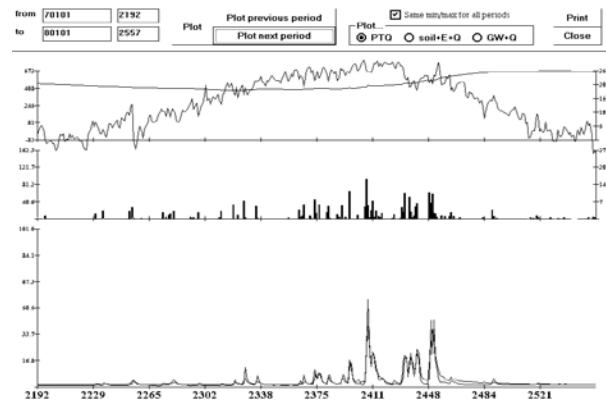


Fig. 5 Model output for the Bukil catchment year 2007

VI. CONCLUSIONS

The HBV-light model was successfully tested in the Uh catchment. The verification of the calibrated parameters proved good results of simulation. The comparison of statistical characteristics of the observed and simulated mean daily discharges for the simulation period proved no significant changes in selected characteristics

<u>Water Balance [mm/year]</u>	
Sum Qsim	= 1198
Sum Qobs	= 1198
Sum Precip.	= 1738
Sum act. ET	= 344
Sum pot. ET	= 772
Contribution of Q2 [-]	= 0.383
Contribution of Q1 [-]	= 0.513

<u>Goodness of simulation</u>	
r ²	: 0.7191
Efficiency of the model	: 0.7095
Efficiency (using ln(Q))	: 0.7138
Mean difference [mm/year]	: 0

Fig. 6 Summary of the simulation results in the Bela River basin

<u>Water Balance [mm/year]</u>	
Sum Qsim	= 1090
Sum Qobs	= 1089
Sum Precip.	= 1342
Sum act. ET	= 573
Sum pot. ET	= 911
Contribution of Q2 [-]	= 0.519
Contribution of Q1 [-]	= 0.205

<u>Goodness of simulation</u>	
r ²	: 0.7298
Efficiency of the model	: 0.7297
Efficiency (using ln(Q))	: 0.7111
Reff_intervall 7	: 0.8663

Fig. 7 Summary of the simulation results in the Bukil River basin

Due to satisfactory results of calibration and verification, the HBV-model in its simple form (HBV-light model) could be a good tool for hydrological studies of rainfall-runoff processes and forecasting in Slovakia, and in Korea.

VII. REFERENCES

- [1] D. Halmova and V. Bacova Mitkova, "Application of the rainfall-runoff model HBV to mitigation of the flood event on the Uh River (in Slovak), *Práce a štúdié*, vol. 65, Bratislava, SHMÚ, pp. 31-48, 2001.
- [2] P. Valent, J. Danekova, and C. Rivero, "Uncertainties in the HBV model calibration," (in Slovak), *Acta Hydrologica Slovaca*, vol. 12(2), pp. 360-367, 2011.
- [3] H. J. Chang, K. Banasik, P. Miklanek, and H. Lee, "Relationship between Calibration of ReFH-Model and Characteristics of Flood Events at Jeungpyeong," *Crisis management theory and practice journal*, (ISSN 1738-8368), to be published.
- [4] A. Krajewski, H. Lee, L. Hejduk, and K. Banasik, "Predicted small catchment responses to heavy rainfalls with SEGMO and two sets of model parameters," *Annals of Warsaw University of Life Sciences – SGGW Land Reclamation* vol. 46(3), pp. 205-220, 2014.
- [5] D. Halmova, P. Pekarova, J. Pekar, and P. Miklanek, "Uncertainties in Runoff Components Modelling and Frequency Analysis," *WSEAS Transactions on Environment and Development*, vol. 10, pp. 374-381, 2014.
- [6] J. Joo, T. Kjeldsen, H.-J. Kim, and H. Lee, "Comparison of Two Event-based Flood Models (ReFH-rainfall Runoff Model and HEC-HMS) at Two Korean Catchments, Bukil and Jeungpyeong," *KSCE Journal of Civil Engineering*, vol. 17(5), pp. 1-15, 2013, DOI 10.1007/s12205-013-0348-3.
- [7] S. Bergström, "The HBV model– its structure and applications," SMHI, Sweden, pp. 1-32, 1992.
- [8] J. Seibert, "User's Manual," Uppsala, Sweden, 30 p., 1998.

Measuring devices for visualization of WJM and AWJM technologies physical factors

Ing. Peter Poór, PhD., doc. Ing. Michal Šimon, Ph.D., doc. Ing. Lýdia Sobotová, PhD, Ing. Monika Karková

Abstract— The article explores with visualization methods of physical factors in water jet technology, measuring devices, characteristics of selected physical factors and of course the actual water jet technology.

Keywords— water jet, visualisation, acoustic emission, measuring.

I. INTRODUCTION

Nowadays addresses the very topical issue of pollution and devastation. This damage is usually caused by satisfying the needs of man and society. Many manufacturing technology was replaced because of negative effects on the environment. Have been introduced, low waste and non-waste production technologies, the introduction of environmental standards and strict rules that oblige protect all components of the environment. In addition, environmental protection and greater emphasis on work environment utilize and generate new progressive technologies, which partly replaced by human

In conclusion, we would like to express thanks for the support of the projects SGS-2012-063 titled “Integrated design of manufacturing system as metaproduct with a multidisciplinary approach and with using elements of virtual reality” and project NEXLIZ – CZ.1.07/2.3.00/30.0038, which is co-financed by the European Social Fund and the state budget of the Czech Republic, and the project KEGA 032TUKE-4/2012, KEGA 049TUKE-4/2012

Ing. Peter Poór, PhD. is with Department of Industrial Engineering and Management, University of West Bohemia, Univerzitní 8, 306 14 Plzeň, Czech Republic, E-mail: poorpeter@gmail.com, Phone: +420 377 638 401 Fax: +420 377 638 402

Doc. Ing. Michal Šimon, Ph.D. is with Department of Industrial Engineering and Management, University of West Bohemia, Univerzitní 8, 306 14 Plzeň, Czech Republic, E-mail: simon@kpv.zcu.cz, Phone: +420 377 638 400 Fax: +420 377 638 402

Ing. Monika Karková. is with Departments of Processing and Environmentalistic Engineering, Technical University of Košice, Park Komenského 5,042 00 Košice, Slovak Republic, E-mail: monika.karkova@tuke.sk, Phone: + 421 55 602 2682, Fax: +421 55 633 2680 and department of Mechanical Engineering, Institute of Technology and Business in České Budějovice Okružní 517/10, 370 01 České Budějovice

Doc. Ing. Lýdia Sobotová, PhD. is with Departments of Processing and Environmentalistic Engineering, Technical University of Košice, Park Komenského 5,042 00 Košice, Slovak Republic, E-mail: lzdia.sobotova@tuke.sk, Phone: + 421 55 602 2682, Fax: +421 55 633 2793

activity, thereby reducing the incidence of occupational diseases in industry and shabbiness of the human body in manufacturing. Water jet technology is one of the progressive technologies with little interference with the environment and its pollution. In water jet technology, with regard to the environment, is occurring physical factors such as noise, vibration and a small amount of heat. For visualizing physical agents currently used various manners from analogy to digital instruments and methods.

II. WATER JET AS A PROGRESSIVE TECHNOLOGY

For centuries water changes the river basins and coasts. The water is the bearer of kinetic energy. The ability to change the water environment is confirmed by observation and experience. In the 19th century, the water began to use the technical objectives. This method of using water was known in the treatment of the outside water flow, especially in the mining and extractive industries.

In this days, one of the unconventional technology of production environmentally friendly technology is cutting water jet.

Demands on the cutting process in recent years are harder due to living and working environment and therefore water jet cutting technology represents a unique opportunity of introducing automation in high-pressure high-performance cutting different types of materials. [17]

Using the kinetic energy of water and a very thin stream of water to achieve a power of the water jet, this is capable of imparting a variety of materials, structures and thickness. From textiles through plastic, stone to steel and cast iron. This technology is one of the technologies segregation of cold.



Figure 1 Cutting head with injection system [20]

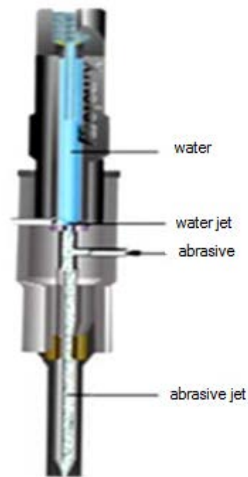


Figure 2 Scheme in the head section [23]

Water in this technology enhances the quality of work, quality of products, equipment life, reduce repair, to reduce wear of nozzles, control valves. Water used in water jet technology division must be free of iron and calcium. The total hardness of the treated water should not exceed 10 mg/l. [11]

Soluble solids are based on the solution and act as an abrasive material. The most affected are the components of the nozzle and high pressure seals. [19]

When creating a high-speed stream of abrasive, the wear occurs in devices which mainly focusing tubes, it means the shocks due to the solid phase to the inner wall of the tube. [16]



Figure 3 Device for cutting water jet [21]

III. VISUALISATION AND MEASURING DEVICE

A. Visualization and visualization techniques

The scientific visualization is an area of research for data collection and presentation. Its boom occurred in the field of information visualization and has become a big part of computer graphics.

In general visualization divided into:

- static parts (images, photos),
- dynamic parts (outputs in the form of films and

animations). [1]

Information accumulated generates data from which only some selected as input into the research. It is good to narrow the field of data entry for clarity studies. [1]

B. Measuring device

An acoustic camera is a device for identifying the acoustic emission using a special microphone system. The device allows frequency analysis of noise sources at a distance of several tens to hundreds of meters. The main assembly acoustic camera, which is shown in Fig. 5 consists of the microphone matrix camera microphone array, hardware and software for recording and processing of data. [2, 3, 4, 5]

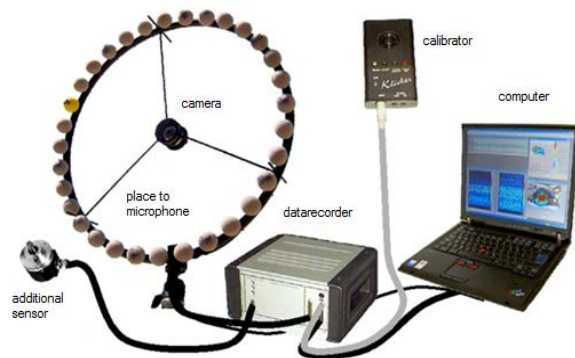


Figure 4 Acoustic camera – complete assembly [4]

The acoustic camera system is composed of a number of microphone units shown in Fig. 6, which are arranged according to the needs of the measurement up to the so-called triangle, star called a circle, ring and the sphere. [5]



Figure 5 Figure 6 Arrays of microphone
a) star b) ring c) sphere

Infrared non-contact measurement system captures the energy and changes it with the detector into electronic signals. The output is the creation of thermal images, as they are modified by the thermo-gram, Fig. 7, and illustrating the temperature curve of the component surface. This method helps to observe of locate temperature anomalies invisible to the human eye, due to the inability to observe in the infrared part of the spectrum.. [8]

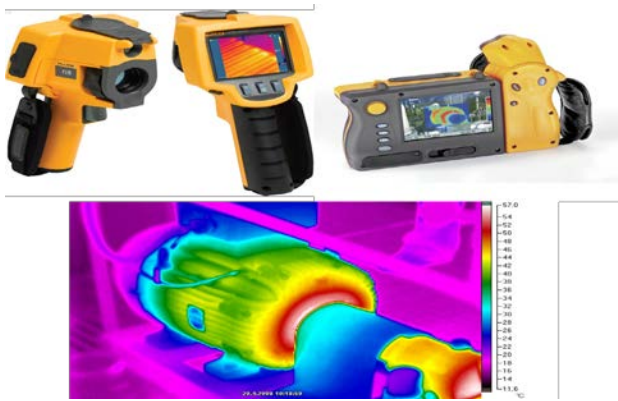


Figure 6 Thermocamera and thermogram of pump [8]

IV. EXPERIMENTAL MEASUREMENT AND EVALUATION

A. Analysis of acoustic emission

This article focuses on the impact of water jet technology work environment, evaluate the selected environmental factors, particularly physical factors that affect the human machine. Physical factors are factors that affect the working environment we advise noise, vibration, climatic conditions, lighting, radiation. [26]

In technology, cutting water jet contribution is defining the physical factors and **vibration**, which can be characterized by oscillating system parameters (speed and acceleration of vibration, amplitude, frequency) and **sound**, which is defined as the mechanical oscillation flexible environment, which progresses from the sound source, and temperature. [26, 27]

In examining the technology to measure vibrations in the cutting process, a pre-defined conditions. In order to determine the effect of vibration given and compare it to define the input parameters of the process of cutting. One of the input parameters, the thickness of the material. Graphical representation is given in the next section of this paper.

In addition to vibration can occur when technology cutting water jet measure and other physical factors such as the aforementioned sound - acoustic signals.

The sound recorded for a given manufacturing process, we can measure:

- in sharing material such as direct production activities,
- in the actual operation, the operation of installations that are part of the technological operations such as pumps to pressurize water and grit into the system, suction pumps.

This type of noise is indicated by the manufacturer and partly influenced by the operator pumps. Noise are shown in Table1.

Table 1 Noise level per pump model [10]

Model of pump	SL-V 30	SL-V 50	SL-V 75	SL-V 100
Level of noise [dB(A)]	72,5	72,5	77,5	77,5

The acoustic signals are in the process of cutting are also for every other steps. Depending on time and type of material - its thickness, complexity and abrasives used shape. The Fig. 8 shows the progress of the acoustic signal, which is recorded, as measured by acoustic emission [11], the article points out that using of the detected acoustic emissions can solve for practical problems encountered in this technology. [11]

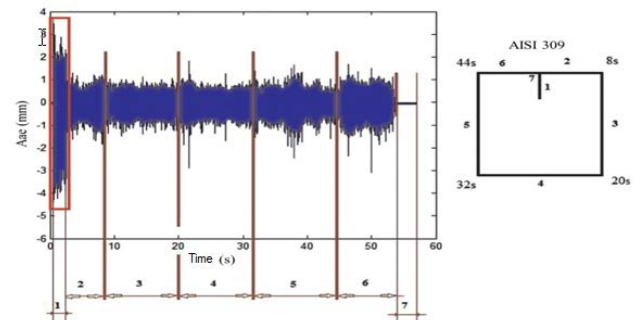


Figure 7 The course of the audio signal in the development of the sample [18]

Figure 8 shows that there is a change of noise especially at the beginning of employment, where the material begins to divide. Phase 1 is marked phase, which is called the "spread it supplies", where water jet hits the material after turning the machine begins to cut and immersed himself in the material. In subsequent phases, the acoustic signal is consolidated. This is because the water jet works evenly divided material and produces the desired pattern. This work is part of a steady pressure. Sliding head pressure to force draws in the direction of the cut and therefore does not thump, thus reducing its intensity signals. The increase in signal in later stages is due to the change of direction of cutting. In the final phase of the signal loses strength and because the resistance of the material is minimal and the beam returned to the place of departure and therefore force interaction is influenced by material force. The material is weakened because of the cut and therefore section 7 (finishing section) is the quietest in the process of measuring the acoustic signal. During the measurements were recorded and vibrations, which are closely related to the measurement of acoustic signals. Acoustic emission depends on the depth of cut in the division AISI 309 with $E = 200 \text{ GPa}$ at the feed speed of the dividing head = 150 mm.min^{-1} (equation 1) and the crushing force (equation 2), which is possible for a better understanding represented graphically. [11]

$$Aae(t) = 0,09851 + 0,11102 \times h(t) \quad (1)$$

$$Aae(t) = 0,14467 + 3,15582 \times Fdef(t) \quad (2)$$

Figure. 9 shows the dependence of acoustic emissions on the depth of cut.

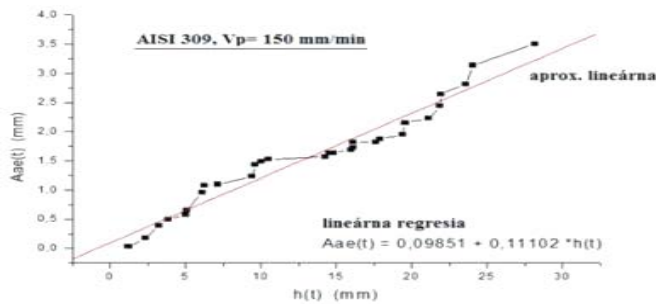


Figure 9 The dependence of acoustic emissions on the depth of cut. [11]

Figure 10 shows the dependence of acoustic emissions on the crushing strength. Addition has increasing character that is meaning that with increasing load, increasing the noise level of the production process.

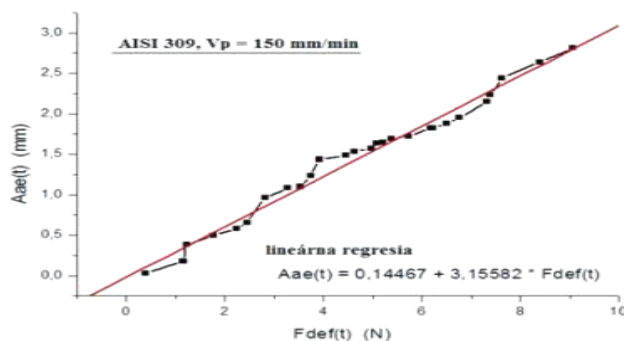


Figure 10 the dependence of acoustic emissions on the crushing strength. [11]

V. THE CUTTING PROCESS AND INFRARED CAMERA THERMO VISION

The aim of the authors of this measurement display output temperature during abrasive water jet cutting. This is carried out under normal working /operating conditions at a room temperature of $T = 293,15$ K. There was used to infrared camera ThermoCAM S65 by manufacturer FLIR Systems. The work piece was made of aluminum 6061-T6 with a width of 46 mm and with the thickness 25.4 mm. Infrared thermal images were recorded with frequency of 25 frames per second. Five thermal images selected from the entire record are shown in Fig.8. [12].

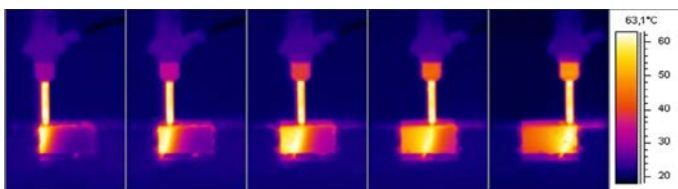


Figure 8 Selected images thermogram of measurement [12]

On-line measurement with a thermal imager, it was found that the maximum temperature during cutting was at 336,15 K.

The heat is already the compression stream of water in a high pressure pump for water pressure of 300 MPa and movement through the transport system of the technology. The speed of cutting head movement is set at 3.23 mm.s-1. [12]

VI. EMISSION OF VIBRATION AT AWJ TECHNOLOGY

The following plot of vibration parameters, shown in Fig. 3 and Fig. 4 it can be seen how the changing values of vibration when changing material thickness of one species. This shows that the type of abrasives, material thickness and topography of the product has a direct impact on the AWJ technology and its quality and vibration. [13]



Figure 9 Orbital parameters - addition (Barton) abrasive grain size, mesh size (50), material thickness 6 mm. [13]

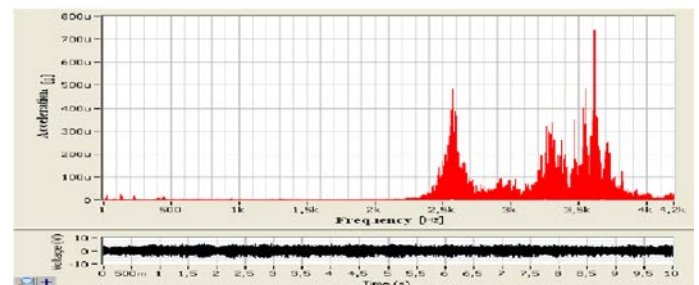


Figure 10 Orbital parameters - addition (Barton) abrasive grain size, mesh size (50), material thickness 15 mm. [13]

VII. CONCLUSION

From this knowledge and measurements are shown the results of the analysis charts, the vibration change during the manufacturing process according to the thickness of the material. The greater thickness of the material by the meter records the greater the intensity of vibration. This increase in vibration intensity has been shown in Fig. 9 and Fig.10. Graphs are used to compare the intensity of vibration at selected thicknesses of one type of material, the thickest and the thinnest material in the same grit abrasives and mesh sizes.

The evaluation of measured and recorded acoustic emissions during material separation as previously negative phenomenon, can contribute to improving the quality of the working environment and the subsequent correction measures and the management process, setting the appropriate technological parameters. From experiments and defining the

manufacturing process mathematical equations, the authors establish a general equation form, which can be used on any material and cutting conditions. [11]

The most significant impact on worker has the technology producing noise arising from the electric motor, high-pressure water pump, water flow through the nozzle, a transport system for abrasive and finally cutting the material. In addition to the water jet technology also create the ambient noise produced by vibration and also the heat during the production process. Adverse effect on the environment can occur in renal water jet cutting system and leakage of oil from the high pressure pump, evasion and avoidance abrasive fluid mixed with abrasive and debris.

Technology cutting water jet largely contributed to environmental protection. Cutting process is clean, does not in fact have any dust, which does not occur by the chemical pollution of the air. Debris, resulting in the cutting process with abrasive is gathered and extracted sludge system. Maximum utilization of material, the use of zero as an emulsion in classical machining, is nowadays regarded as a strength of the production technology

ACKNOWLEDGMENT

In conclusion, we would like to express thanks for the support of the projects SGS-2012-063 titled "Integrated design of manufacturing system as metaproduct with a multidisciplinary approach and with using elements of virtual reality" and project NEXLIZ – CZ.1.07/2.3.00/30.0038, which is co-financed by the European Social Fund and the state budget of the Czech Republic, and the project KEGA 032TUKE-4/2012, KEGA 049TUKE-4/2012

REFERENCES

- [1] KORINEK, P.: Vizualizácia vybraných algoritmov a vlastnosti z teórie grafov. Diplomová práca. Bratislava: UK FMFI, 2006. 70 s.
- [2] BADIDA a kol.: Uplatnenie akustickej kamery v priemysle. In Strojársstvo. roč. 2012, číslo 4, s 2-5.
- [3] Akustická kamera [online]. [cit. 2014-04-3]. Available at: <<http://www.ekolagroup.cz/cs/akusticka-kamera/>>.
- [4] Uplatnenie akustickej kamery v priemysle [online]. [cit. 2014-04-3]. Available at: <<http://www.design.engineering.sk/index.php/clanky2/stroje-a-technologie/937--uplatnenie-akustickej-kamery-v-priemysle>>.
- [5] Microphone arrays [online]. [cit. 2014-04-3]. Available at: <<http://www.acoustic-camera.com/en/products/microphone-arrays.html>>.
- [6] Norsonic sources [online]. [cit. 2014-04-3]. Available at: <http://www.norsonic.com/en/products/noise_sources/>.
- [7] SMETANA, C. a kol.: Hluk a vibrace, měření a hodnocení. Praha. Praha, 1988. 188 s. ISBN 80-901936-2-5.
- [8] Termovízná diagnostika [online]. [cit. 2014-04-3]. Available at: <http://www.unms.sk/?termovizna_diagnostika>.
- [9] HRETHA, P. et al.: Analysis of acoustic emission recorded during monitoring of abrasive waterjet cutting of stainless steel AISI 309. In: Technical Gazette. Volume 19, 2012, issue 2, p. 355-359.
- [10] BADIDA, M., J. KMEC, L. SOBOTOVÁ, Ľ. BIČEJOVÁ a M. GOMBÁR, 2013 : Hydroerosion and Environment. Edition first, Lüdenscheid, Germany : Ram-Verlag. 131 p.. ISBN 978-3-942303-20-0.
- [11] LAZAR, I.: Využitie akustických emisií v technológii hydorabrazívneho delenia, In: MM průmyslové spectrum, rubrika trendy/ Obrábění, roč. 2011, č.6, s.45-47, ISSN 1212-2572
- [12] LEBAR, A. et al.: Method for online quality monitoring of AWJ cutting by infrared thermography. In: CIRP Journal of Manufacturing Science and Technology. Volume 2, 2010, issue 3, p. 170-175.
- [13] BIČEJOVÁ, Ľ.: Abrasive kind and granularity changes affects to water jet technology head vibration during cutting HARDOX material thickness alternation process, IN: Operation and diagnostics of machines and production systems operational state, 2007, p.270-275, ISBN 9788073996345
- [14] BADIDA, M., SOBOTOVÁ, L., KMEC, J.: Environmental approach to abrasive recycling for AWJ, In :SGEM 2012, Conference Proceedings : 12th International Multidisciplinary Scientific Geoconference, 2012, č.4,693-700 s., ISSN:1314-2704
- [15] HLAVÁČ, L. M., I. M. HLAVÁČOVÁ, L. GEMBALOVÁ, J. KALČINSKÝ, S. FABIAN, J. MEŠTÁNEK, J. KMEC a V. MÁDR. 2009 : Experimental method for the investigation of the abrasive water jet cutting quality. In: Journal of Materials Processing Technology. Vol. 209, no. 20, 6190-6195 p., ISSN 0924-0136 Spôsob prístupu: <http://www.sciencedirect.com>.
- [16] KMEC, J., D. KUČERKA, M. GOMBÁR, Ľ. BIČEJOVÁ, L. SOBOTOVÁ, L. OPEKAROVÁ, J. STRAKOVÁ, A. VAGASKÁ a R. HRMO, 2014 : Waterjet for Practice. Edition second, Lüdenscheid, Germany : RAM- Verlag. 150 p.. ISBN 978-3-942303-27-9
- [17] KMEC, J., D. KUČERKA, M. GOMBÁR, R. HRMO a Ľ. BIČEJOVÁ. 2014 : Delenie materiálov. 1. vyd. Košice: Technická univerzita v Košiciach, 287 s.. ISBN 978-80-553-1872-1.
- [18] Salesmen presentation; KMT GmbH-KMT Waterjet System : KMT Creating value through precision,15slide, Germany 77 s
- [19] KMEC, J., E. SPIŠÁK, D. KUČERKA, S. RUSNÁKOVÁ, R. HRMO, M. GOMBÁR a Ľ. BIČEJOVÁ., 2014 : Materiály pre automobilový priemysel. 1. vyd. Košice: Technická univerzita v Košiciach, 220 s.. ISBN 978-80-553-1862-2. Podrobnejšie : <https://is.vstecb.cz/publication/25981>
- [20] https://www.google.cz/search?q=delenie+vodn%C3%BDm+1%C3%BA%C4%8Dom&espv=2&biw=1920&bih=955&source=lnms&tbm=isch&sa=X&ei=CczlVNTTG4PuUkQWhLAO&ved=0CAYQ_AUoAQ#imgdii=&imgsrc=ivcPMOXyHE99eM%253A%3BErZR6rHLAznwrM%3Bhttp%253A%252F%252Fwww.revolt.sk%252Fuploads%252Fprojects_fotky%252F640e0a4ab8ef7fc25ceca83ab2481886.jpg%3Bhttp%253A%252F%252Fwww.revolt.sk%252Fsk%252Frezanie-vodnym-lucom%3B1024%3B768
- [21] <http://www.microstep-europa.de/sk/produkty/rezacie-zariadenia/zariadenia-na-rezanie-vodnym-lucom.aspx?ProdID=38>
- [22] <http://www.techpark.sk/technika-52009/rezanie-materialov-vodnym-lucom-v-hazardnom-prostredi.html>
- [23] Xinology Co.: Water jet cutting machine , 1989– 2013, Available at: <http://xinology.com:888/GlassProcessing-Equipments-Supplies-onsumables/glass-cutting/water-jet-cutting/overview/twotypes-of-water-jet.html>
- [24] JANUŠKA, M., ŠŤASTNÁ, L. Industrial Engineering in the Non-Manufacturing Processes. In Proceedings of The 22nd International Business Information Management Association Conference. neuveden: International Business Information Management Association (IBIMA), 2013. s. 747-766. ISBN: 978-0-9860419-1-4
- [25] JANUŠKA, M. Communication as a key factor in Virtual Enterprise paradigm support. In Innovation and Knowledge Management: A Global Competitive Advantage. Kuala Lumpur: International Business Information Management Association (IBIMA), 2011. s. 1-9. ISBN: 978-0-9821489-5-2
- [26] LUMNITZER, E., BADIDA, M. ROMANOVA, M.: Hodnotenie kvality prostredia, Košice 2007, 281 s., ISBN: 978-80-8073-836-5
- [27] Nový, R.: Hluk a chvění, ČVUT, Praha 2000, 389 s., ISBN: 80-01-02246-3
- [28] Podafil, M., A. Kubala, D. Kučerka, J. Kmec a J. Cech : Frames for cycles. The European Community design (Evropský průmyslový vzor Společenství) č. 002592626, Alicante Spain, OHIM – OFFICE FOR HARMONIZATION IN THE INTERNAL MARKET. TRADE MARKS AND DESIGNS. Registered 08/12/2014, No 002592626-0001, 4 p.
- [29] Podafil, M., A. Kubala, D. Kučerka, J. Kmec a M. Mládek : Frames for cycles. The European Community design (Evropský průmyslový vzor Společenství) č. 002592626, Alicante Spain, OHIM – OFFICE FOR HARMONIZATION IN THE INTERNAL MARKET. TRADE MARKS AND DESIGNS. Registered 08/12/2014, No 002592626-0002, 4 p.

- [30] Podařil, M., A. Kubala, D. Kučerka, J. Kmec a J. Duchoň : Frames for cycles. The European Community design (Evropský průmyslový vzor Společenství) č. 002592626, Alicante Spain, OHIM – OFFICE FOR HARMONIZATION IN THE INTERNAL MARKET. TRADE MARKS AND DESIGNS. Registered 08/12/2014, No 002592626-0003, 4 p.
- [31] SPIŠÁK, E., J. MAJERNÍKOVÁ, M. GOMBÁR, A. VAGASKÁ, J. KMEC a F. STACHOWICZ, 2014 : Experimental study of the physical factors' influence on microhardness of AAO layers generated on material's AW-1050A. In: Acta Metallurgica Slovaca. Roč. 20, č. 2, s. 160-166. - ISSN 1335-1532. Spůsob přístupu: <http://www.ams.tuke.sk/>.
- [32] VAGASKÁ, A., J. KMEC, M. GOMBÁR a P. MICHAL. 2014 Implementation of method and structure handling manipulation operations to hydroabrasive process. In: Applied Mechanics and Materials, Switzerland: Trans Tech Publications, č. 616, s. 35-43. ISSN 1660-9336. doi:10.4028 /www.scientific.net/AMM.616.35. Podrobněji : <https://is.vstecb.cz/publication/25483>.
- [33] MICHAL, P., A. VAGASKÁ, M. GOMBÁR a J. KMEC. 2014 : Mathematical modelling and optimization of technological process using design of experiments methodology. In: Applied Mechanics and Materials, Switzerland: Trans Tech Publications, s. 61-68. ISSN 1660-9336. doi:10.4028/www.scientific.net/ AMM.616.61. Podrobněji: <https://is.vstecb.cz/publication/25863>.
- [34] MICHAL, P., A. VAGASKÁ, M. GOMBÁR, J. KMEC, E. SPIŠÁK a M. BADIDA. 2014 : Prediction of the effect of chemical composition of electrolyte on the thickness of anodic aluminium oxide layer. International Journal of Mathematical Models and Methods in Applied Sciences, USA: North Atlantic University Union NAUN, vol. 8, č. 1, p. 152-155. ISSN 1998-0140. Podrobněji : <https://is.vstecb.cz/publication/25781>.
- [35] BADIDA, M., L. SOBOTOVÁ a J. KMEC, 2012 : Environmental approach to abrasive recycling for AWJ. 1. elektronický optický disk (CD-ROM). In: SGEM 2012 : 12th International Multidisciplinary Scientific GeoConference : conference proceedings : Volume 4 : 17-23 June, Albena, Bulgaria. Sofia : STEF92 Technology Ltd., p. 693-700. ISSN 1314-2704.
- [36] Rusnáková, S.- Kučerka, D.-Podařil, M.-Kmec, J.-Rusnák, V.-Bičejová, V.: Influence of Processing Parameters Production of Sandwich Composite Structures Designed Especially for the Construction of Machine Tool Parts. In: Applied Mechanics and Materials (Volume 616). Editor: Stanislav Fabian and Tibor Krenicky, 2014.s.333-343.
- [37] RUSNÁKOVÁ, S.- KUČERKA, D.-HUSÁR, Š.-HRMO, R.- KUČERKOVÁ, M.- RUSNÁK, V.: Education in Composite Materials. 16 International Conference on Interactive Collaborative Learning. ICL 2013: sborník příspěvků. 1. vyd. Kazaň: CTI Villach, Kazan National Research Technological University, 2013. s. 216-221, 6 s. ISBN 978-1-4799-0152-4.
- [38] KUČERKA D., RUSNÁKOVÁ S., HUSÁR Š., KUČERKOVA M., HRMO, R.: Research in engineering pedagogy. 16 International Conference on Interactive Collaborative Learning : sborník příspěvků. 1. vyd. Kazaň: CTI Villach, Kazan. National Research Technological University, 2013. s. 30-35, 6 s. ISBN 978-1-4799-0152-4.
- [39] HRMO, R., KUČERKA, D., KRIŠTOFIAKOVÁ, L.: Developing the Information Competencies via E-learning and Assessing the Qualities of E-learning Text. 15th International Conference on Interactive Collaborative Learning and 41st International Conference on Engineering Pedagogy. Villach, Austria, 26 – 28. 9. 2012, s. ISBN 978-1-4673-2426-7.
- [40] HRMO, R.- KUČERKA, D. Information competence and evolution of e-learning text with the fog index. Interactive Collaborative learning: 14th International Conference on Interactive Collaborative Learning (ICL2011) □ 11th International Conference Virtual University, Piešťany, 21.-23. september 2011, s. 390-394. ISBN 978-1-4577-1746-8.
- [41] TREBUŇA, P. - KLIMENT, M. - FILO, M.: Optimization and Elimination of Bottlenecks in the Production Process of a Selected Company / Peter Trebuňa, Marek Kliment, Milan Filo - 2014. In: Applied Mechanics and Materials. Vol. 611 (2014), p. 370-375. - ISSN 1660-9336
- [42] KLIMENT, M. - TREBUŇA, P. - STRAKA, M.: Tecnomatix plant simulation, its features and its integration into business processes in logistics systems / Marek Kliment, Peter Trebuňa, Martin Straka - 2014. In: American Journal of Mechanical Engineering. Vol. 2, no. 7 (2014), p. 286-289. - ISSN 2328-4102

THE WATER TEMPERATURE SIMULATION IN THE MORAVA RIVER BASIN WATERCOURSES

Dana Halmova, Pavla Pekarova, Jan Pekar, Katarina Kucarova

Abstract— The study is focused on water temperature simulation in watercourses in the Morava River basin and its dependence on expected increase of maximum daily air temperature. Our aim is to assess influence of possible air warming on water temperature increase in watercourses. In the process of data handling have used: series of average daily water temperature measured in 21 watercourses in the Morava River basin and mean daily air temperature series at Bratislava Airport, period 2006–2011. Scenarios for extreme monthly air temperatures at station Bratislava Airport have been calculated on the basis of statistical analysis of daily air temperatures for period 1951–2011. Extreme water temperatures have been simulated from the scenario of air temperatures by calibrated ARIMA models. Results of simulations show, that in case of maximum air temperature increase by 1°C the water temperature will rise by 0.7°C–0.9 °C, depending on models used.

Keywords— autoregressive models, ARIMA models, water temperature simulation, climate change.

I. INTRODUCTION

THE water temperature is one of the main physical characteristics of the surface water. It directly influences the biota of the streams and adjacent land. The water temperature significantly influences other physical and chemical properties of the water. The productivity of the total water ecosystem does not only depend on the water temperature, but it is in great extent limited by the water temperature [1]. The factors that affect the water temperature can be generally divided into four groups [2]:

1. Atmospheric conditions - solar radiation, air temperature,

This work was supported in part by Agency VEGA under the contract VEGA 2/0009/15 and results from the project implementation of the “Centre of excellence for integrated flood protection of land” (ITMS 26240120004) supported by the Research & Development Operational Programme funded by the ERDF.

D. Halmova is with Institute of Hydrology Slovak Academy of Sciences, Raciarska 75, 831 02 Bratislava, Slovakia, (e-mail: halmova@uh.savba.sk).

P. Pekarova is with Institute of Hydrology Slovak Academy of Sciences, Raciarska 75, 831 02 Bratislava, Slovakia (phone: +4212 44259311, Fax: +4212 44259311, e-mail: pekarova@uh.savba.sk).

J. Pekar is with the Faculty of Mathematics, Physics and Informatics, Comenius University, Bratislava, Slovakia (e-mail: pekar@fmph.uniba.sk).

K. Kucarova is with Ministry of Environment of the Slovak Republic, (e-mail: katarina.kucarova@enviro.gov.sk).

wind speed, precipitation, evaporation, condensation...

2. Topographic conditions - altitude, latitude basin, flow orientation, coastal vegetation, subsoil...

3. The hydrological regime of flow - discharge, flow velocity and depth of stream, level and temperature of groundwater...

4. Anthropogenic activities in the basin - discharge of urban and industrial waste water, flow reduction [3], artificial reservoirs [4] and diversion canals and removal of riparian vegetation [5].

Some Slovak hydrologists dealt with statistical analysis of low flows in water streams in Eastern Slovakia, to which is attached the low water level in the stream [6]. The main objective of their work was to identify low flow trends in the selected 63 river stations in Eastern Slovakia in time period 1975–2012.

II. MORAVA RIVER BASIN CHARACTERISTIC

The Morava River is a left tributary of the Danube and Morava basin is mostly located in the Czech Republic. Catchment area of Morava River in estuary into the Danube is about 26 580 km², of which in Slovakia is only 2 282 km², representing 8.6% of the whole catchment area and 4.65% of the Slovak Republic area, (Fig. 1).

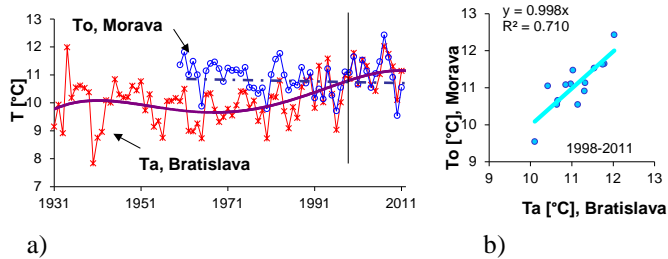


Fig. 1 Morava River basin at the national level

In terms of water balance, sub-basin of Moravia is the catchment lowest rainfall (614 mm) as well as outflow (109 mm). The Morava River basin is characterized by

a drainage system with a maximum average monthly flows during the spring season (March and April) and smallest average monthly discharges in the summer - autumn (August and September). The regime of small water levels is an important phase of the hydrological cycle, which is associated with the occurrence of minimum flows. Low flows are concentrated during two periods: summer-autumn period with a minimum in the months of August to October, and in winter depression usually with a minimum in January.

Fig. 2 shows the relation between the mean annual water temperature (T_o) of the Morava River at station Záhorská Ves and the mean annual air temperature (T_a) in station Bratislava Airport, 1956–2011. In Fig. 2a we can see that the mean annual temperatures of both series are identical since the year 1991. The mean annual water temperature corresponds to the mean annual temperature of the environment through which the river flows. The air temperature increased in the period 1971–1998. In case of water temperature the increase was much more moderate in last twenty years.



a) Fig. 2 a) Long-term trend of the mean annual air temperature (T_a) in Bratislava (1931–2011) and of the mean annual water temperature (T_o) of the Morava River at station Záhorská Ves (1955–2011). b) Relation between mean annual water temperature (T_o) of the Morava River at station Záhorská Ves and the air temperature (T_a) in Bratislava, period 1998–2011.

Since the period of introducing the automatic measuring stations the mean annual air and water temperatures are identical and the relation between them is very close (Fig. 2b). The long-term water temperature trend of the Morava river was evaluated from the series of mean annual water temperature (T_o) and maximal annual water temperature (T_o, \max) in the period 1956–2010. The mean annual water temperature of the Morava River was decreasing in 1956–1996, but since 1996 the trend is increasing. The series of maximal annual water temperature does not show neither increasing nor decreasing trend, [7].

Average daily water temperature at selected stations Morava River basin indicate the type-specific and seasonal course of temperature (Fig. 3).

Specific decreasing trend in water temperature was observed at the gauging station Myjava: Myjava (dark green) in the period 2009–2011.

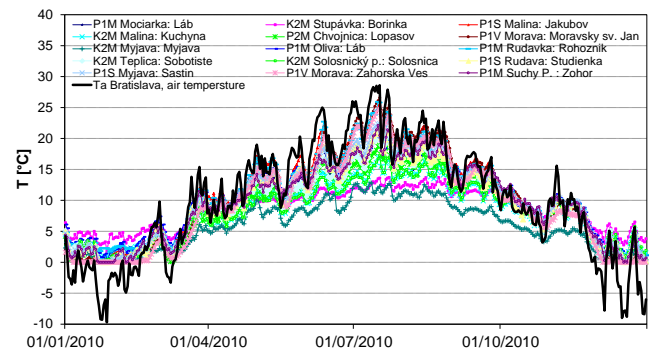


Fig. 3 Measured water temperature T during the year 2010 at chosen gauging stations in the Morava River basin, T_a - air temperature - Bratislava

III. THE SIMULATION OF THE WATER TEMPERATURE DEVELOPMENT

A. Autoregressive Models

Linear autoregressive models represent the very suitable means to describe the periodic time series with strong stochastic character. They are simple autoregressive models of the processes AR (p), MA (q) and the combination of ARMA (p, q) as well as the integrated form ARIMA (p, d, q). ARIMA model has several advantages. It is highly flexible, fast responds and adapts to changing the nature of the test process. The model is able to model the stochastic seasonality even trend better than the classical time series analysis [8]–[14]. In this work we have used several types of ARIMA models with additional regression component - the air temperature.

B. Input data

Input data for autoregressive models testing are monthly series of the maximum average daily water temperature in selected rivers in the Morava River basin (Myjava: Šaštín–Stráže, Močiarka: Láb, Morava: Záhorská Ves and Stupávka: Borinka), Fig. 4.

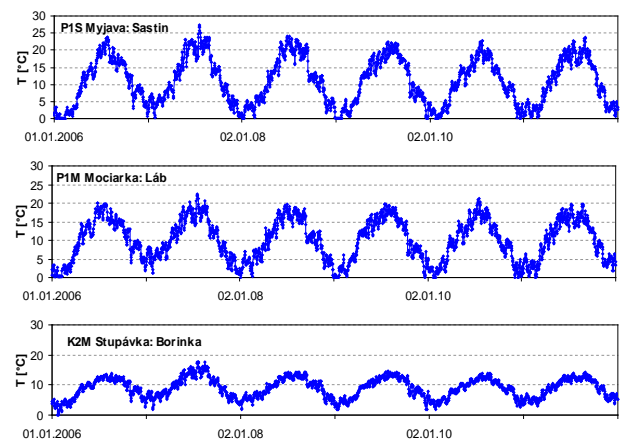


Fig. 4 Measured water temperature T at station Myjava: Šaštín–Stráže, Močiarka: Láb and Stupávka: Borinka in the Morava River basin. (Axis-x period 2006–2011).

Selected hydrometric stations represent three types of rivers (small, medium and large) and in their surrounding area was not located significant source of anthropogenic effects. As a regressor the monthly series of maximum average daily air temperature in the Bratislava Airport station were used. For the statistics processing the average daily water temperatures series, calculated from hourly data, are used.

C. Model calibration and verification

Six years period 2006–2011 was used for calibration. The choice of the time period was associated with a gradual transition to the automatic hourly hydrological data collection since 2006 and thus better comparability of water temperature measurements of. That period also includes the period with average water temperatures as well as a period of hydrological and climatic extremes (drought, flood period). The models were verified such a way that a period of parameters calibration was reduced by one year (2006–2010), and the last year 2011 (12 values) was used for model verification.

D. Choice of the autoregressive model

The process of model selection is presented on data from gauging stations Myjava: Šaštín–Stráže for the period 2006–2011. Following autoregressive models simulations were tested (with air temperature as regressor): (A) ARIMA(1,0,1)x(1,0,1)12 + 1 regressor; (B) ARIMA(1,0,0) + 1 regressor; (C) ARIMA(1,0,0) with constant + 1 regressor; (D) ARIMA(1,0,1) + 1 regressor; (E) ARIMA(1,0,1) with constant + 1 regressor.

Procedure for autoregressive models testing is shown in the model simulation (A). When testing other model simulations of (B)–(E), we proceed by analogy. The regressor was the monthly maximum of mean daily air temperature at station Bratislava Airport for the same time period. The resultant parameters of the model simulation (A) ARIMA (1,0,1)x(1,0,1)12+1 regressor are given in Table 1. The values of the significance of each model parameters were less than 0.05, so any parameter of the model has not excluded. The comparison of the prediction results is in Table 2 for selected five models.

Table 1 Parameters of the model ARIMA (1,0,1) x (1,0,1) 12 + 1 regressor Tam Br (air temperature Bratislava Airport)

Parameter	Estimate	Std. Error	T-test	P-value
AR(1)	0.101838	0.0419494	2.42764	0.017850
MA(1)	-0.490689	0.1147440	-4.27637	0.000061
SAR(1)	0.112752	0.0334248	3.37329	0.001230
SMA(1)	-0.707946	0.0794354	-8.91222	0.000000
Tam Br	0.661843	0.0295140	22.42470	0.000000

Where: AR (1) - autoregressive member, MA (1) - moving average model, SAR (1) - seasonal autoregressive member, SMA (1) - Member of the seasonal moving averages, Tam Br - air temperature at the Bratislava Airport, Estimate - Preliminary calculation, Std. Error - standard deviation, T-test verification of normal distribution, P-value - significance level; thereby the value P is higher the dependency is lower. P-values less than 0.05 indicate a significant dependence.

Table 2 Comparison of predictions for the 5 selected models

Model	RMSE	RUNS	RUNM	AUTO	MEAN	VAR
(A)	1.11349	OK	OK	**	OK	OK
(B)	1.58388	OK	**	***	OK	***
(C)	1.45784	OK	**	OK	OK	**
(D)	1.43085	OK	OK	**	OK	OK
(E)	1.38074	OK	OK	OK	OK	OK

Where: RMSE = residual standard deviation; RUNS = number of rising and falling courses; Runm = number of traces above and below the median; AUTO = Box-Pierce test of auto-correlative course; MEAN = t-test; VAR = F-test; OK = not significant ($p \geq 0.10$), * = 90% limit/interval of reliability/confidence interval, ** = 95% limit/interval of reliability/confidence interval, *** = 99% limit/interval of reliability/confidence interval.

Based on the results from the statistical characteristics and the characteristics of the degree of accuracy of the individual models tested, the most suitable for the specified criteria appear models with the parameters A and E.

IV. RESULTS OF WATER TEMPERATURE SIMULATION

The objective of the simulation was to predict the effect of increasing of the maximum monthly air temperature to the maximum monthly water temperature of selected types of flows. For this purpose it was necessary to create a scenario of maximum monthly air temperatures in the Bratislava Airport using measured daily air temperatures during the period 1951–2010.

Following scenarios of maximum monthly air temperature were created: 1. The first scenario (Scen1) represents the maxima of monthly maximum air temperature during 60-years period 1951–2011; 2. The second scenario (Scen1+1) was created adding 1°C to Scen1; 3. The third scenario (Scen+2) was created adding 2°C to Scen1.

The simulation results of the maximum monthly water temperatures of the Myjava River at Šaštín–Stráže station are in Table 3 according to two autoregressive models for one air temperature scenarios Scen1+1, see also Fig. 5.

Table 3 Results of maximum daily water temperature simulation To in Myjava River based on scenario Scen1 + 1 according to two models

month	Model A ARIMA(1,0,1)x(1,0,1)12 + 1 regressor			Model E ARIMA(1,0,1) with constant + 1 regressor		
	To[°C]	To, upper limit [°C]	To, lower limit [°C]	To[°C]	To, upper limit [°C]	To, lower limit [°C]
I.	8.6	11.0	6.2	10.6	13.4	7.9
II.	11.7	14.4	9.0	12.8	16.0	9.7
III.	14.6	17.3	11.9	14.9	18.1	11.8
IV.	16.0	18.7	13.3	17.9	21.0	14.7
V.	22.9	25.6	20.2	22.2	25.3	19.0
VI.	24.4	27.1	21.7	24.3	27.5	21.2
VII.	26.0	28.7	23.3	26.4	29.5	23.2
VIII.	26.0	28.8	23.3	26.1	29.2	22.9
IX.	22.9	25.6	20.2	23.3	26.4	20.1
X.	17.7	20.5	15.0	19.3	22.4	16.1
XI.	14.1	16.8	11.4	16.5	19.7	13.4
XII.	12.0	14.7	9.2	12.9	16.1	9.7

Values in Table 3 show that in case of maximum air temperature increase by 1°C the water temperature will rise by 0.7°C according to model A. The upper 95% limit represents the extreme water temperatures that could be achieved.

Analogically the water temperature simulations were calculated for stations Morava: Záhorská Ves and Stupávka: Borinka.

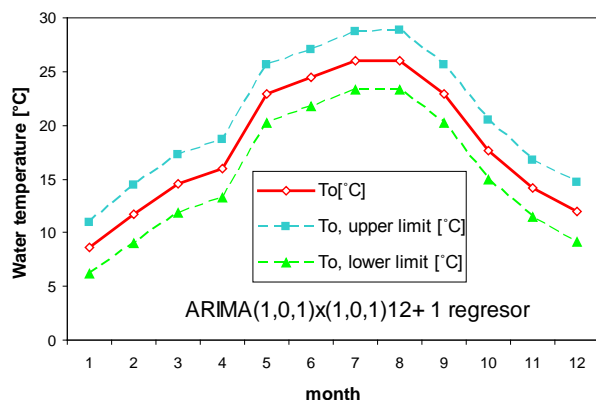


Fig. 5 Results of maximum daily water temperature simulation in gauging stations at Myjava: Šaštín-Stráže, based on scenario Scen1+1 (solid line) according to two models A, upper and lower 95% limit (dashed lines).

V. CONCLUSION AND DISCUSSION

The paper is focused on one of the most recent topics: development of water temperature in streams in the context of climate change [15].

The Morava River basin has been chosen as a pilot area. Within this area were selected 3 hydrometric stations. The aim was to assess the effects resulting from possible warming air to water temperature. For this purpose 3 scenarios of extreme monthly air temperatures in the Bratislava Airport were prepared. It can be concluded that the increase of the maximum air temperature by 1°C water temperature causes increase of water temperature by an average of 0.7°C (model A) and of 0.9°C (model E) respectively. Between small, medium and large rivers no significant difference was found. It should be noted that this case is a case study processed based on selected criteria for 3 hydrometric stations where the air temperature as regressor has priority. When testing the water flow as regressor no significant dependence of water flow and water temperature was demonstrated. This may be caused by high dependence of air temperature and water temperature, which was more dominant than the dependence of water temperature and flow. The water temperature increases with increasing air temperature and flow rates mostly decline (particularly dry summer months). It is possible that, for a constant flow rate test vs. scenarios of temperature fluctuations, the mutual regression could show a stronger dependence for small, medium and large flows.

Water temperature plays a key role in environmental, biochemical as well as chemical point of view. Increase in

water temperature, e.g. during extreme and long-lasting heat waves and drought, can cause undesirable chemical and biochemical reactions. The adverse reactions may be primary or secondary affect the quality as well as status of surface water possibly groundwater. Water temperature for its high correlation with air temperature belongs to the parameters within which are not directly propose measures for its reduction.

REFERENCES

- [1] T. Derka, <http://www.fns.uniba.sk/prifuk/skripta/kek/t2.htm>, 1999.
- [2] D. Caissie, "The thermal regime of rivers: a review," *Freshwater Biology*, 51, 1389–1406, 2006.
- [3] B. A. Sinokrot and J. S. Gulliver, "In-stream flow impact on river water temperatures," *Journal of Hydraulic Research*, 38, 339–349, 2000.
- [4] Lowney, C.L., "Stream temperature variation in regulated rivers: evidence for a spatial pattern in daily minimum and maximum magnitudes," *Water Resources Research*, 36, 2947–2955, 2000.
- [5] S. L. Johnson and J. A. Jones, "Stream temperature response to forest harvest and debris flows in western Cascades, Oregon," *Canadian Journal of Fisheries and Aquatic Science*, 57, 30–39, 2000.
- [6] M. Zelenakova, P. Purcz, T. Solakova, and D. Simonova, "Statistical Analysis of Low Flows in Eastern Slovakia," *Advances in Environmental Sciences, Development and Chemistry*, 181–185, 2014.
- [7] K. Kucarova, M. Valuchova, I. Bartik, K. Melova, and R. Magulova, "Evaluation of the ecological status of rivers in Slovakia," (in Slovak) Part 4: Podporné prvky kvality - fyzikálno-chemické a hydromorfologické, *Vodohospodársky spravodajca*, 11-12, ISSN: 0322-886X, 2008.
- [8] G. E. P. Box, G. M. Jenkins, and G. C. Reinsel, "Time Series Analysis, Forecasting and Control," 3rd ed. Prentice Hall, Englewood Cliffs, NJ., 1994.
- [9] M. Komornikova, J. Szolgay, D. Svetlikova, and D. Szokeova, "Combined deterministic – stochastic forecasting of monthly river flows," *Geophysical Research Abstracts*, EGU General Assembly, Vol. 10, EGU2008-A-05501, SRef-ID: 1607-7962/gra/EGU2008-A-05501, 2008.
- [10] M. Komornikova, J. Szolgay, D. Svetlikova, D. Szokeova, and S. Jurcak, "A hybrid modeling framework for forecasting monthly reservoir inflows," *J. Hydrol. Hydromech.*, 56, 3, 145–162, 2008.
- [11] D. Svetlikova, M. Komonikova, S. Kohnova, J. Szolgay, and K. Hlavcova, "Analysis of discharge and rainfall time series in the region of the Káštorské lúky wetland in Slovakia," XXIVth conference of the Danubian countries on the hydrological forecasting. Conference E-papers. Bled, 12 pp., 2008.
- [12] T. Burt and F. Worrall, "Non-stationarity in long time series: some curious reversals in the 'memory' effect," *Hydrological Processes*, 21, 3529–3531, 2007.
- [13] P. Pekarova, Miklanek, and J. Pekar, "Long-term prediction of the draughts in the Danube and Elbe basins: role of NAO and use of periodicities," In Pollution and Water Resources, Columbia University Seminar Proceedings: Environmental Protection of Central Europe and USA. vol. XL, 2010-2011. - Bratislava; Pécs: Institute of Hydrology SAS: Hungarian Academy of Sciences, 208–236, 2011.
- [14] J. Pekar, "Autoregression models of gross domestic product," (in Slovak). UK Bratislava, Slovakia, 146 pp., 2004.
- [15] WFD (Water Frame Directive) 2000/60/EC of the European Parliament and of the Council of the 23 October 2000, establishing a framework for Community action in the field of water policy.

Measurement results of longitudinal dispersion coefficient in urban sewer networks under dry weather conditions.

Marek Sokáč, Yvetta Velísková

Abstract— One of the main tasks of water management is to achieve good water quality. Important auxiliary tools in this case are mathematical models that currently are incorporated in almost every mathematical model, used to solve problems in everyday practice of water. A dispersion coefficient is one of the crucial input parameters of transport processes.

The paper is focused on determination of dispersion coefficients in sewers, as in prismatic and straight stream channel with relatively constant roughness of streambed. Field experiments were performed in a straight sewer sections under dry weather flow conditions, i.e. with relatively low pipe filling, discharges and velocities. Consequently the dispersion coefficient in a sewer line with various direction changes was determined.

In the end of the paper the observed effect of "dead zones" is described, which theoretically should not occur in conditions of our experiment (prismatic channel with no obstacles) and explain its root cause.

Keywords—Dispersion, flow with free surface, longitudinal dispersion coefficient, sewer network.

I. INTRODUCTION

Dispersion, from hydrodynamic point of view, is the spreading of mass from highly concentrated areas to less concentrated areas in flowing fluid. Mass in flowing water is not transported only in the reach of streamline, but it is also gradually spreading to outside in consequence of velocity pulsations and mass concentration differences. Mass dispersion with advection is basic motion mechanics of particles, transported in water. Reductions of maximum concentrations are results of their effects. The main characteristics of dispersion are dispersion coefficients in relevant directions. Determination of these dispersion characteristics is the key task for solving problem of pollutant transport in streams and for modelling of water quality.

The most simple description of the mass spreading in water is one-dimensional advection-dispersion equation, which

describes the phenomenon in longitudinal direction x (well-proportioned distribution of a mass concentration is required along a depth and a width of a stream). The form of this equation is:

$$\frac{\partial AC}{\partial t} + \frac{\partial QC}{\partial x} - \frac{\partial}{\partial x} \left(AD_L \frac{\partial C}{\partial x} \right) = -AKC + C_s \cdot q \quad (1)$$

where: C is a mass concentration (g.l^{-1}); D_L is the longitudinal dispersion coefficient ($\text{m}^2.\text{s}^{-1}$) - $D = df + \varepsilon$, where df is the coefficient of turbulent diffusion, ε is the coefficient of molecular dispersion, df is often disregarded, because $\varepsilon \gg df$; A is a discharge area in a stream cross-section (m^2), Q is a discharge in a stream ($\text{m}^3.\text{s}^{-1}$), K represents a rate of growth or decay of contaminant (s^{-1}), C_s is the concentration of a source, q is a discharge of a source, x is a distance (m), t is time (s).

Such one-dimensional approach is applicable for rivers or streams with comparatively non-wide channel or e.g. for sewers. In this case the pollutant spreading has markedly one-dimensional character.

As it follows from the abroad references [1], [3], [4], [5], [6], [7], [10], [12], [13], as well from our local ones [8], [11], the longitudinal dispersion coefficient D_L derivation is achieved by several ways: from the own experience or that from the references, over the qualified estimates, up the special calculations application. As dispersion coefficient value is determined by the turbulence intensity in the given stream section, its magnitude depends upon its main hydraulic characteristics: form and magnitude of its cross section profile, its flow velocity and its longitudinal slope.

Most of the published relations for the D_L determination are based on experimental results from laboratory physical models, or directly from the field measurements on the rivers. Such relationships are often in the following form:

$$D_L = p \cdot h \cdot u_* \quad (2)$$

where p is the empirical dimensionless coefficient, h is the mean river section depth (m), u_* is the friction velocity (m.s^{-1}).

Other form of equation for D_L prediction, which is based on

This work was supported in part by the project implementation ITMS 26240120004, by the 7th FP project „Goldfish“, FP7-ICT-2009-6, Grant agreement no: 269985 and VEGA project Nr. 1/0691/13.

Marek Sokáč is with the Department of Sanitary and Environmental Engineering, Faculty of Civil Engineering, Slovak University of Technology, Bratislava, phone +421 2 59274286, e-mail: marek.sokac@stuba.sk

Yvetta Velísková is with the Institute of Hydrology Slovak Academy of Science, Bratislava, e-mail: veliskova@uh.savba.sk

hydraulic parameters, is expressed in form [4]:

$$D_L = q \frac{u^2 B^2}{u_* h} \quad (3)$$

where q is the empirical dimensionless coefficient (according Fischer $q=0,011$), u is the mean velocity (m.s^{-1}), B is the surface width (m).

II. MATERIAL AND METHODS - FIELD MEASUREMENTS

The field measurements were performed near to the experimental hydrological base of Institute of Hydrology in Liptovský Mikuláš (Slovakia). The part of sewer network which was built in 2004-2005 under EU Cohesion Fund project „Environmental improvement of the Liptov region“ (more specifically the connecting collector between Liptovský Hrádok and Liptovský Mikuláš) was selected for field measurements.

The collector has profile DN 500 mm with slopes in range from 2‰ to 9.5 ‰. After more detailed reconnaissance there were selected two areas for field experiments – the first one is a straight sewer section above Podtureň village and the second part is closely to the place Borová Sihot', near Liptovský Hrádok. In both areas were several sewer sections with various length selected, with diverse tracer inlets and measuring stations (manholes). In every section was the experiment repeated at least three times to obtain three valid tracer concentration time courses.

In the second section there are three sewer direction changes (30° , 45° a 90°) in which the distributions of tracer concentration in time were measured at various parts of sewer. The aim was to determine the influence of these trajectory diversions on the dispersion coefficient.

The common (kitchen) salt (NaCl) was used as a tracer and this one influenced on the variation of wastewater flow conductivity. The coloring agent (fluorescein) was added to the tracer to monitor the passage of tracer substance in measuring profile. The dosage of tracer was 5 l and it was discharged to sewer instantly.

The measurement of conductivity was performed with electric conductivity meter device in measuring manhole. The conductivity meter probe was situated in the center of wastewater stream.

All measurements were performed in dry weather conditions, so the pipe filling ranges from 10 up to 25% of the pipe diameter. Velocity in the pipe was in range from 0.25 up to 1.2 m/s. A total of 61 tracer experiments were performed, but only about 54 datasets are identified as reliable for further data processing. The most common cause for dataset excluding was a missing part or irregular shape of the conductivity distribution in time due to measurement devices failures, etc.

The determination of longitudinal dispersion coefficient from experiment results was performed in two ways: the first one consists in simulation of tracer experiment (concentration

distribution) for various values of longitudinal dispersion coefficient.

The base for this numerical simulation is the analytical solution of (1) for instantaneous injection of tracer [2]:

$$C(x,t) = \frac{G}{2A\sqrt{\pi D_L t}} \cdot \exp\left[-\frac{(x - \bar{u}t)^2}{4 D_L t}\right] \quad (4)$$

where $C(x,t)$ is a mass concentration (g/l) in a place and time; D_L is the longitudinal dispersion coefficient (m^2/s); A is a discharge area in a stream cross-section (m^2), G is the mass of a tracer (kg), u is a mean velocity (m/s), x is a distance (m), t is time (s).

The difference between the measured and simulated values was evaluated. The minimum of difference squares determines the value of the longitudinal dispersion coefficient for each one of experiments. Although the probe was located in streamline it was ignored irregular distribution of concentration (conductivity) along the width of measuring profile. Due to this fact, we add a correction coefficient to the model calculations, which comes out from ratio of inflow and outflow tracer volume.

The second way for evaluation of the longitudinal dispersion coefficient is based on direct determination of the statistical parameters (σ , standard deviation) of the acquired conductivity time courses. Principle of this method is to find the time, corresponding to the 15.87 and 84.13 percentile of the cumulative concentration curve [14]. Distance of these two points is equal to 2σ and dispersion coefficient can be determined as

$$D_L = \frac{u^2 \sigma^2}{2t} \quad (5)$$

III. RESULTS

Output of field measurements is the record of tracer concentration time courses, deducted from the wastewater conductivity time courses in sewer. All results of field measurements in dimensionless form of time courses are shown on Fig 1. The examples of graphic expression of a single tracer time courses records (in real units) are shown in Fig. 2 and 3.

The evaluation of experiment results consists in simulation of tracer experiment (concentration distribution) for various values of longitudinal dispersion coefficient. The base for this numerical simulation is the analytical solution of (1) for instantaneous injection of tracer (4).

For experiment series with the lower discharge (and thus also the lower water level), the measurement processing revealed, that in the given measurement section, there are some stream flow (pipe) irregularities, creating a kind of the „dead zone“ in it. Most significantly this phenomenon showed up in section with the 90o curve (here were also the lowest

water depths) as shown on Fig. 2.

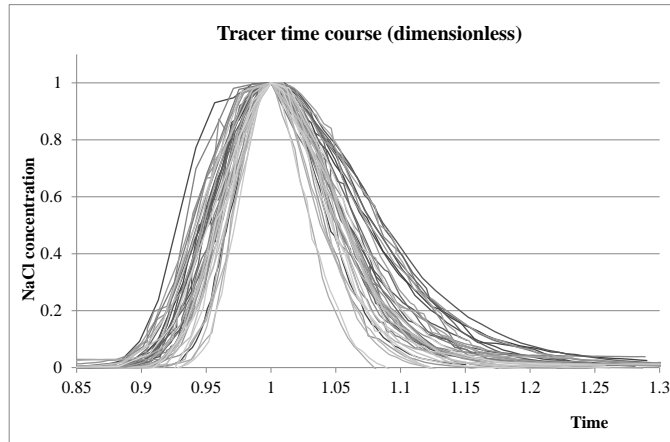


Fig. 1 Dimensionless graph of all traces experiments (max. concentration is equal to 1 in time equal to 1, background concentration is equal to zero)

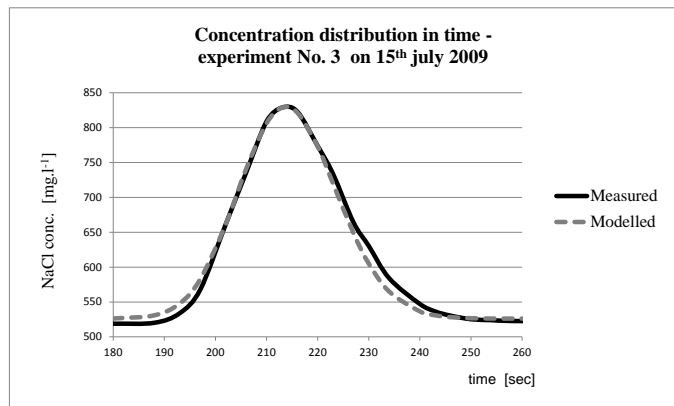


Fig. 2 Behaviour of concentration distribution in measuring profile (manhole Nr. 164), experiment Nr. 3, 15th July 2009 (inlet of tracer – manhole Nr. 166)

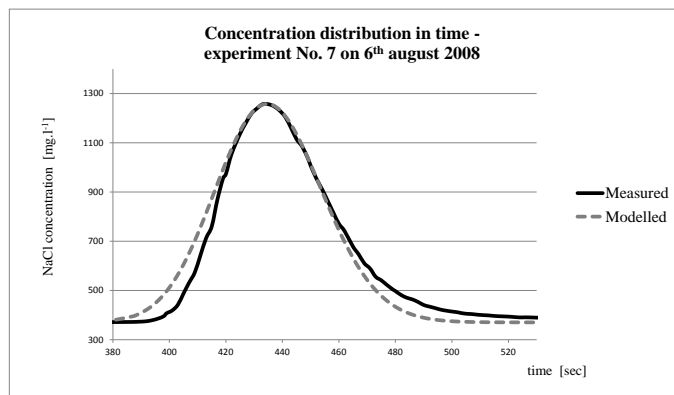


Fig. 3 Behaviour of concentration in measuring profile (manhole Nr. 127), experiment Nr. 7, 6th August 2008 (inlet of tracer – manhole Nr. 133)

In this dead zone the tracer has been accumulated and released gradually later. That distorts the conductivity time course curve, it becomes asymmetrical, and becomes a „tail“,

because of the later tracer release. This can be seen on both figures (Fig. 1. and Fig. 2).

IV. DISCUSSION AND CONCLUSION

The evaluation of longitudinal dispersion mass rate in surface streams is related closely to determination of the longitudinal dispersion coefficient. Its magnitude is influencing strongly the simulation and calculation results, related to this phenomenon. Therefore, it is necessary to determine its value most correctly.

It has to be reached by specification of information about the crucial input characteristics of transport processes and by formulating of relationships for determination of dispersion coefficients. The tracer experiments were located to the straight part and to the part with directional changes of sewer line. The analysis of measurement results and determination of dispersion coefficients for particular parts and measurements using both evaluation methods are shown in Table 1.

Conclusion after comparing both ways for determining the dispersion coefficient is, that the model approach generally gives lower values of D_L approximately by 10% (the range is from 50 to 110 %, average 89.2%), relating to the direct statistical parameters determination. Especially problematic were experiments with bigger irregularities (asymmetry) in shape of conductivity time courses.

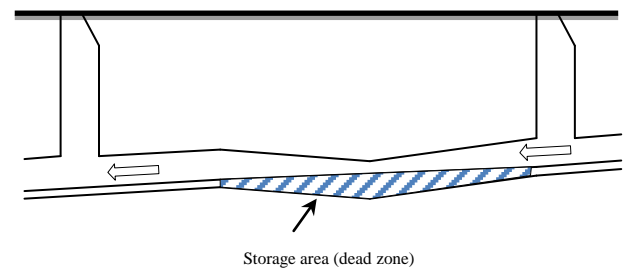


Fig. 4 Local backwater effects, acting as “dead zones” and causing tracer time course asymmetry

Explanation of the time course asymmetry, mentioned in previous chapter can be as following: time course of the tracer is principle always asymmetric, because of the advection and dispersion in flowing water related to the stationary placed measurement device; it results inter alia from the form of analytical solution (4). Further asymmetry related to the analytical solution is probably caused by local backwater effects (see Fig. 4), caused by irregular sewer pipes slope.

Table 1. Statistical results of field experiments

Evaluation method		Model approach			Statistical approach		
	Unit	Straight sewer line	Part with directional changes	Both parts together	Straight sewer line	Part with directional changes	Both parts together
Nr. of experiments	-	24	30	54	24	30	54
Average	$\text{m}^2 \cdot \text{s}^{-1}$	0,14	0,06	0,10	0,19	0,07	0,12
Max.	$\text{m}^2 \cdot \text{s}^{-1}$	0,20	0,24	0,24	0,65	0,24	0,65
Min.	$\text{m}^2 \cdot \text{s}^{-1}$	0,09	0,02	0,02	0,12	0,03	0,03
Std. deviation σ	$\text{m}^2 \cdot \text{s}^{-1}$	0,025	0,056	0,059	0,102	0,03	0,010

Such backwater acts in dry weather condition as tracer (pollutant) storage, it accumulate the tracer and slowly releases the tracer into the main stream. We assume that this phenomenon becomes evident especially in conditions of low discharges (dry weather flows) and of course in case of lower sewer construction quality (irregular slopes, sewer settlement due to the ground consolidation). These conclusions are confirmed also by fact, that in the section with lowest water depths (section with the 90° curve) was the time course asymmetry most evident.

This phenomenon should be taken into account also in models, simulating waste water quality in sewer networks.

ACKNOWLEDGMENT

This paper was prepared with the support of the Scientific Grant Agency VEGA within the scientific project Nr. VEGA 1/0691/13 "Increase of stormwater runoff retention and detention in urban catchments" and the 7th FP project "Detection of Watercourse Contamination in Developing Countries using Sensor Networks", Acronym: Goldfish., FP7-ICT-2009-6, Grant agreement no: 269985. It is also the result of the project implementation ITMS 26240120004 Centre of excellence for integrated flood protection of land supported by the Research & Development Operational Programme funded by the ERDF.

REFERENCES

- [1] Bansal, M. K. (1971) Dispersion in natural streams. J. Hyd. Division, ASCE, 97(HY11), Nov., pp. 1867-1886.
- [2] Cunge, J.A., Holly, F.M. and Verwey, A.: Practical aspects of computational river hydraulics. Moskva, Energoatomizdat 1985 (in Russian)
- [3] Elder, J. W. (1959) Dispersion of marked fluid in turbulent shear flow. J. Fluid Mech., 5, Part 4, 544-560.
- [4] Fischer, H. B. et al. (1979) Mixing in inland and coastal waters. Academic press, New York.
- [5] Jolánkai, G. (1992) Hydrological, chemical and biological processes of contaminant transformation and transport in river and lake systems. A state of the art report, UNESCO, Paris.
- [6] Karcher, M.J. et al. (2004) The dispersion of 99Tc in the Nordic Seas and the Arctic Ocean: A comparison of model results and observations. Journal of Environmental Radioactivity, 74 (1-3), pp. 185-198.
- [7] Krenkel, P.A., Orlob, G. (1962) Turbulent diffusion and reaeration coefficient. J. Sanitary Engineering Div., ASCE, 88, SA2 - March, pp. 53-83.
- [8] Kosorin, K. (1995) Dispersion Coefficient for Open Channels Profiles of Natural Shape. J. Hydrol. Hydromech., 43, 1-2, pp. 93-101.
- [9] Kováčová V. (2009) The analysis of salinization and alkalization of the soil profile on the South part of Danube Lowland. Acta Hydrologica Slovaca, 10 (1) ISSN 1335-6291, pp. 44-54 (in Slovak).
- [10] Parker, F. L. (1961) Eddy diffusion in reservoirs and pipelines. J. Hyd. Div., 87, HY3, pp. 151-171.
- [11] Pekárová, P., Velísková, Y. (1998) Water quality modelling in Ondava catchment, VEDA – ÚH SAV, Bratislava, ISBN 80-224-0535-3 (in Slovak).
- [12] Říha, J. et al. (2000) Water quality in surface streams and its mathematical modelling. NOEL, Brno, ISBN 80-86020-31-2. (in Czech)
- [13] Swamee, P. K. et al. (2000) Empirical relations for longitudinal dispersion in streams. Journal of Environmental Engineering. 126 (11), pp. 1056-1062.
- [14] Socolofsky S. A., Jirka G. H. CVEN 489-501(2005) Special Topics in Mixing and Transport Processes in the Environment. Engineering. Lectures. 5th Edition, Coastal and Ocean Engineering Division, Texas A&M University, M.S. 3136, College Station, TX 77843-3136.

Grey water system application – water savings and use in the hotel building

Martina Rysulová, Daniela Káposztássová, Zuzana Vranayová

Abstract—What is grey water and how we can use it? There are lots of proven and operating grey water systems in the world. Slovakia is in this regard quiet lagging country, where system doesn't have this position, neither instance of application. Due to approach the topic of reuse systems, this article describes grey water system reuse and its brief characteristic. The main aim of this article is to describe the grey water system, its design and water treatment on the case study by pointing out its saving potential. Therefore this study confirms, that system of alternative recycled water use, can save particular source of potable water, where the water is unnecessarily wasted and used where drinking water quality is no needed. In parallel to water savings, grey water system can bring financial savings, which are relevant especially for users at decision-making processes. It is obviously that system have advantages and disadvantages, but if we are sustainable thinking, we have to refer about every drop of water we can save, and we can consider that grey water system is the way we can reach it.

Keywords—water demand, water production, saving potential, system design, grey water, white water

I. INTRODUCTION

THE reuse of waste water represents common part of building water cycle in most countries. We can say that for Slovakia is using of recycled water entirely new concept. For end users are in particular the best known terms like using rainwater, or in case of sufficient groundwater sources using water from the well. But it is important point to the fact, that there exist another alternative source of water supply, which is daily available during our routine using of water in buildings.

The main topic of this article is to describe, how we can treat with this source of water, and demonstrate its potential utilization, which means saving particular source of potable water and in parallel to water savings, bring financial savings

II. DESCRIPTION OF GREY WATER SYSTEM

Grey water system can be described as system which is

This work was supported by projects VEGA n. 1/0202/15: Sustainable and Safe Water Management in Buildings of the 3rd Millennium.

This work was supported by The APVV - SK-CZ-2013-0188 Lets Talk about the Water – An Essential Dimension of Sustainable Society of the 21. Century.

M. Rysulová, Technical University of Košice, Faculty of Civil Engineering (e-mail: martina.rysulova@tuke.sk).

D. Káposztássová, Technical University of Košice, Faculty of Civil Engineering (e-mail: daniela.ocipova@tuke.sk).

Z. Vranayová, Technical University of Košice, Faculty of Civil Engineering (e-mail: zuzana.vranayova@tuke.sk).

oriented on capturing waste water before its discharging from building. If we want to apply this system, the waste water has to be separated on grey water and black water.

There are a lot of descriptions, what grey water means, and according to British Standard, we can consider grey water as domestic wastewater excluding faecal matter and urine [1]. This characteristic specifies using waste water from sanitary appliances, which are not expected high rate of water pollution. Usually that are sinks, baths and showers, also can include washing machines, but with sufficient cleaning process, which ensure the required quality of water for its further use.

The significant part of the system is to provide the appropriate treatment system for grey water, which depends on the types of contaminants removed [2] and required quality of white water that returns back to building.

III. CASE STUDY OF GREY WATER APPLICATION

A. Designing the system

At this stage it is important to define grey water system parts for proposed building. Determine what we can consider as grey water production and white water demand. Depending on this specification and according to chosen types of sanitary we can estimate amount of water pollution and according to target utilization estimated the require water quality, which will be reuse in building water cycle.

B. Building characteristics

As an example we used the hotel building. The building has four floors; on the first floor we can find reception, fitness, restaurant, kitchen and technical room. The rest floors are approximately identical, with only one difference on the second floor, where hotel rooms are placed instead of conference rooms. Hotel provides accommodation for 128 people.



Fig. 1 Southeast view of the hotel

C. Grey water system in hotel building

Due to ensure the natural water system in building, with minimal use of additional energy the self-gravity grey water discharge system from sanitary was designed. Therefore the technical room, where is placed wastewater treatment plant and storage tanks for grey and white water, are placed on the first floor, the water was collected only from the second to fourth floor.



Fig. 2 Schema of the 1st and typical floor with grey water use

Sanitary appliances which will produce grey water are sinks, kitchen sinks, showers and baths. Cleaned white water will be used for toilets and urinal flushing, cleaning and from May to September also for irrigation.

D. Amount of water in system

During calculation it is important to establish daily production of grey water and daily demand of white water and the comparison has to fulfill following condition:

$$Q_{\text{prod}} \geq Q_{24} \quad (1)$$

Q_{prod} - volume of produced grey water per day (l/day)

Q_{24} - volume of white water demand per day (l/day)

When this condition is fulfilled, we can consider that system has potential for grey water use.

Following calculation was transferred according to calculation [3].

Daily production of grey water

Determination of daily production of grey water per day, was based on a number of sanitary appliances which produce grey water. We selected 139 appliances.

Tab. 1 Amount of sanitary produced grey water

Sanitary appliances	Sanitary amount	Grey water production q_{prod} (l/day)
Shower	52	90
Bath	7	150
Kitchen sink	3	5
Sink	77	-

$$Q_{\text{prod},i} = \sum_{i=1}^m (q_{\text{prod},i} \cdot n_{\text{mj},i}) \quad (2)$$

$$Q_{\text{prod}} = (q_{\text{prod,shower}} \cdot n_{\text{bed}} + q_{\text{prod,bath}} \cdot n_{\text{bed}} + q_{\text{prod,sink}} + q_{\text{prod,kitchen,sink}} \cdot n_{\text{person}}) \quad (2)$$

Q_{prod} - volume of produced grey water per day (l/day)

$q_{\text{prod},i}$ - grey water production per unit or day (l/day)

$n_{\text{mj},i}$ - amount of the same measuring units

If the production per unit or day is missing, as it is in this case, it can be determined according to this relation:

$$q_{\text{prod, sink}} = q_c \cdot n_c \quad (3)$$

q_c - grey water production for relevant activity (l)

n_c - amount of the same units performing within one day

$$q_{\text{prod, sink}} = 3 \cdot ((2 \cdot 128) + (2 \cdot 8) + (2 \cdot 12) + (2 \cdot 120)) \quad (3)$$

$$q_{\text{prod, sink}} = 1\,608 \text{ l/day} \quad (3)$$

$$Q_{\text{prod}} = (90 \cdot 112 + 150 \cdot 16 + 1\,608 + 5 \cdot 12) \quad (2)$$

$$Q_{\text{prod}} = 14\,148 \text{ l/day} \quad (2)$$

According to calculation is hotels grey water production 14 148 l/day.

Daily demand of white water

Daily demand of white water is created by 86 sanitary appliances and water demand for cleaning and irrigation.

Tab. 2 Amount of sanitary utilizing white water

Sanitary appliances	Sanitary amount	Flushing volume q_0 (l)
Toilet	80	6
Urinal	6	4

Tab. 3 White water demand for cleaning and irrigation

Type of water demand	Area A (m ²)	White water demand q (l/m ²)
Cleaning	2 086,7	0,1
Irrigation	930,6	1

$$Q_{24} = (q_{\text{wc}} \cdot n_{\text{person}} + q_{\text{pis}} \cdot n_{\text{person}} + q_{\text{clean}} \cdot n_{\text{clean}} + q_{\text{irr}} \cdot A_{\text{irr}}) \quad (4)$$

Q_{24} - volume of white water demand per day (l/day)

$q_{\text{n},i}$ - white water demand per unit or day (l/day)

$n_{\text{mj},i}$ - amount of the same measuring units

A_{irr} - irrigated area (m²)

Water demand for flushing toilets and urinals is determined by following relation:

$$q_{wc} = q_0 \cdot p = 6 \cdot 4,42 = 26,52 \text{ l} \quad (5)$$

$$q_p = q_0 \cdot p = 4 \cdot 3 = 12 \text{ l} \quad (5)$$

q_0 - flushing volume (l)

p - number of uses

$$Q_{24} = (26,52 \cdot 195 + 12 \cdot 65 + 0,1 \cdot 2 \cdot 086,7 + 1 \cdot 1 \cdot 230,6) \quad (4)$$

$$Q_{24} = 7 \, 390,67 \text{ l/day} \quad (4)$$

Daily amount of required white water for purposed building at maximum occupancy and in months when we consider irrigation 7 390,67 l/day.

During months when irrigation is unnecessary, is the amount of white water demand 6 160,07 l/day.

E. Potential of grey water use

According to calculated values, we can estimate the potential of grey water system for this building

$$Q_{prod} \geq Q_{24} \quad (1)$$

$$14 \, 148 \geq 7 \, 391 \text{ l/day include irrigation} \quad (1)$$

$$14 \, 148 \geq 6 \, 160 \text{ l/day without irrigation} \quad (1)$$

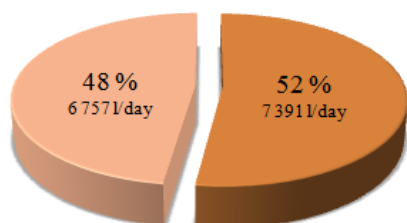


Fig. 3 White water demand for cleaning and irrigation

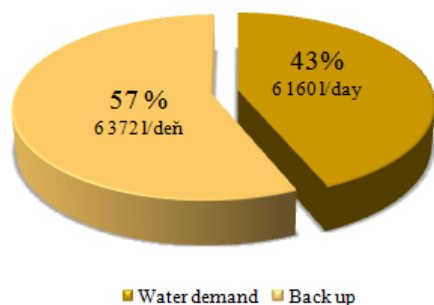


Fig. 4 White water demand for cleaning and irrigation

This specific case proves that condition is fulfilled and the production of grey water covers the daily requirement of white water. Grey water production also creates the substantial amount of back up, which can supply building during unexpected water demands. In possibility of no utilization for back up, water can be safely discharged from building by waste water drainage.

F. Amount of water in system according to real conditions

The calculation was provided with 100 percent hotel occupation, what we can consider as a rare event. For example

how can the water production and white water demand look like, we can mention the comparison of real occupancy of hotel in Liptovský Mikuláš during 2014th year.

Tab. 4 Annual grey water production

Month	Days	Grey water production Fully hotel occupancy		Hotels occupancy [%]	Grey water production [l/month]
		Daily [l/day]	Monthly [l/month]		
January	31	14 148	438 588	22,6	99 121
February	28		396 144	96,1	380 694
March	31		438 588	45,12	197 891
April	30		424 440	13,42	56 960
May	31		438 588	17,97	78 814
June	30		424 440	35,02	148 639
July	31		438 588	77,88	341 572
August	31		438 588	83,33	365 475
September	30		424 440	26,75	113 538
October	31		438 588	15,58	68 332
November	30		424 440	8,4	35 653
December	31		438 588	18,73	82 148

Tab. 5 Annual white water demand

Month	Days	White water demand Fully hotel occupancy		Hotels occupancy [%]	White water demand [l/month]
		Daily [l/day]	Monthly [l/month]		
January	31	6 160	190 960	22,6	43 157
February	28		172 480	96,1	165 753
March	31		190 960	45,12	86 161
April	30		184 800	13,42	24 800
May	31	7 391	229 121	17,97	41 173
June	30		221 730	35,02	77 650
July	31		229 121	77,88	178 439
August	31		229 121	83,33	190 927
September	30	6 160	221 730	26,75	59 313
October	31		190 960	15,58	29 752
November	30		184 800	8,4	15 523
December	31		190 960	18,73	35 767

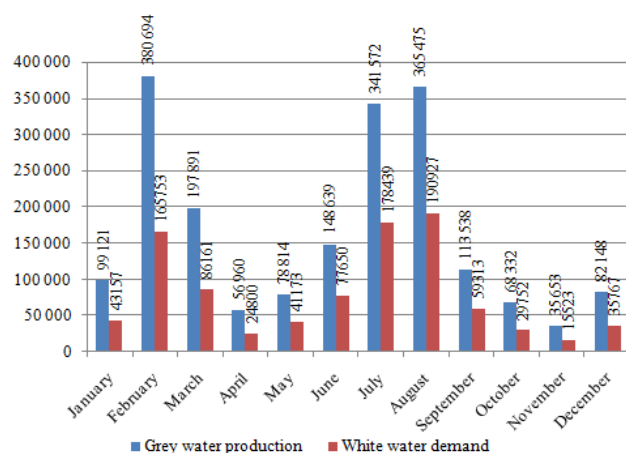


Fig. 8 Comparison of the grey water production and white water demand according to hotels occupancy

IV. DISCUSSION

We can consider that this example of grey water application prove that system has some saving potential especially for potable water. If we are considering with the occupancy of hotel above, our annual saves will values 948 m³ of potable water. It is understood that with water savings, we save some sort of financial sources. For this specific case it represent 1 035,40 € savings per year, with actual price for water supply 1,0922 €/m³ [4] in Liptov region, and 1 259,10 € per year for discharging water to public sewer. Actual price for water discharging in Liptov region is 1,3282 €/m³ [4]. Overall savings on water supply and discharging water will be 2 294,5 €

V. CONCLUSION

The modern decentralized water infrastructure can include site-collected rainwater, grey water, storm water, and black water systems. The main goal is to point out a need for standardization to protect the public and to ensure that reliable systems are designed, installed and maintained. It is necessary to define regulation and set standards for designing hybrid systems for example according to foreign national standards and performed experiments in Slovak conditions. From this example of grey water application we can consider, that system is efficient in terms of saving potable water. It is clear that the changing of hotel occupation will have impact on the water and financial savings. The target of this article was to introduce the grey water system and pointed out that with this system we can save certain amount of potable water, which is used for purpose where it is with its quality unnecessarily wasted.

REFERENCES

- [1] BS 8525-1:2010 Greywater systems Part 1: Code of practise. UK: BSI, 2010
- [2] Chaitidak D. M., Yadav K.D., Characteristics and treatment of greywater-review. *Anviron Sci Pollut Res* (2013) 20:2795-2809. DOI 10.1007/s11356-013-1533-0

- [3] Srážkové a šedé vody aneb "colors of water". Conference proceedings. 2013. www.asio.sk
- [4] Ceny vodného a stočného. [online]. [cit.2014-12-26]. Available on the internet: <http://www.lvsas.sk/ceny-vodneho-a-stocneho>
- [5] M. Zeleňáková, P. Purcz, I. Gargar, H. Hlavatá, "Research of Monthly Precipitation Trends in Libya and Slovakia," Proceedings of the 2014 International Conference on Environmental Science and Geoscience (ESG '14) p.46, March 15-17, 2014, Venice, Italy
- [6] Afonso S., et al. Grey water in buildings. The Portuguese approach. IN: Proceedings of 37th International Symposium CIB W062 on Water Supply and Drainage for Buildings, Aveiro 2011, ISBN: 978-989-97476-0-9
- [7] Kaposztasova D., et al.: Grey water as a part of in-building water cycle, IN: Proceedings of 40th International Symposium CIB W062 on Water Supply and Drainage for Buildings, Sao Paolo 2014.
- [8] Markovič G., Zeleňáková M., Measurements of quality and quantity of rainwater runoff from roof in experimental conditions - 2014. In: ICITSEM 2014 : International conference on innovative trends in science, engineering and management 2014 : 12th and 13th February 2014, Dubaj, UAE. - [Bangalore]: Mudranik Technologies, 2014 P. 145-151. - ISBN 978-93-83303-19-9

Martina Rysulová is a PhD. student at the Faculty of Civil Engineering, Technical University of Kosice. She is specialised in water supply and drainage systems. Recently she has been concentrated on the field of grey water reuse.

Daniela Kaposztasova is lecturer at the Faculty of Civil Engineering, Technical University of Kosice. She is specialised in Water supply and drainage systems. Recently she has been concentrated on the field of rainwater use and grey water reuse. She is a vice dean for education

Zuzana Vranayova is the professor at the Civil Engineering Faculty, Technical University of Kosice, Department of Building Services. She is conducting various researches on her major field of study of water supply and drainage system in buildings. She is also actively involved in governmental and academic institutions and committees related to her field of study as chief coordinator and board member.

Infiltration efficiency of percolation facility for its safety operation

Gabriel Markovič, Daniela Kaposztásová, Zuzana Vranayová

Abstract— Facilities for percolation of rainwater are devices designed for fluent and natural infiltration of rainwater from the roofs of buildings and other paved surfaces. The basic principle and function of all types of infiltration facilities as quickly as possible to divert rainwater to infiltration zone and there it infiltrates into the surrounding soil. Every construction should be secure with a drainage system to remove rainwater from the roof, or other paved surfaces without causing damage to the construction or endangering the health and safety of people in and around the building. Infiltration facilities must be designed correctly. There are a number of cases, when from the incorrect design of infiltration facilities insufficiently or only partly fulfil their function, and in many cases there has been damage of property.

Keywords— percolation, rainwater, runoff, safety, shaft.

I. INTRODUCTION

EVERY building and paved surfaces must be designed and constructed with a surface water drainage system. This drainage system must ensure the disposal of surface water without threatening the building and safety of the people [12]. Suitability of choice of type of infiltration facility is dependent on local conditions. It is necessary to take into account the principles of design of these facilities, for example separation distance from buildings, groundwater level, infiltration coefficient etc. Therefore, in each case, it is to be considered carefully, which drainage concept in combination with the percolation of precipitation is ecologically sensible, technically possible and economically justifiable.

This work was supported by the VEGA 1/0202/15 Sustainable and Safe Water Management in Buildings of the 3rd. Millennium and APVV-SK-CZ-2013-0188 Lets Talk about the Water – An Essential Dimension of Sustainable Society of the 21.Century.

The Centre was supported by the Slovak Research and Development Agency under the contract No. SUSPP-0007-09.

Ing. Gabriel Markovič, PhD., Technical University of Košice, Faculty of Civil Engineering, Institute of Architectural Engineering, Vysokoškolská 4, 042 00 Košice, mail: gabriel.markovic@tuke.sk

Ing. Daniela Kaposztásová, PhD., Technical University of Košice, Faculty of Civil Engineering, Institute of Architectural Engineering, Vysokoškolská 4, 042 00 Košice, mail: daniela.ocipova@tuke.sk

doc. Ing. Zuzana Vranayová, PhD., Technical University of Košice, Faculty of Civil Engineering, Institute of Architectural Engineering, Vysokoškolská 4, 042 00, Košice, e-mail: zuzana.vranayova@tuke.sk.

II. IMPORTANT DESIGN PRINCIPLES FOR CORRECT DESIGN

A. Distance from buildings

It always should be respected a minimum distance from buildings, basement of the buildings and the average amount of groundwater levels. These dimensions can vary from a few decimetres to several meters. Figure 1 and 2 represent minimum distance from buildings. The same rules apply for underground infiltration facilities.

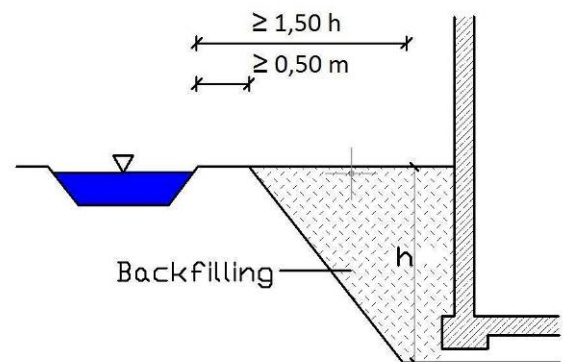


Fig. 1. The minimum distance of the decentralized infiltration facilities from building without waterproofing [6]

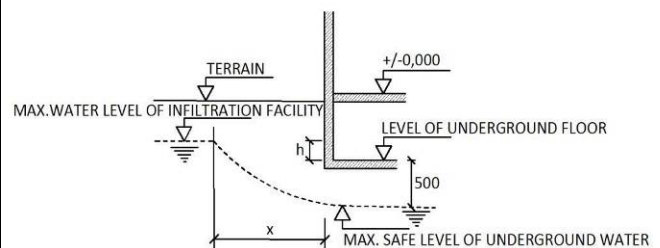


Fig. 2. Required separation distance from buildings [13]

Recommended minimum distances from the infiltration facility:

- 5 m from residential buildings without waterproof
- 2 m from residential buildings with waterproof
- 3 m from local vegetation (trees, bush etc.)
- 2 m from the property line, public communication, etc
- 1,5 m from gas pipelines and water pipelines
- 0,8 m from power lines

- 0,5 from telecommunication lines
- 1 m from ground water level

B. The permeability of infiltration area

The most important design parameter of infiltration facilities is to determine the infiltration coefficient k_f in the interest area, respectively infiltration coefficient of the soil where is planned to place an infiltration facility. Infiltration coefficient k_f generally represents an efficiency of infiltration facilities, respectively infiltration capability of the soil to absorb inflow water.

Permeability of the infiltration zone is a main qualitative and quantitative requirement for rainwater infiltration. Permeability of loose rock depends primarily on the size and distribution of the particles and compactness, in soils is critical soil structure and water temperature and is given by the infiltration coefficient. Permeability of loose rock varies in general between $1 \cdot 10^{-2}$ and $1 \cdot 10^{-10}$ m/s (figure 3). The k_f values apply to the process of infiltration water in the saturated zone. The range of values for the filtration coefficient for technical drainage ranges from $1 \cdot 10^{-3}$ and $1 \cdot 10^{-6}$ m/s [14].

The k_f values greater than $1 \cdot 10^{-3}$ m/s cannot be reached for rainwater runoff and low depth of groundwater level the sufficient pretreatment through chemical and biological processes. If the k_f values are smaller than $1 \cdot 10^{-6}$ m/s, the percolation facilities are loaded very long time. For this reason, anaerobic processes in the unsaturated soil, which resulting in adverse effects on retention and capacity capabilities of the soil can occur.

Therefore, the most important design parameter of the infiltration facilities is to determine the filtration coefficient k_f on-site.

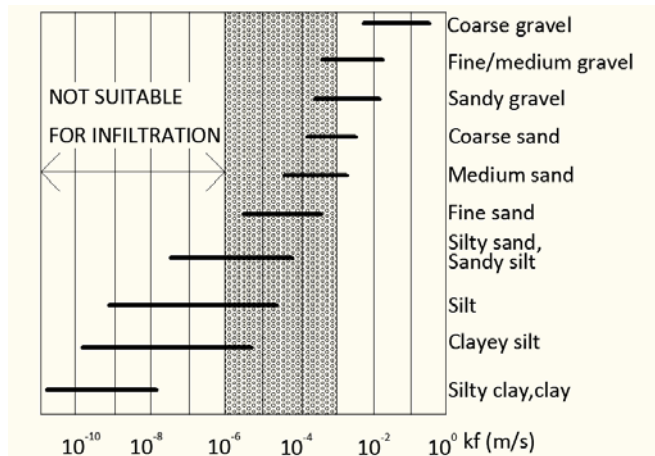


Fig.3 Recommended values of the infiltration coefficient

The importance of knowledge of the hydrogeological conditions at the site of the proposal of infiltration facility is evident from table 1. Table 1 shows theoretical calculation for infiltration coefficient from k_f 10^{-2} to 10^{-7} m/s and attributable required times for rainwater infiltration. Calculated time represent required time for infiltration only one (critical) rainfall event. Calculation is for infiltration facility – infiltration shaft - with real dimensions of infiltration shaft

which will be mentioned in the next chapter.

Tab. 1 Required time for rainwater infiltration in shaft depending of the infiltration coefficients from theoretical calculation

Infiltration coefficient	Rainfall periodicity	V (required accumulation volume in m ³)	t (time of infiltration in hours)
$k_f = 10^{-2}$	$r_D(0,5)$	0,16 m ³	t = 0,05 h
$k_f = 10^{-3}$	$r_D(0,5)$	1,49 m ³	t = 0,13 h
$k_f = 10^{-4}$	$r_D(0,5)$	3,77 m ³	t = 1,4 h
$k_f = 10^{-5}$	$r_D(0,5)$	6,26 m ³	t = 14 h
$k_f = 10^{-6}$	$r_D(0,5)$	7,27 m ³	t = 143 h (6 days)
$k_f = 10^{-7}$	$r_D(0,5)$	7,40 m ³	t = 1432 h (60days)

III. RESEARCH OF INFILTRATION EFFICIENCY IN REAL CONDITIONS

A. Experimental research in the campus of TU Košice-city

We have started our research and own measurements in scope of stormwater quantity and quality parameters at the campus of Technical University of Košice within the project relating to the management of stormwater. The objects of research represent two infiltration shafts in the campus of TU Kosice that were made before the start of our research. These infiltration shafts represent drainage solution for real school building PK6 and All of the runoff rainwater falling onto the roof flows into these underground shafts (figure 4) [1].

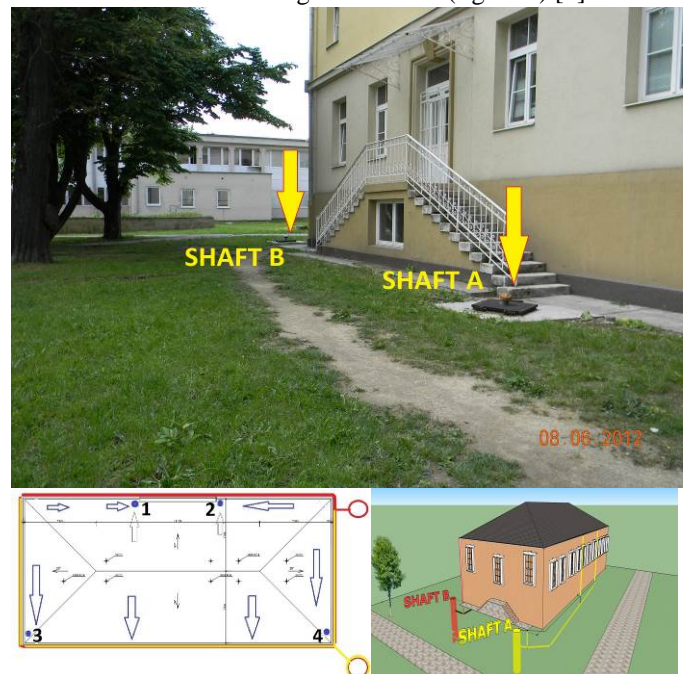


Fig.4 Location of drainage shafts near the PK6 building [3]

The measuring devices for information about volume of incoming rainwater from the roof of the building PK6 and also information about the quality of rain water are located in both infiltration shafts [1]. All devices are connected with registration and control unit M4016. Unit M4016 automatically sent measured and archived data into the server database (data hosting) via GPRS in regular intervals [8]. Under inflow, respectively rain outlet pipe in the shaft, there are measurement flumes for metering of inflow rainwater from the roof of a building PK6 in both of infiltration shafts. Rainwater from the roof of the building PK6 is fed by rainwater pipes directly into measurement flumes, which are placed under the ultrasonic level sensor which transmitting data of the water level in the measurement flumes to the data unit M4016 (figure 5). Water level at the bottom of shafts is measured by pressure sensors type LMP307 (figure 5) [2].



Fig. 5. Measurement devices - Data unit M4016 in shaft A, Measurement flume with ultrasonic level sensor, Pressure sensor LMP307

B. Experimental research in peripheral part of Prešov-city

Second experimental research of infiltration efficiency is located in Šarišské Lúky near Prešov-city. Rainwater infiltration as a drainage solution is from bridge road after its reconstruction. The infiltration gallery from infiltration units was designed in the monitored area by theoretical calculation.

Bridge object (Figure 6) is located on road 1/8 between Prešov and Kapušany. Approached two-way road on the bridge contains 4 lanes. It is bridge road over the train and local road MK Sekčov and road III/06815. Roadway on the bridge has one-sided slope 1,5% [7].

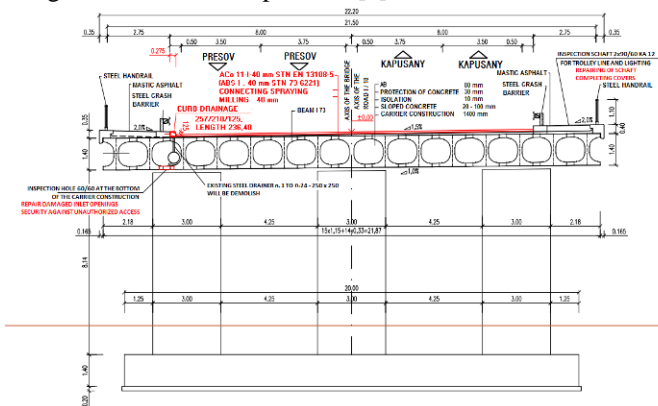


Fig. 6. Bridge object

Figure 7 shows the location of measuring equipment and objects for research. Rainwater from the bridge flows into filter shaft (1), which serves for capture and sedimentation of coarse and fine impurities. The rainwater subsequently flows into the infiltration gallery (2), where the water is filtered

during infiltration to the soil. Measuring devices for volume of rainwater are the same as in infiltration shaft in campus of TU Kosice. A flow meter is located in the filter shaft, which record incoming rainwater in l/s. The water level in the infiltration gallery can be monitored by means of the float-gauge which is located in inspection shaft (3). Near this infiltration gallery is located rain-guage (4).

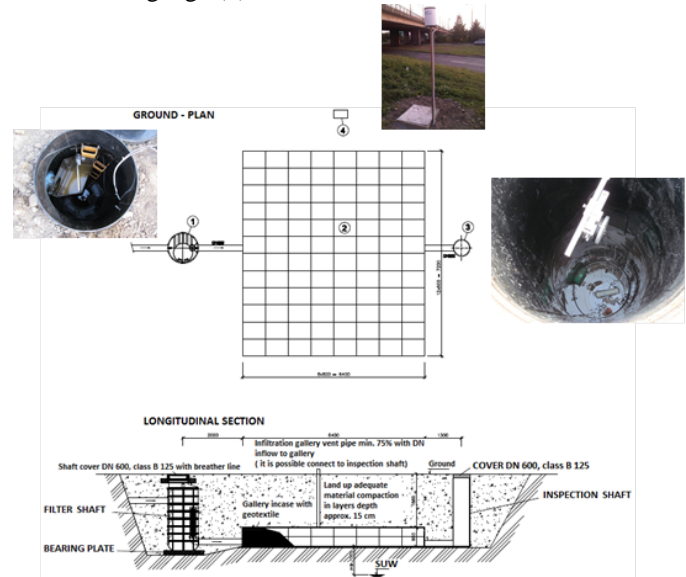


Fig. 7. Infiltration gallery – situation [9]

IV. MEASUREMENT AND EVALUATION

A. Experimental research in the campus of TU Košice-city

Figures 8-11 represent typical process of flow rate and next percolation of rainwater during rainfall events in percolation shafts [3,10]. Figures 8-11 shows 2 selected rainfall events from year 2013 and 2014 with high rainfall intensity. All data from research show, the total infiltration of runoff inflow into the infiltration shafts from roof of PK6 building take place at the same time of duration of rainfall events, respectively very short-time after. This represents a high infiltration rate of this infiltration shafts. It is given by the coefficient of infiltration of soil at the bottom of shaft determined as $k_f = 1.10^{-3}$ m/s.

The maximum water level at the infiltration shaft A, measured during the research period 2011-2014 is 1,28 m, which is less than 1/3 filling depth of infiltration shaft A and maximum water level at the infiltration shaft B, measured during the research period is 1,31 m, which is less than 1/3 filling depth of infiltration shaft B too.

If we compared size of area for infiltration of runoff with other types of infiltration facilities (for example infiltration units) this size is several times smaller against another types of infiltration facilities. But the infiltration coefficient of surveyed infiltration shafts $k_f = 1.10^{-3}$ m/s ensures percolation of rainwater in required time so represents safe disposal of surface runoff for the object PK6 [11].

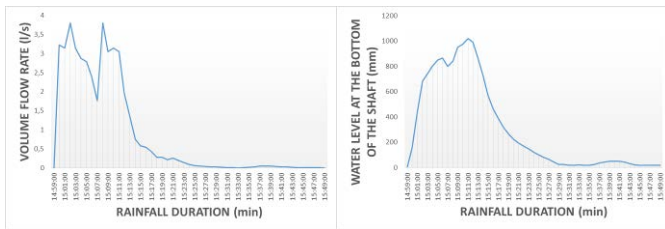


Fig. 8. Volume flow rate and water level changes at the bottom of shaft A during rainfall 30.7.2013

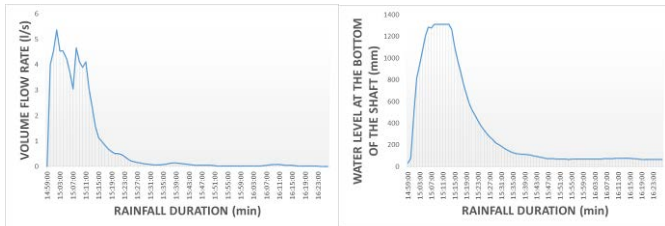


Fig. 9. Volume flow rate and water level changes at the bottom of shaft B during rainfall 30.7.2013

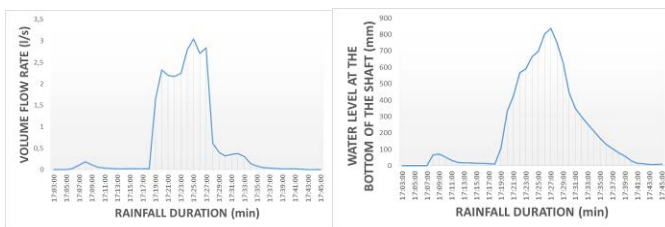


Fig. 10. Volume flow rate and water level changes at the bottom of shaft A during rainfall 10.6.2014

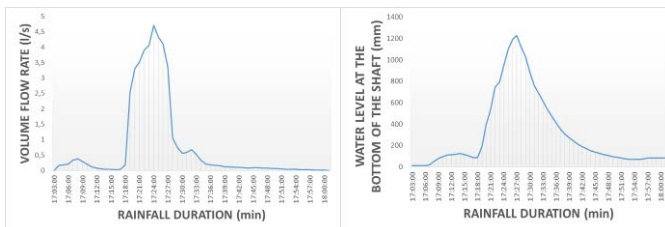


Fig. 11. Volume flow rate and water level changes at the bottom of shaft B during rainfall 10.6.2014

B. Experimental research in peripheral part of Prešov-city

The percolation gallery is formed by plastic units. The percolation area of the infiltration gallery is 46,08 m². Its surface is rectangular. The volume of rainwater draining into infiltration gallery and water level changes at the bottom are monitored with devices in the filter shaft.

During the design phase of the infiltration gallery the infiltration coefficient was estimated by designer as $8,2 \cdot 10^{-5}$ m/s. All parameters of infiltration gallery were calculated with this infiltration rate which should ensure a sufficient and suitable percolation characteristics for this facility.

But results from laboratory test set infiltration coefficient in area of interest as $4,84 \cdot 10^{-7}$ m/s! It means about 100 times lower infiltration efficiency and also lower accumulation volume of infiltration gallery as was design for safe disposal of rainwater runoff. This results to insufficient infiltration rate of this percolation gallery. Infiltration coefficient $4,84 \cdot 10^{-7}$ m/s represents practically impermeable type of soil not suitable for

infiltration facilities. Unfortunately this inaccurate design caused flooding and silting all infiltration gallery and result to failure of installed devices for research – figure 12.



Fig. 12. Volume flow rate and water level changes at the bottom of shaft B during rainfall 30.7.2013

Figures 13-14 represent typical process of rainwater percolation in infiltration gallery respectively water level in gallery during the month. Data from research showed that there was continuously high water level in percolation gallery. This represents a very low infiltration rate of this infiltration gallery what is given by the coefficient of infiltration of soil at the bottom of gallery determined as $k_f = 4,84 \cdot 10^{-7}$ m/s and also means overflow of percolation gallery (figure 13-14).

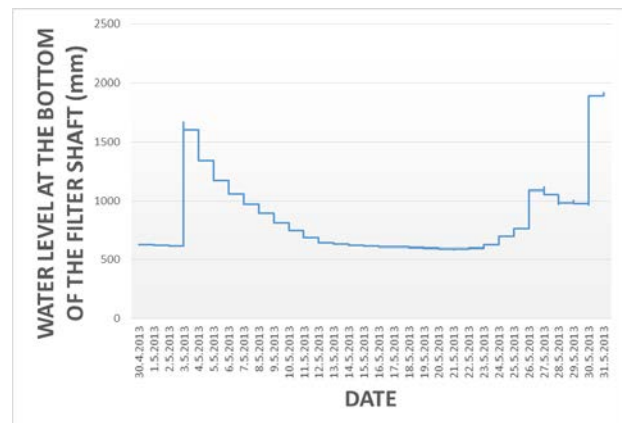


Fig. 13. Water level changes at the bottom of filter shaft during May 2013

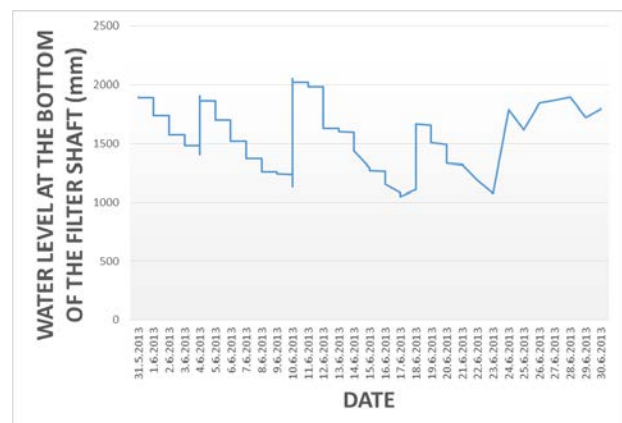


Fig. 14. Water level changes at the bottom of filter shaft during June 2013

V. CONCLUSION

Percolation of rainwater as a part of stormwater management is quite a new topic in Slovakia. There is no legal framework as well as standards or guidelines how to apply sustainable stormwater management techniques especially in field of percolation of rainwater. Percolation drainage systems are technical solutions that provide an alternative to the traditional direct channelling of surface water through networks of pipes and sewers to wastewater treatment plant or watercourses. But these systems must be designed with regard of threatening the building and safety of the people.

As was mentioned above, suitability of type of infiltration facility is dependent on local conditions. Of course, it is necessary to take into account the principles of design of these facilities, for example separation distance from buildings, groundwater level, infiltration coefficient etc. In this study, the results obtained through the research on the percolation facilities, demonstrated how coefficient of infiltration depend to efficiency of percolation facility in real conditions. So for correct operation of these facilities its necessary has knowledge of hydrogeological conditions in site of design.

REFERENCES

- [1] G. Markovič, Z. Vranayová 2013 Infiltration as a means of surface water drainage, Košice: TU
- [2] G. Markovič, D. Kaposztasova, Z. Vranayová 2014 The Analysis of the Possible Use of Harvested Rainwater and its Potential for Water Supply in Real Conditions, WSEAS Transactions on Environment and Development. Vol. 10, p. 242-249.
- [3] M. Zeleňáková, P. Purcz, I. Gargar, H. Hlavatá, "Research of Monthly Precipitation Trends in Libya and Slovakia," Proceedings of the 2014 International Conference on Environmental Science and Geoscience (ESG '14) p.46, March 15-17, 2014, Venice, Italy
- [4] A. Bucur, J. L.López-Bonilla, "An Approach to the Quality of Drinking Water as a Matter of Multicriterial Decision, Recent advances in energy, environment, ecosystems and development (EEED '13), p.43, July 16-19, 2013, Rhodes island, Greece
- [5] H. Raclavska, J. Drozdova, S. Hartmann, "Municipal Waste Water Toxicity Evaluation with Vibrio Fisheri, "Recent advances in environment, energy, ecosystems and development (EEEAD 2013), p.226, September 28-30, 2013, Venice, Italy
- [6] DWA-A 138E: Planning, Construction and Operation of Facilities for the Percolation of Precipitation Water, 2005.
- [7] Technical report – I/18 Šarišské Lúky bridge reconstruction (in Slovak) No.18-449. Prodosing s. r. o., Bardejovská 13, 080 06 Ľubotice, 2012.
- [8] Technical documentation Fiedler-magr – Manual M4016.
- [9] M. Zeleňáková, G. Rejdovjanova, The importance of hydrogeological and hydrological investigations in the residential area: a case study in Presov, Slovakia - 2014. In: Infraeko 2014 : 4 International Conference of Science and Technology : 29-30 May 2014, Krakow. - Rzeszow: Politechnika Rzeszowska, 2014 P. 319-325. - ISBN 978-83-7199-937-2
- [10] M. Zeleňáková, P. Purcz, I. Gargar, H. Hlavatá, M. M. Portela 2014 Statistical Trends of Precipitation in Chosen Climatic Station in Slovakia and Libya, WSEAS Transactions on Environment and Development, Vol. 10, p. 298-305.
- [11] G. Markovič, M. Zeleňáková, D. Kaposztasova, G. Hudakova, Rainwater infiltration in the urban areas - 2014. In: Environmental Impact 2. - Southampton : WITT press, 2014 Vol. 181 (2014), p. 313-320. - ISBN 978-1-84564-762-9 - ISSN 1743-3541
- [12] P. Stahre, (2006): Sustainability in Urban Storm Drainage, Planning and examples, Svenskt Vatten, 81 p.
- [13] Z. Žabička, "Technická řešení vsakovacích zařízení", in Proceedings of 15th International Conference Sanhyga, Piešťany, Slovakia, October 14-15, 2010.
- [14] J. Vrána, (2010), "Dimenzování vsakovacích zařízení v ČR", in Proceedings of 15th International Conference Sanhyga, Piešťany, Slovakia, October 14-15, 2010.

Gabriel Markovič is researcher at the Faculty of Civil Engineering, Technical University in Kosice. He is specialised in Water supply and drainage systems. Recently he has been concentrated on the field of rainwater harvesting and rainwater infiltration systems.

Daniela Kaposztasova is lecturer at the Faculty of Civil Engineering, Technical University in Kosice. She is specialised in Water supply and drainage systems. Recently she has been concentrated on the field of hot water distribution systems and rainwater reuse.

Zuzana Vranayova is the professor at the Civil Engineering Faculty, Technical University in Kosice, Department of Building Services. She is conducting various researches on her major field of study of water supply and drainage system in buildings. She is also actively involved in governmental and academic institutions and committees related to her field of study as chief coordinator and board member. She is a vice dean for education

Migration of Travel time in a common-shot gather by Structural Similarity

Hernando Castañeda M , José Luciano Maldonado ,Rómulo Sandoval F

Universidad de Pamplona, Grupo CICOM y PANGA

hcastaneda@unipamplona.edu.co, maldonaj@ula.ve, romusanflo@unipamplona.edu.co

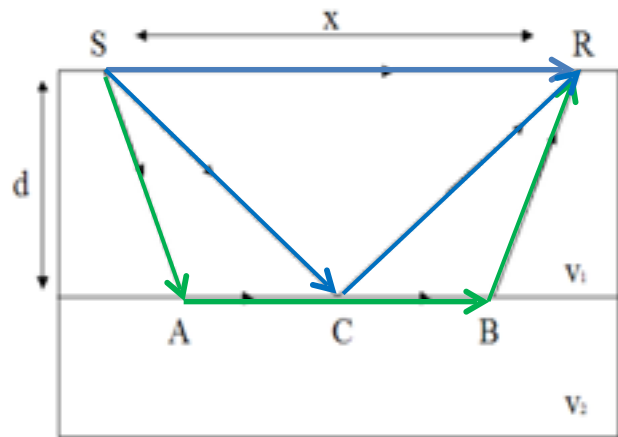
Abstract: This paper presents a method of seismic migration, specified with the concept of structural similarity, its purpose is to find seismic velocity of the ground layers and identify the location of the reflectors from the travel time and slowness. Seismic attributes in this research are the slope and curvature of the wave propagation time. In particular, the seismic group is split in segments using the concept of structural similarity that have matching in its shape and temporal evolution. Inout information is used to process migration method that does not require a model of seismic velocity. The migration is performed directly through patterns derived from the first and second derivative of travel-time regarding the offset address and the depth and in accordance with the estimated effective slowness.

Keywords: Seismic Migration, Structural Similarity, System Identification.

Introduction

The seismic acquisition process is based on techniques of reflections and refractions [2,3], when generate short pulse from an acoustic source (tremor) and it's to register in receivers. Data include the travel time consisting of the temporal duration between pulse emission and the arrival in one of the receivers. Figure 1 illustrates a model of abstraction of the phenomenon characterized by Wave front in a homogeneous medium. This process of seismic data acquisition data are inputs for the processes of seismic inversion and reconstruction of the wave field, which requires specific techniques to implement them in a practical way by means of computer programs.

The methods of seismic tomography [12.14] are used in this application, it is based on concepts of slowness and travel time, the first and second derivate of travelttime with respect to position of the receivers is use specifically , with the purpose of estimating the matrix where its represent the structure of slowness.



This is a problem of the waves tomography in their first arrivals [6] (points of reflection and refraction), in the shell model of the Earth with their respective forms structural (the position of reflectors). its descriptors are the curvature and the slopes derived from the trajectories that generate the travelttime and its allows a process of temporal grouping is motivated by change of temporal behavior of the path in feature space (slope ,curvature). Data from each segment of the travelttime are the inputs to develop the method of identifying with restriction of the eigenvalues, using the method of least squares with approximate solution and it is fitting with the use of the estimation of a regularization parameter.

The figure 2 illustrates the geometry of the relationship between travelttime behavior and the horizontal distance in a point of reflection-refraction of a wave front in an environment characterized by the seismic change.

Description of the Problem.

The understanding of the proposed problem [4] makes it necessary to start from a graphical representation to

explain (see Figure 2) the vision of the receiver of a trace from a reflected source wave emitted from a source. This is illustrated in geometry (2D) a reflective process with their respective seismic objects that are specified below:

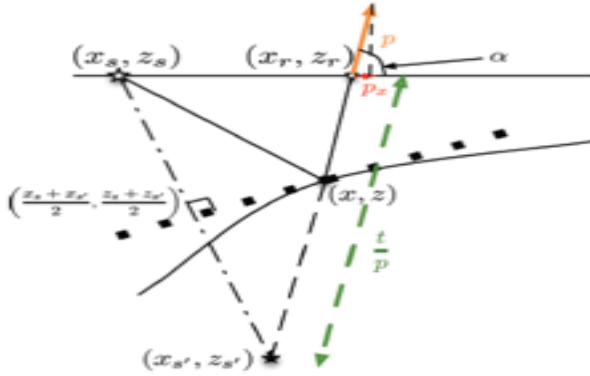


Fig. 2 Geometry of the vision of a receiver from a reflected source

- Specific position of the source (x_s, y_s) and position of the receiver (x_r, z_r) .
- Positions of a point of the reflector (x, z) (x_s', z_s')
- Positions of the image (x_s', z_s') and half the distance between the source and the image $(\frac{x_s + x_{s'}}{2}, \frac{z_s + z_{s'}}{2})$
- The descent (lines to points) in the reflection point and the distance of effective slowness p and its first derivative with respect to the position of the receiver p_x .
- The angle of reflection α and $\frac{t}{p}$ it is the distance between the surface and the position of the image.

From the illustration and geometry specified above are derived then mathematical expressions for first and second derivative of the slowness with respect to the positions of the receivers.

That , propagation time of a signal from a source pins with location given by the coordinates to the

receiver located in (x_r, z_r) , then , horizontal slowness on the receiver is defined as:

$$p_x = \frac{\partial t}{\partial x_r} \quad (1)$$

Propagation wave through a constant effective velocity of the medium with slowness $p = \frac{1}{v}$, where v is the

effective velocity, which can be found at a point of reflection through search the image. The coordinates of the image shall be given by the following equations:

$$z_s' = z_r + \frac{t}{p} \sqrt{1 - \left(\frac{p_x}{p}\right)^2} = z_r + \frac{t}{p^2} \sqrt{p^2 - p_x^2} \quad (2)$$

$$x_s' = x_r - \frac{tp_x}{p^2} \quad (3)$$

As illustrated in Figure 3, the reflection point is located at the line of intersection that passes through the receiver and the source image, indicated by the green dashed line.

$$(z_s' - z_r)(x - x_r) = (x_s' - x_r)(z - z_r)$$

With the line that is normal to the line source and the reflected source what is passing through the middle of the line indicated by dotted black line.

$$\left(x - \frac{x_r + x_s}{2}\right)(x_s' - x_r) + \left(z - \frac{z_r + z_s}{2}\right)(z_s' - z_r) = 0$$

The coordinates of the point are derived from the last two equations and are formulated thus:

$$x = \frac{x_r(x_s'^2 - x_s^2 + (z_s - z_s')^2)}{2((x_r - x_{s'}) (x_s - x_{s'}) + (z_r - z_{s'}) (z_s - z_{s'}))} + \frac{x_{s'}(x_s'^2 - x_s^2 + x_s'^2 - z_s'^2 + 2z_r(z_s - z_{s'}))}{2((x_r - x_{s'}) (x_s - x_{s'}) + (z_r - z_{s'}) (z_s - z_{s'}))}$$

$$z = \frac{2(x_r x_s z_{s'} - x_s x_{s'} z_r - x_r x_{s'} z_{s'})}{2((x_r - x_{s'}) (x_s - x_{s'}) + (z_r - z_{s'}) (z_s - z_{s'}))} + \frac{x_{s'}^2(z_r + z_{s'}) + (z_r + z_{s'})(x_s'^2 + z_s'^2 - z_s^2)}{2((x_r - x_{s'}) (x_s - x_{s'}) + (z_r - z_{s'}) (z_s - z_{s'}))}$$

Substituting equations 2 and 3 in the previous equations and expressing in terms of propagation time $t_0 = 2zp$

towards vertical double will reach the following expressions:

$$x = \frac{2p^2 x_r (t + \sqrt{p^2 - p_x^2} (z_r - z_s))}{2p^2 (t + p_x (x_s - x_r) + \sqrt{p^2 - p_x^2} (z_r - z_s))} + \frac{p_x (p^2 (x_s^2 - x_r^2) + (z_r - z_s)^2 - t^2)}{2p^2 (t + p_x (x_s - x_r) + \sqrt{p^2 - p_x^2} (z_r - z_s))} \quad (4)$$

$$t_o = \frac{\sqrt{p^2 - p_x^2} (t^2 - p^2 ((x_r - x_s)^2 + z_s^2 - z_r^2))}{2p^2 (t + p_x (x_s - x_r) + \sqrt{p^2 - p_x^2} (z_r - z_s))} + \frac{2p^2 z_r (t - p_x (x_r - x_s))}{2p^2 (t + p_x (x_s - x_r) + \sqrt{p^2 - p_x^2} (z_r - z_s))} \quad (5)$$

To use these expressions, it is necessary to know the effective slowness p with the stated equilibrium condition that exists when only values of slowness can be found if and only if it does so that the reflector can be approximated to a plane.

The preceding statement implies that the derivatives with respect to x_r , the equations (10 and 11) and then equal to zero. To Carrying out this derivation gives the following equations:

$$0 = 1 - \left(\frac{z_s}{p} \right)^2 - \frac{t}{p^2} p_{xx} \quad (6)$$

$$p^2 = p_x^2 + t p_{xx} \quad (7)$$

Where p is the effective slowness and $p_{xx} = \frac{\partial^2 t}{\partial x^2}$ is















the second derivative (curvature) To obtain the analytical expression for time migration for effective steady velocity.

Structural Similarity and Clustering Method.

The structural similarity, refers to the behavior of the temporal patterns of the time of propagation of the waves, as a "change in form in time" [9] and is considered a

novel technique to recognize the behavior of the waves emitted through the layers in the subsoil and in order to understand these complex dynamic systems, such as the seismic computational. The following hypothesis arises: "What are the essential dynamic seismic behavior shapes?" An initial strategy is to use seven unique behavior patterns derived from the first and second curvature of the time of propagation with respect to the positions of the receivers.

Table 1 Set of patterns based on the values of the features

Slope Value	Curvature Value	Symbol Label	Alphabet Symbol	Pattern Abstract
S=0	C=0		Y	
S=0	C=0		X	
S=0	C=0		L	
S=0	C=0		M	
S=0	C=0		F	
S=0	C=0		S	
S=0	C=0		E	

S

The trend in the absolute values in the changes of the net rates can be used to identify and recognition even unique patterns of behavior [3].

- The first pattern is balanced, with linear behavior when there is balance. Label with yellow color.
- The second pattern is the linear growth, has a monotonous behavior of growth. Label with black color.
- The third pattern is called as growth strengthened, which is characterized by a concave upwards behavior with monotonous growth. Label with light blue color.
- The fourth pattern is linear fall with linear decrease behavior. Label with purple color.
- The fifth pattern is known as: fall forced with concave down behavior with monotonous decrease. Label with red.
- Sixth pattern is referred to as growth in balance, has concave down behavior with monotonous increase. Label with blue color.
- The seventh pattern is called fall in equilibrium, is concave upward with monotonous increase. Label green color.

Method of identification of reflectors (investment)

The identification of parameters from a set of training data, begins with the specification of the restrictions suggested by Jacques Hadamard (existence, uniqueness, stability of the solution or solutions), the condition of stability is that most often are breaks and to avoid this condition is implemented in this work a method of identifying restrictions on the eigenvalues which is one of the way of analyzing this condition of stability. (A path is called stable if, for $t \rightarrow \infty$, $x_1(t), x_2(t)$ they converge at the point of equilibrium).

If the temporary range $[b, e]$ an i -nth sequence of propagation times $[t_b, \dots, t_e]$ It is a set of explicit data that satisfies the discrete equation of a system dynamic of the form:

$$T_k^{(i)} = A_i T_{k-1}^{(i)} + G_i^{(i)} \quad (8)$$

Where A_i is the matrix of transition (array of seismic speed) A_i and G_i bias vector.

Given a sequence of continuous States mapped from a space of observation, the estimation of the parameters of a A_i transition matrix from the vector sequence of continuous temporary States $[t_b^{(i)}, \dots, t_e^{(i)}]$ It corresponds to a problem of minimization of forecast errors, where propagation using time segments are specified thus:

$$T_0^{(i)} = [t_b^{(i)}, \dots, t_{e-1}^{(i)}], T_1^{(i)} = [t_{b+1}^{(i)}, \dots, t_e^{(i)}] \quad (9)$$

This estimate of the parameters correspond to a problem of minimization of errors of prediction [[8], replacing the discrete equation specified above. The vector of errors equation may be expressed as:

$$\varepsilon_t = t_k - A^{(i)} t_{k-1} + G_i \quad (10)$$

where A_i the transition matrix and G_i vector of bias and are parameters to be estimated. The sum of the square norm of $[b, e]$ all vectors of errors in the range I will then be:

$$\sum_{t=b+1}^e \|\varepsilon_t\|^2 = \sum_{t=b+1}^e \|t_k - A^{(i)} t_{k-1} + G_i\|^2 \quad (11)$$

To estimate A_i the matrix and G_i vector, initially specified segments using the respective diversion To estimate the matrix and vector, initially specified segments using the respective deviation with their $[m_0^{(i)}, m_1^{(i)}]$ average values] and expressed as: with their average values] and expressed as:

$$\begin{aligned} T_0^{(i)} &= [t_b^{(i)} - m_0^{(i)}, \dots, t_{e-1}^{(i)} - m_0^{(i)}] \\ T_1^{(i)} &= [t_{b+1}^{(i)} - m_1^{(i)}, \dots, t_e^{(i)} - m_1^{(i)}] \end{aligned}$$

From equation 4, it makes use of the invariant properties known as the trace of a matrix and then derives the expression that is derived with respect to these parameters, obtaining the following expressions:

$$A^{*(i)} T_0^{(i)} T_0^{(i)T} = T_1^{(i)} T_1^{(i)T} \quad (12)$$

As it is necessary to determine it is necessary to use the properties of the pseudo inverse of Moore-Penrose [5], reaching the following expression:

$$A^{*(i)} = T_1^{(i)} T_0^{(i)T} (T_0^{(i)} T_0^{(i)T})^{-1} \quad (13^a)$$

$$E^{(i)} = m_1^{(i)} - A^{*(i)} m_0^{(i)} \quad (13b)$$

With the purpose of preventing the over fitting of the parameters into consideration, factor specified by the following mathematical expression Tikhonov regularization is used:

$$A = \min_{\lambda} (T_0^{(i)} T_1^{(i)T} + \delta^2 I)^{-1} \quad (14)$$

where I represents the unitary matrix and δ^2 . It is a positive real value, known as a factor of adjustment [8]. [8].

A Stable Dynamic Estimation.

To identify the system parameters seismic from a small amount of training of some state variables data, needs to be restriction on the values derived from the transition matrix and reach a dynamic appropriate supported in that its concentration consists in extracting the behavior of segments of the observed trajectories, for example Atomic linear behavior patterns exponential and logarithmic, however the restriction must be based on the dynamic stability, it must be available to find moves that

converge to certain States from an initial position. The key idea to estimate the stable dynamics is the method of restriction in the eigenvalues on condition that all values must be less than 1.

Seismic model.

In order to illustrate this approach used the model proposed by Gerard T. Schuster in his work "Seismic interferometry"(<http://utam.gg.utah.edu/Inter.LAB1/>)

Which specifies the following information: are 400 shooting eventually displaced on a surface and 12 Geophones eventually displaced from the Center (3000m offset) in a range of 1900 to 2100 meters in depth? To address this problem, a new method for determining the speed of migration that requires only the domain data is formulated offset-time (time series); using the first and second derivative of the propagation time of the waves with respect to the location of the receiver from a family of common shooting.

A graph (see Figure 3) data entry of the proposed problem is the behavior of the density in different strata at known depths. This field work is called data models. .

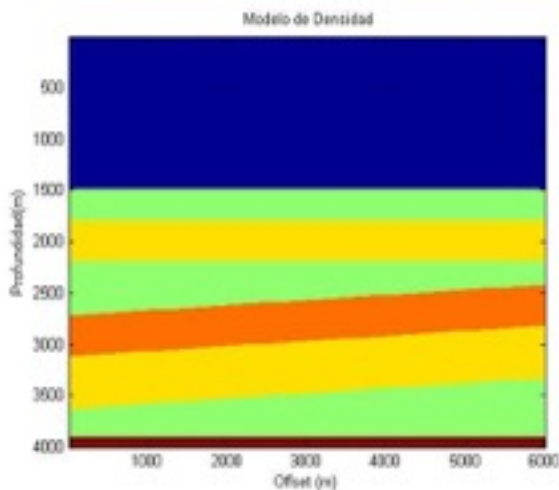


Fig 3. Seismic density model

The behavior of the propagation time of the waves in the Offset (position of Geophones) term is illustrated in Figure 4. This propagation time is the result of using "forward" methods for ray-tracing

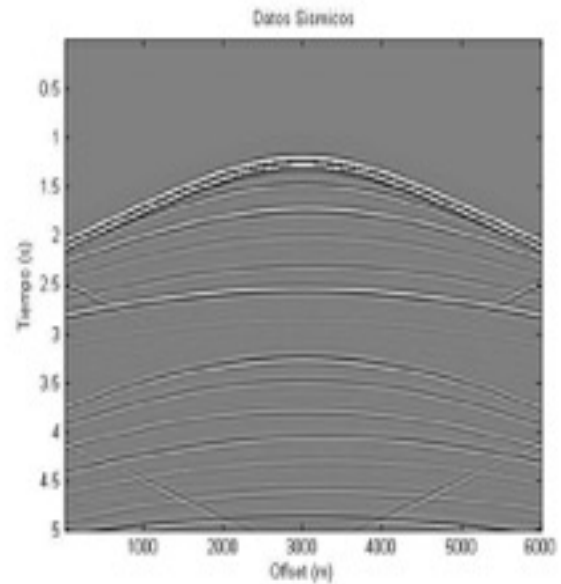


Fig 4. Seismic data travel time

Experimental Results.

In Figure 5, illustrated in the area of traits (slope-curvature) the concordance of a history of the propagation time of a trace, represented by dynamic average values (top) and temporal dynamic points green, red, blue, black and Brown) according to the concept of structural similarity. You can see all the segments represented by sequences of the same color to converge to zero.

The application of the concept of structural similarity for the "Travel time" paths is generate from each of the shots from one or more sources.

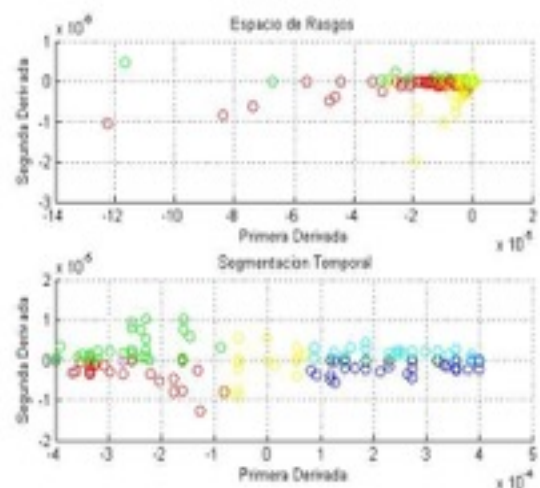


Fig. 5. Space of **feature** (Slope-Curvature)

Dynamic grouping begins with the process of extraction of the features (derivation of his first and second derivative with respect to the distance between sources and receivers) and the operation of conjunction that relates them to their respective values of slope and curvature resulting in a method of grouping is labeled by different colors. As shown in the figure above, for shooting 100, 200, 300 and 400 with respect to the positions of the receivers.

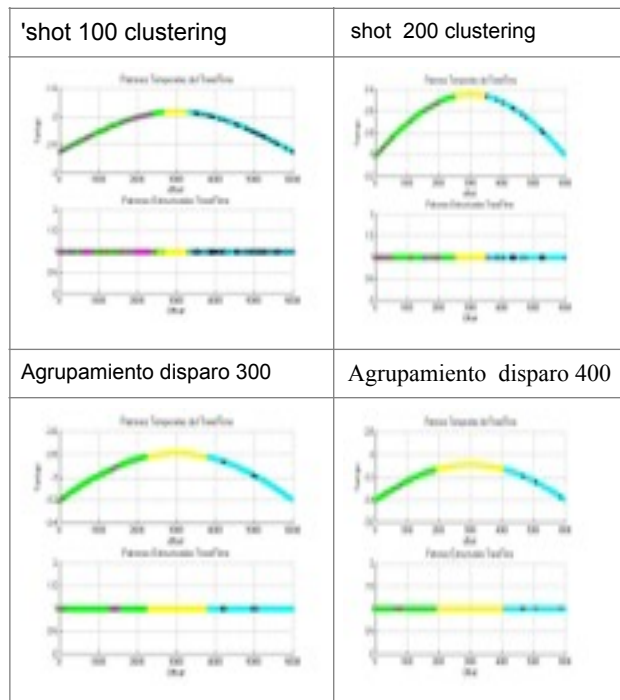


Fig. 6 Temporal clustering travel time in offset

These examples illustrate the diversity of the forms of the curves of the propagation time of the waves, that can result from simple changes in e ; I inland subsoil. From the [standpoint of geology becomes complex, the resulting complexities increases at the point where the identification simply cause and effect is impossible].

Implementation was carried out with discrete data, we used the central approach of the partial derivatives of the propagation time differences and from equation 5 is estimated the effective "slowness".

Computational methods, its result is illustrated in Figure 7, and is called speed. Represents the behavior of speed in space offset-(inverse of the seismic delay) depth of 400

shots and are derivatives with finite differences of first and second degree of propagation of the waves (trace) times.

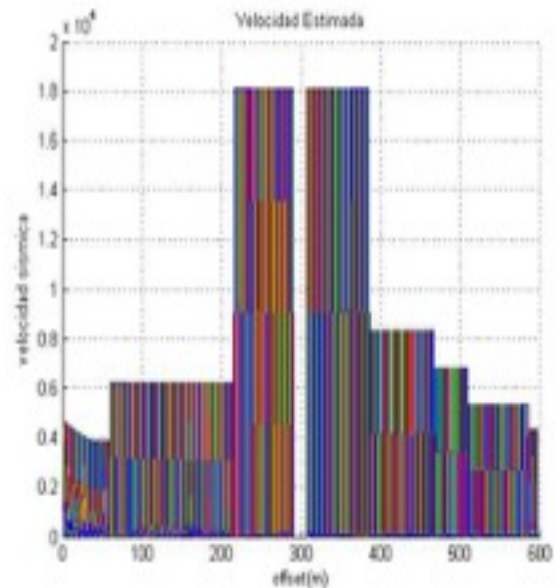


Fig. 7 Model of effective speed in the group travel time

The hypothesis of the research process that originates this document can be stated thus: the location of reflectors is presented in the change of pattern using the grouping method using structural similarity (see table 1) and based on the I -change of speed are formalized by Snell's law and of Huygens's principle in the propagation of waves in continuous media.

To demonstrate the above hypothesis, were tested with each of the traces of the "travel time" and determined the graphic concordance (see graphic 8) between the change of speed of the respective plots (see equation 7) and dynamic clustering (structural similarity) derived from the conjunctiva implementation between the values of the slope and curvature in differential form.

In addition, we present results of migration widespread in three dimensions. To get the speed of migration may be similar to the obtained expressions mediate you consideration of stationary points of the coordinates of the image reflected with respect to the changes from (y_r) depth and is thus formalized:

$$p^2 = p_y^2 + t_{p_{yy}}$$

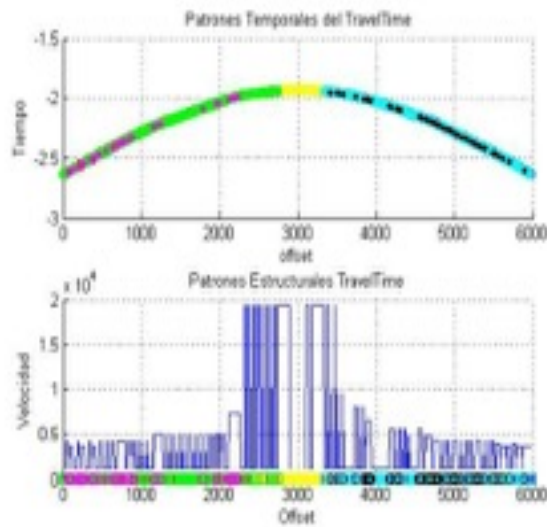


Fig.8. Matching between the change of dynamic pattern in the offset and change of seismic speed

Migration speed is determined by the second derivative of the propagation time with respect to a single coordinate of the receiver. This means that it is not necessary to have the same data sampled in x directions or to find the second derivative of the "travel time" with respect to the location of the receiver. To find the speed of migration, you can use the derivative along the direction of the receiver with the finer separation. As shown in Figure 8.

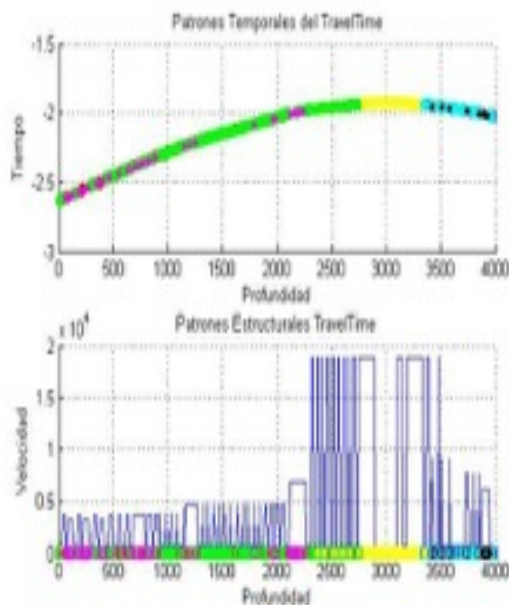


Fig.7 matching between the change of dynamic pattern in depth and seismic velocity change

The above results shows that migration speed is given by the shape of the curve "travel time" in the vicinity of the zero offset value for each group generated at the source. If the speed doesn't change much from each shot of the group, then the image presented is a migration in time with a speed corresponding to the speed constant migration.

Figure 9 illustrates the speed changes with instances in 100,200,300,400 in depth; you can see the difference in speed changes (characterized in the dynamic grouping and the implementation of the calculation of the effective speed) in a shot of each group. The behavior of time-series presents seismic coherence.

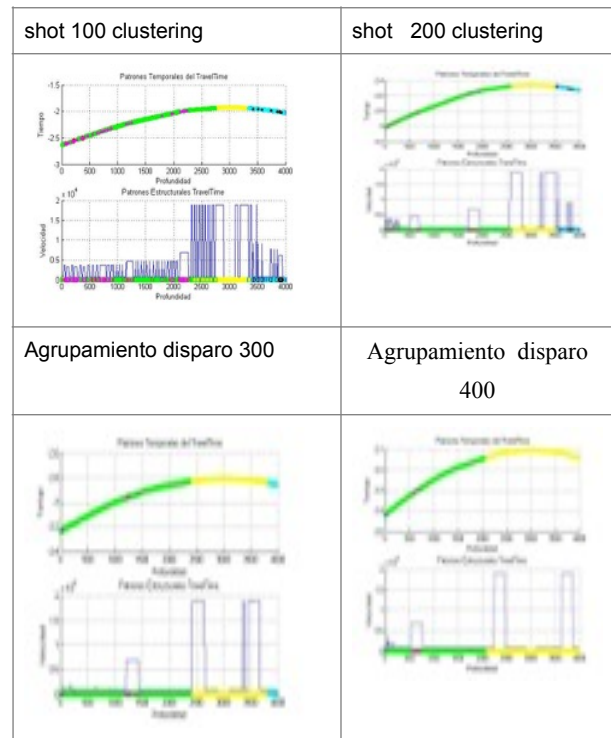


Fig. 9 Positions of reflectors in depth

The migration method using the estimate of the first and second derivative of the trajectory of the propagation time requires smoothing of the data processes. However the method of structural similarity in the estimation of these parameters is sensitive to noise in varying degrees. Publications exist to compare the estimate of the local slopes including methods of stacking, destroyers of plane waves, errors of prediction and "curvelet" filters, methods for the estimation of the second derivative are less numbers, sketch analyses are the most common. The methods of estimation of the second derivative in the presence of noise are still an open problem.

Seismic migration is a process whereby the seismic events is geometrically relocate in space or time, location an event occurs in the subsurface in the place where you registered on the surface, thus creating a more accurate picture of the subsurface. This process is necessary to overcome the limitations of geophysical methods imposed by areas of complex geology, such as: failure, saline bodies, and seismic varieties.

The simplest form of migration is the migration graphic. Graphical migration assumes a world of constant velocity and zero correction data, a geophysicist draws circles or spheres from the receiver to the location of the event for all events. The intersection of the circles and then form the 'real' the location of the reflector in time or space.

According to the demonstration of the hypothesis put forward in the research work and illustrated in figures 6,7,8; the purpose of this application with the comparison and identification of reflectors in space (offset-depth) derived coordinates locations, a from evolution of the propagation time of the grouped waves with the use of the structural similarity. According to this comparison and identification of the location of the reflectors you can graphically represent the model of migration.

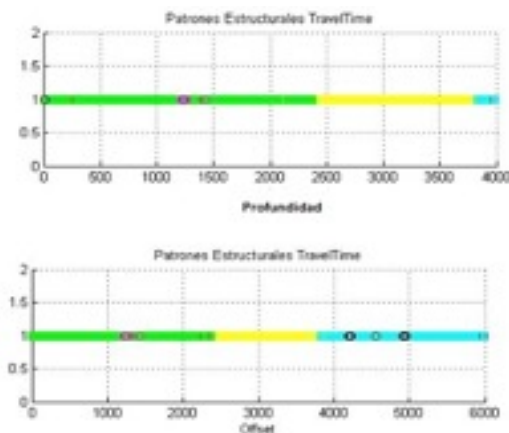


Fig. 10 Comparison de "travel time" en offset -depth

The method of migration of data from a group of shooting has an optimal implementation for synthetic data and a possible application for the method of imaging during seismic. acquisition.

Figure 11, illustrates the results (an instance) method of clustering and identification with restriction on the values [1] matrices of transition and its respective bias (noise) as

specified in equations 10 and 11. The different colors mean different ranges at high speed in the x-z space.

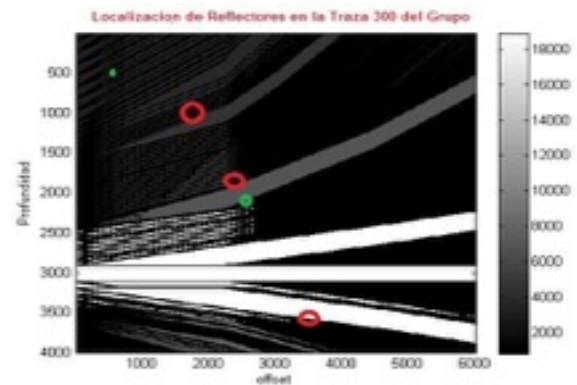


Fig. 11 Location of reflectors in a trace

Conclusions

Starting from the hypothesis, whose statement is "the possible location of the reflectors using the concept of structural similarity which match this specified on the form and evolution of trajectories?".

It has been assumed that the effective speed is constant and that reflectors are locally planes that did not affect the computational applicability to certain geological situations as demonstrated through the proposed example.

The presented method depends only on the shot group and it is not necessary to know the relative positions between sources and receivers, which are replaced by the slopes and local horizontal and vertical curvatures.

In conclusion it method has many advantages over existing methods of speed-independent migration processes. The method is computationally fast and requires little memory, is an extension of the method of grouping proposed Colina-castaneda for the method of clustering and identification of linear dynamical systems with restrictions on the eigenvalues.

Standard migration techniques require a speed model. Consider this new and fast method of migration in pre-stack time and discovering the potential features of processes of segmentation by structural similarity and the recognition of dynamic patterns in temporal trajectories.

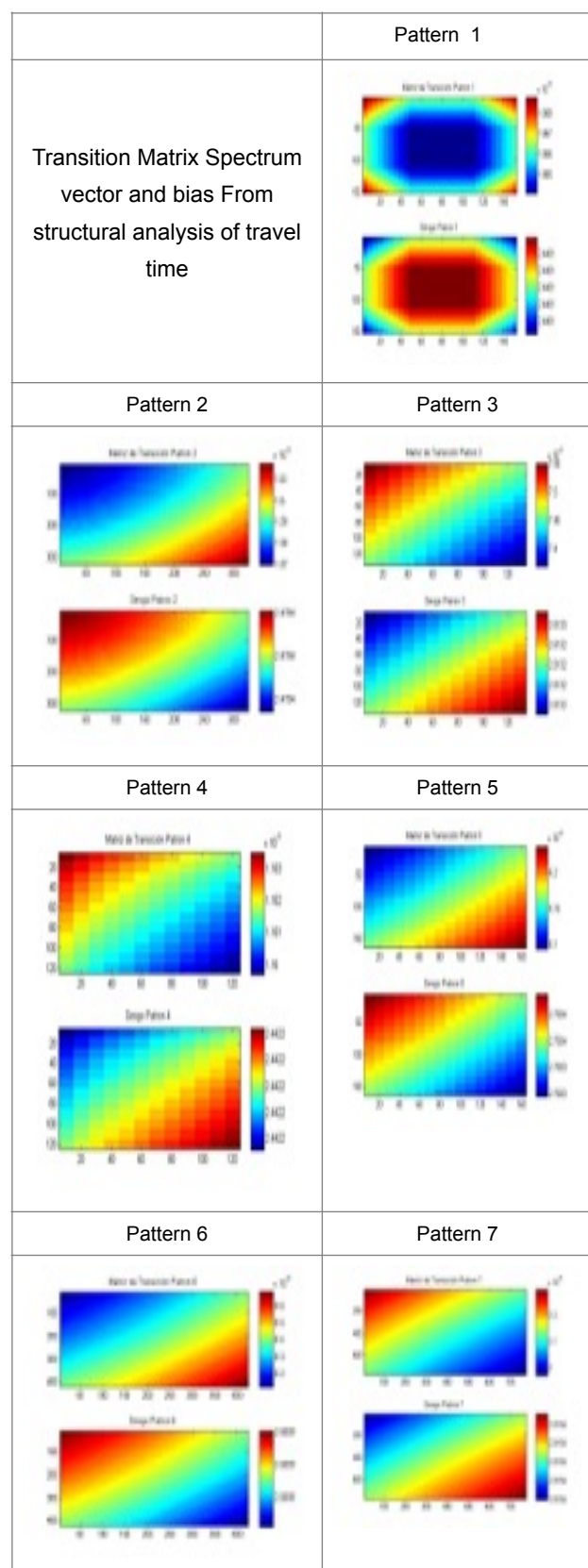


Fig. 12 slowness matrix estimate

Acknowledgments

We thank to the universities of los Andes and Pamplona for the dedication of its faculty in the participation of the calls of Colciencias and other institutions as Ecopetrol .

References

- [1] Berryman G. James, Seismic cross hole Tomography and Nonlinear constrained optimization, University of California, Lawrence Livermore National Laboratory, P.O. Box 808 L-156, Livermore, CA94550
- [2] Billette Frédéric, Velocity macro model estimation in seismic reflection by Stereo tomography, PHD Thesis, Denis Diderot University, 17 Dec 1998.
- [3] Casanta Lorenzo, Fomel Sergey, Velocity-Independent τ -p move out in a Horizontally –layered VTI medium, Geophysics 76, no 4,U45-U57,(2011)
- [4] Cooke D,Bóna A,Hansen B,Geophysic vol 74 , No 6, (November –december 2009)
- [5] Moret J.M.,Clement William P.,Knoll Michael and Barrash Warren,Vsp travel time inversion: Near Surface Issues, Geophysics , Vol 69, No 2 (March-April) 2004, computational intelligency, Sankt, augusting, p 98-105.
- [6] Kawashima, H., Matsuyama, T. , Proc. 3rd International Conference on Advances in Pattern Recognition (S. Singh et al. (Eds.): ICAPR 2005, LNCS 3686, Springer), pp. 229-238, 2005
- [7] Joentgen., Mikenina. Weber, R., Zimmerman, H.-J., (1998), Dynamic Fuzzy Data Analysis: Similarity between Trajectories. In: Bauer. (Ed.) Fuzzy Neuro System' 98, computational intelligency, Sankt, augusting, p 98-105
- [8] T. Sabsevary,A.Talebi, R. Adarkanian,A. Shamsai,A steady saturation model to determine the subsurface travel time (STT) in complex hill slopes, Hydrology and Earth System Science , Copernicus Publication on behalf of the European Geosciences union, 4 June 2010
- [9] Schuster Gerard T, Seismic interferometry,Cambidge , 2009, isbn: 9780521871242
- [10] Stephen Ralph , Harding Alistair ,Travel time Analysis of Borehole Seismic Data, redistribution subject to SEG , 29 Mar 2013.
- [11] Zhang Jie, Toksoz Nafi, Nonlinear refraction travel time tomography, Geophysics Vol 63,No 5 , September – October 1998.

Taking account of covariance estimation uncertainty in spatial sampling design for prediction with trans-Gaussian random fields

Gunter Spöck¹ and Jürgen Pilz^{2,*}

^{1 2}*Department of Statistics, Alps-Adria University Klagenfurt, Klagenfurt, Austria*

Correspondence*:

Jürgen Pilz

Department of Statistics, Alps-Adria University Klagenfurt, Universitätsstrasse 65-67, 9020 Klagenfurt, Austria, juergen.pilz@aau.at

ABSTRACT

Recently, Spöck and Pilz [10], demonstrated that the spatial sampling design problem for the Bayesian linear kriging predictor can be transformed to an experimental design problem for a linear regression model with stochastic regression coefficients and uncorrelated errors. The stochastic regression coefficients derive from the polar spectral approximation of the residual process. Thus, standard optimal convex experimental design theory can be used to calculate optimal spatial sampling designs. The design functionals considered in this paper did not take into account the fact that the kriging predictor actually is a plug-in predictor, where the estimated covariance function is plugged into the best linear predictor. Because the design criterion did not consider the uncertainty of the covariance function the resulting optimal designs were close to space-filling designs.

In this paper we assume the covariance function to be estimated, too, e.g., by restricted maximum likelihood (REML), and we develop a design criterion that fully takes account of the fact that the kriging predictor is a plug-in predictor. The designs resulting from this criterion are less regular and space-filling as before but also require samples very close to each other in order to get the covariance function well estimated. We also dismiss the assumption of Gaussian observations and assume the data to be transformed to Gaussianity by means of the Box-Cox transformation. The resulting

prediction method is known as trans-Gaussian kriging. We apply the Smith-Zhu [9] approach also to this kriging method and show that resulting optimal designs are then also dependent on the available data. As illustrative data set serve monthly rainfall measurements from Upper Austria.

Keywords : planning of monitoring networks, polar spectral representation, spatial design, Smith and Zhu [9] design criterion, trans-Gaussian kriging, rainfall data.

1 INTRODUCTION

A standard approach in geostatistics is to estimate the covariance function by means of weighted least squares or restricted maximum likelihood and then to plug-in this estimate into the formula for the kriging predictor. This plug-in kriging predictor is no longer linear nor optimal. This approach does not matter so far as one considers the variance of this plug-in predictor not to be best estimated by the so-called plug-in kriging variance, where the covariance estimate is plugged into the standard expression for the kriging variance. Harville and Jeske [4] and Abt [1] show that the plug-in kriging variance underestimates the true variance of the considered plug-in kriging predictor in certain cases to a large amount and give corrections to this plug-in variance. Zhu and Stein [14] apply this correction also to a design criterion for spatial sampling design and calculate almost optimal designs by means of simulated

annealing and a two-step algorithm. As a first step they adopt simulated annealing to the plug-in kriging variance to find many design locations that have good predictive performance and then as a second step adopt simulated annealing again but this time to the corrected plug-in variance to get also some design locations with good estimative performance for covariance estimation. Smith and Zhu [9] give a new interpretation of this design criterion as measuring the average lengths of estimated predictive intervals having no coverage probability bias. Up to date simulated annealing algorithms are a gold standard for calculating spatial sampling designs, see for example Diggle and Lophaven [2], because the design criteria seem to be mathematically intractable.

In this paper we will make no usage of stochastic search algorithms but will derive a mathematically tractable structure of the investigated design criteria so that deterministic design algorithms can be used. We are going to show certain advantageous mathematical properties of the complicated Smith and Zhu [9] design criterion like continuity and demonstrate that for optimizing this design criterion and finding optimal design locations no stochastic search algorithms like simulated annealing are necessary. On the contrary, spatial sampling designs can be found by means of methods and deterministic algorithms from the standard theory of convex optimization and classical experimental design. The theoretical developments are illustrated with a dataset taken from rainfall monitoring.

For a survey of model-based spatial sampling design we refer to Spöck and Pilz [10].

2 BAYESIAN SPATIAL LINEAR MODEL AND CLASSICAL EXPERIMENTAL DESIGN PROBLEM

We consider a mean square continuous (m.s.c.) and isotropic random field $\{Y(x) : x \in \mathbf{X} \subseteq R^2\}$ such that

$$Y(x) = \mathbf{f}(x)^T \beta + \varepsilon(x), \quad E\varepsilon(x) = 0,$$

where $\mathbf{f}(x)$ is a known vector of regression functions, $\beta \in R^r$ a vector of unknown regression

parameters and

$$\text{Cov}(Y(x), Y(y)) = C(\|x - y\|); \quad x, y \in \mathbf{X}.$$

Spöck and Pilz [10] demonstrate that in accordance with Yaglom [13], one can get an arbitrarily close approximation to the isotropic random field in form of a mixed linear model

$$Y(x) \approx \mathbf{f}(x)^T \beta + \mathbf{g}(x)^T \alpha + \varepsilon_0(x). \quad (1)$$

Here the components of the additional regression vector $\mathbf{g}(\cdot)$ are made up of the following radial basis functions (cosine-sine-Bessel-harmonics); assuming polar coordinates (t, ϕ) these are

$$g_{m,i}(t, \varphi) = \cos(m\varphi) J_m(\omega_i t); \quad (2)$$

$$m = 0, \dots, M; i = 1, \dots, n$$

$$g_{m,i}(t, \varphi) = \sin((m - M)\varphi) J_{m-M}(\omega_i t);$$

$$m = M + 1, \dots, 2M; i = 1, \dots, n$$

and derive from the so-called polar spectral approximation of the error process $\varepsilon(x)$. The random regression parameter vector α has mean $\mathbf{0}$, and a diagonal covariance matrix \mathbf{A} , whose variance components can be calculated from the isomorphic correspondence of the isotropic covariance function to its polar spectral distribution function. Actually the continuous spectrum of the residual process $\varepsilon(x)$ is approximated by a discrete spectrum represented by a piecewise constant function with discontinuities at $\omega_1, \dots, \omega_n$ serving as an approximation of the polar spectral distribution function.

Starting from the spatial mixed linear model (1), (2) we may gain further flexibility with a Bayesian approach incorporating prior knowledge on the trend. To this we assume that the regression parameter vector β is random with

$$E(\beta) = \mu \in R^r, \quad \text{Cov}(\beta) = \Phi \quad (3)$$

This is exactly in the spirit of Omre [6] who introduced Bayesian kriging this way. He used physical process knowledge to arrive at “qualified guesses” for the first and second order moments, μ and Φ , respectively. On the other hand, the state of prior ignorance or non-informativity can be modelled by setting $\mu = \mathbf{0}$ and letting Φ^{-1} tend to the matrix of zeros, thus passing the “Bayesian bridge” to universal kriging, see Omre and Halvorsen [7].

Now, combining (1), (2) and (3), we arrive at the **Bayesian spatial linear model** (BSLM)

$$Y(x) = \mathbf{h}(x)^T \gamma + \varepsilon_0(x) \quad (4)$$

where

$$\mathbf{h}(x) = \begin{pmatrix} \mathbf{f}(x) \\ \mathbf{g}(x) \end{pmatrix}, \gamma = \begin{pmatrix} \beta \\ \alpha \end{pmatrix},$$

$$E\gamma = \begin{pmatrix} \mu \\ 0 \end{pmatrix}, \text{Cov}(\gamma) = \begin{pmatrix} \Phi & 0 \\ 0 & A \end{pmatrix} =: \Gamma$$

Here $\varepsilon_0(x)$ is white-noise with variance σ_0^2 . (Actually we assume that the variation in the original error process, which the term $\mathbf{g}(x)^T \alpha$ does not take into account, can be approximated sufficiently closely by the uncorrelated white noise term $\varepsilon_0(x)$). Spöck and Pilz [10] demonstrate that Bayesian linear trend estimation in the above BSLM actually approximates Bayesian linear kriging in the original model arbitrarily closely. The same is true for the total mean squared error (TMSEP) of the trend prediction and the TMSEP of Bayesian kriging.

Thus, taking the TMSEP of the trend prediction in the approximating model as a substitute for the Bayes kriging TMSEP, we arrive at the following classical experimental design problem for so-called I-optimality:

$$\int_{\mathbf{X}} \mathbf{h}(x_0)^T (\mathbf{H}^T(d_n) \mathbf{H}(d_n) + \sigma_0^2 \Gamma^{-1})^{-1} \mathbf{h}(x_0) dx_0 \rightarrow \min_{d_n}. \quad (5)$$

Here $d_n = \{x_1, x_2, \dots, x_n\}$ collects either the design points to be added to the monitoring network or in the case of reducing the network the design points remaining in the monitoring network. $\mathbf{H}(d_n) = \sum_{i=1}^n \mathbf{h}(x_i) \mathbf{h}(x_i)^T$ denotes the design matrix, which explicitly depends on the design points in the set d_n .

At this point we advise the reader not familiar with Bayesian experimental design theory to read the Appendix of Spöck and Pilz [10]. The key point in this theory is that the above so-called concrete design problem, which is mathematically

intractable, may be expanded to a so-called continuous design problem that has the nice feature of being a convex optimization problem. Thus, the whole apparatus of convex optimization theory is available to approximately solve the above design problem for I-optimality. In particular, directional derivatives may be calculated and optimal continuous designs may be found by steepest descent algorithms. Continuous designs are just probability measures ξ on \mathbf{X} and may be rounded to exact designs d_n . Defining the so-called continuous Bayesian information matrix

$$\mathbf{M}_B(\xi) = \int_{\mathbf{X}} \mathbf{h}(x) \mathbf{h}(x)^T \xi(dx) + \frac{\sigma_0^2}{n} \Gamma^{-1} \quad (6)$$

and

$$\mathbf{U} = \int_{\mathbf{X}} \mathbf{h}(x_0) \mathbf{h}(x_0)^T dx_0, \quad (7)$$

it may be shown that the set of all such information matrices is convex and compact and that the extended design functional

$$\Psi(\mathbf{M}_B(\xi)) = \text{tr}(\mathbf{U} \mathbf{M}_B(\xi)^{-1}) \quad (8)$$

is convex and continuous in $\mathbf{M}_B(\xi)$. The above design functional $\Psi(\cdot)$ thus attains its minimum at a design $\xi^* \in \Xi$, where Ξ is the set of all probability measures defined on the compact design region \mathbf{X} , see Pilz [8]. The closeness of exact designs d_n to the optimal continuous design ξ^* may be judged by means of a well-known efficiency formula (cp. the Appendix of Spöck and Pilz [10]).

The idea to approximate the random field by a mixed model is not new. Actually, Fedorov [3] was the first to do this. He made use of the so-called Karhunen-Loeve approximation to the error process. This approach has the disadvantage that a complicated Eigen-problem has to be solved, whereas the calculation of the polar spectral approximation, which is used here, is easier and more accessible, see Spöck and Pilz [10].

3 THE SMITH AND ZHU (2004) DESIGN CRITERION TAKING ACCOUNT THAT THE COVARIANCE FUNCTION IS ESTIMATED

In real world applications the isotropic covariance function $C_\theta(t)$ is always uncertain and has to be

estimated. The kriging predictor used is then based on this estimated covariance function. Thus, the kriging predictor is always a plug-in predictor with the estimate for the covariance function inserted into the formula for the kriging predictor and the reported (plug-in) kriging variance may be shown to underestimate the true variance of this plug-in predictor [4].

Smith and Zhu [9] consider spatial sampling design by means of minimizing the average of the lengths of estimated $1 - \alpha$ predictive intervals:

$$\frac{1}{|\mathbf{X}|} \int_{\mathbf{X}} \{\text{length of estimated } 1 - \alpha \text{ predictive interval at } x_0\} dx_0 \rightarrow \underset{d_n=\{x_1, \dots, x_n\}}{\text{Min}}$$

Here $|\mathbf{X}|$ denotes the area of the design region. Their predictors of the $\alpha/2$ and $1 - \alpha/2$ quantiles of the predictive distributions are selected in such a way that the corresponding estimated predictive intervals have coverage probability bias 0 to order $O(n^{-1})$, where n is the number of observations. That means, $\mathbf{E}\{\Phi(\hat{y}_{1-\alpha/2}(\mathbf{Y}), \theta_0)\} = 1 - \alpha/2$ to order $O(n^{-1})$, where $\hat{y}_{1-\alpha/2}(\mathbf{Y})$ is the estimated $(1 - \alpha/2)$ predictive quantile and $\Phi(\cdot, \theta_0)$ is the true, unknown predictive cumulative distribution function, i.e., a Gaussian distribution with mean equal to the true unknown universal kriging predictor and variance equal to the true unknown universal kriging variance, both based on the true unknown covariance parameters θ_0 . The above expectation is taken with respect to the true unknown Gaussian distribution of the data \mathbf{Y} . The estimates $\hat{y}_{\alpha/2}(\mathbf{Y})$ and $\hat{y}_{1-\alpha/2}(\mathbf{Y})$ of the mentioned quantiles are essentially the plug-in universal kriging predictor based on restricted maximum likelihood (REML) estimation of the covariance parameters plus/minus a scaled plug-in kriging standard deviation term that is corrected to take account of REML estimation, see (35) and [9]. Based on Laplace approximation of the true predictive density Smith and Zhu [9] show that the above design criterion, up to order $O(n^{-2})$, is equivalent to:

(9)

$$\begin{aligned} \int_{\mathbf{X}} [\sigma_{\hat{\theta}}^2(x_0) + \text{tr}(\kappa_{\hat{\theta}}^{-1} \{ \frac{\partial \lambda_{\hat{\theta}}(x_0)}{\partial \theta^T} \}^T \mathbf{K}_{\hat{\theta}} \frac{\partial \lambda_{\hat{\theta}}(x_0)}{\partial \theta^T}) \\ + y_{1-\alpha/2}^2 \{ \frac{\partial \sigma_{\hat{\theta}}(x_0)}{\partial \theta} \}^T \kappa_{\hat{\theta}}^{-1} \frac{\partial \sigma_{\hat{\theta}}(x_0)}{\partial \theta}] dx_0 \\ \rightarrow \underset{d_n=\{x_1, \dots, x_n\}}{\text{Min}} \end{aligned}$$

Obviously the above design functional is evaluated at $\hat{\theta}$, the REML estimate of the covariance parameters. Above

$$(\kappa_{\hat{\theta}})_{i,j} = \text{tr}(\mathbf{W}_{\hat{\theta}} \frac{\partial \mathbf{K}_{\hat{\theta}}}{\partial \theta_i} \mathbf{W}_{\hat{\theta}} \frac{\partial \mathbf{K}_{\hat{\theta}}}{\partial \theta_j}) \quad (10)$$

is the Fisher information matrix for REML estimation of θ ,

$$\mathbf{W}_{\hat{\theta}} = \mathbf{K}_{\hat{\theta}}^{-1} - \mathbf{K}_{\hat{\theta}}^{-1} \mathbf{F} (\mathbf{F}^T \mathbf{K}_{\hat{\theta}}^{-1} \mathbf{F})^{-1} \mathbf{F}^T \mathbf{K}_{\hat{\theta}}^{-1}, \quad (11)$$

$y_{1-\alpha/2}$ is the $1 - \alpha/2$ -quantile of the standard normal distribution, $\sigma_{\hat{\theta}}^2(x_0)$ is the universal kriging variance at x_0 and $\lambda_{\hat{\theta}}(x_0)$ is the universal kriging weights vector for prediction at x_0 so that the universal plug-in kriging predictor reads

$$Y_{UK, \hat{\theta}}(x_0) = \lambda_{\hat{\theta}}(x_0)^T \mathbf{Y}$$

The design criterion given above takes both prediction accuracy and covariance uncertainty into account. A design criterion similar to the Smith and Zhu [9] criterion was considered also by Zimmerman [15].

4 EXPERIMENTAL DESIGN THEORY APPLIED TO THE SMITH AND ZHU (2004) DESIGN CRITERION

Sections 2 and 3 have demonstrated that by using the BSLM (4) as approximation to the true isotropic random field the I-optimality design criterion (5) can be completely expressed in terms of the Bayesian information matrix

$$\mathbf{M}_B = \mathbf{H}^T \mathbf{H} + \sigma_0^2 \mathbf{\Gamma}^{-1}.$$

and that it is convex on the set of all such information matrices. Thus, classical convex experimental design algorithms could be used to find optimal spatial sampling designs minimizing

the criterion (5).

The aim of this section is to demonstrate that the Smith and Zhu [9] design criterion has some favourable properties, too, which allow the application of classical convex experimental design theory to this design criterion:

Theorem : Expression (9) can be expressed completely in terms of the Bayesian information matrix \mathbf{M}_B . The design functional is continuous on the convex and compact set of all matrices $\mathbf{M}_B(\xi)$. This allows us to make use of classical experimental design algorithms to find spatial sampling designs.

4.1 THE DESIGN CRITERION CAN BE EXPRESSED IN TERMS OF THE BAYESIAN INFORMATION MATRIX \mathbf{M}_B

Assuming the BSLM (4), the covariance function actually is parametrized in the diagonal matrix \mathbf{A} and the nugget variance σ_0^2 . Since the Smith and Zhu [9] design criterion assumes the covariance parameters to be estimated by restricted maximum likelihood we actually estimate this diagonal matrix \mathbf{A} and σ_0^2 by this methodology. The a priori covariance matrix $\Phi = \text{Cov}(\beta)$ must be given almost infinite diagonal values because the Smith and Zhu [9] approach assumes the trend parameter vector β to be estimated by generalized least squares and $\Phi \rightarrow \infty$ bridges the gap from Bayesian linear to generalized least squares trend estimation. The a priori mean $\mu = E(\beta)$ can be set to 0 then.

According to the polar spectral representation given in Spöck and Pilz [10], several values in the diagonal matrix \mathbf{A} are identical:

$$\mathbf{A} = \text{diag}(\{d_m a_i^2\}_{m=0,\dots,M; i=1,\dots,n; k=1,2}), \quad (12)$$

where the definitions of the a_i^2 's, -the discrete spectra-, and the indexing derive from the polar spectral representation given in Spöck and Pilz [10]. $k = 1, 2$ index the sine-Bessel term and the cosine-Bessel term in formula (2); and $d_m = 1$ for $m = 0$ and $d_m = 2$ for $m \geq 1$. For restricted maximum likelihood estimation of \mathbf{A} we have two possibilities:

- We can leave the discrete spectra a_i^2 unspecified: This approach is almost nonparametric because a lot of a_i 's and corresponding frequencies w_i are needed to get the isotropic random field properly approximated and corresponds to a semiparametric estimation of the spectral distribution function via a step function.
- We can specify a parametric model for the a_i^2 's: The polar spectral density function for an isotropic random field over R^2 possessing for example an exponential covariance function $B(h) = C \exp(-\frac{3h}{\alpha})$ is given by

$$g(w) = \frac{C \frac{3}{\alpha} w}{((\frac{3}{\alpha})^2 + w^2)^{3/2}}.$$

The polar spectral density function is defined as the first derivative of the polar spectral distribution function $G(w)$, see Spöck and Pilz [10]. A possible parametrization for the a_i^2 's:

(13)

$$\begin{aligned} a_i^2 &= 0.5(g(w_i) + g(w_{i-1}))(w_i - w_{i-1}), \\ i &= 1, 2, \dots, n, \end{aligned}$$

where $0 = w_0 < w_1 < \dots < w_n$ are fixed frequencies.

In the following we will deal with both approaches for spatial sampling design. One may want to skip the following subsections at a first reading. It is just shown there that the Smith and Zhu [9] design criterion can be expressed as a function of the information matrix \mathbf{M}_B .

4.1.1 Kriging variance $\sigma_{0,K}^2$, kriging weights vector λ and \mathbf{W} expressed by \mathbf{M}_B . According to (5) the kriging variance can be expressed as

$$\sigma_{0,K}^2 = \sigma_0^2(1 + \mathbf{h}(x_0)^T \mathbf{M}_B^{-1} \mathbf{h}(x_0)).$$

The kriging weights vector may be written

$$\lambda = \mathbf{H} \mathbf{M}_B^{-1} \mathbf{h}(x_0),$$

and the matrix

$$\mathbf{W} = \frac{1}{\sigma_0^2} (\mathbf{I} - \mathbf{H} \mathbf{M}_B^{-1} \mathbf{H}^T), \quad (14)$$

where \mathbf{I} is the identity matrix. All these expressions derive from the application of the Sherman-Morrison-

Woodbury matrix inversion formula

$$\begin{aligned} (\mathbf{A} + \mathbf{UCV})^{-1} &= \\ &= \mathbf{A}^{-1} - \mathbf{A}^{-1}\mathbf{U}(\mathbf{C}^{-1} + \mathbf{VA}^{-1}\mathbf{U})^{-1}\mathbf{VA}^{-1}, \end{aligned}$$

from the fact that $\mathbf{GA}g(x_0)$ and $\sigma_0^2\mathbf{I} + \mathbf{GA}g^T$ are the vector of covariances and covariance matrix of observations, respectively, and that the kriging weights vector for Bayesian kriging may be written as

$$\lambda = (\mathbf{K} + \mathbf{F}\Phi\mathbf{F}^T)^{-1}(\mathbf{c}_0 + \mathbf{F}\Phi\mathbf{f}(x_0)),$$

where \mathbf{F} is the design matrix of the linear regression that is based on the drift function $\mathbf{f}(x)$.

4.1.2 Partial derivatives of \mathbf{M}_B^{-1} . Let $\mathbf{M}_B = \mathbf{H}^T\mathbf{H} + \sigma_0^2\mathbf{\Gamma}^{-1}$ be the Bayesian information matrix. Using the matrix identity

$$\frac{\partial \mathbf{M}^{-1}}{\partial t} = -\mathbf{M}^{-1} \frac{\partial \mathbf{M}}{\partial t} \mathbf{M}^{-1},$$

the partial derivative of \mathbf{M}_B^{-1} with respect to σ_0^2 may be calculated as

$$\frac{\partial \mathbf{M}_B^{-1}}{\partial \sigma_0^2} = -\mathbf{M}_B^{-1} \mathbf{\Gamma}^{-1} \mathbf{M}_B^{-1}. \quad (15)$$

Defining

$$\begin{aligned} \gamma_{m,i,k} &= d_m a_i^2, \\ m &= 0, \dots, M; \\ i &= 1, \dots, n; \\ k &= 1, 2 \end{aligned}$$

we obtain

$$\frac{\partial \mathbf{M}_B^{-1}}{\partial \gamma_{m,i,k}} = \frac{\sigma_0^2}{\gamma_{m,i,k}^2} \mathbf{M}_B^{-1} \mathbf{E}_{m,i,k} \mathbf{M}_B^{-1},$$

where $\mathbf{E}_{m,i,k}$ is a matrix of 0's, with only the m, i, k -th diagonal element being 1. Setting

$\gamma_{m,i,k} = d_m a_i^2$ and using

$$\frac{\partial \mathbf{M}_B^{-1}}{\partial a_i^2} = \sum_{m=0}^M \sum_{k=1,2} \frac{\partial \mathbf{M}_B^{-1}}{\partial \gamma_{m,i,k}} \frac{\partial \gamma_{m,i,k}}{\partial a_i^2}$$

one gets

$$\frac{\partial \mathbf{M}_B^{-1}}{\partial a_i^2} = \frac{\sigma_0^2}{a_i^4} \mathbf{M}_B^{-1} \mathbf{J}_i \mathbf{M}_B^{-1}, \quad (16)$$

where

$$\mathbf{J}_i = \sum_{m=0}^M \frac{1}{d_m} \sum_{k=1,2} \mathbf{E}_{m,i,k}.$$

For the parametric model (13) partial derivatives may be calculated by using

$$\begin{aligned} \frac{\partial \mathbf{M}_B^{-1}}{\partial \alpha} &= \sum_{i=1}^n \frac{\partial \mathbf{M}_B^{-1}}{\partial a_i^2} \frac{\partial a_i^2}{\partial \alpha} \\ \frac{\partial \mathbf{M}_B^{-1}}{\partial C} &= \sum_{i=1}^n \frac{\partial \mathbf{M}_B^{-1}}{\partial a_i^2} \frac{\partial a_i^2}{\partial C}. \end{aligned}$$

Defining

$$\begin{aligned} \mathbf{J}_\alpha &= \sigma_0^2 \sum_{i=1}^n \frac{1}{a_i^4} \frac{\partial a_i^2}{\partial \alpha} \mathbf{J}_i, \\ \mathbf{J}_C &= \sigma_0^2 \sum_{i=1}^n \frac{1}{a_i^4} \frac{\partial a_i^2}{\partial C} \mathbf{J}_i \end{aligned}$$

one obtains

$$\frac{\partial \mathbf{M}_B^{-1}}{\partial \alpha} = \mathbf{M}_B^{-1} \mathbf{J}_\alpha \mathbf{M}_B^{-1} \quad (17)$$

$$\frac{\partial \mathbf{M}_B^{-1}}{\partial C} = \mathbf{M}_B^{-1} \mathbf{J}_C \mathbf{M}_B^{-1} \quad (18)$$

Note, these expressions are dependent on the spatial design only via the Bayesian information matrix \mathbf{M}_B .

4.1.3 Partial derivatives of $\sigma_{0,K}$ and λ . Using the partial derivatives of \mathbf{M}_B^{-1} given in subsubsection

4.1.2 and the expressions for $\sigma_{0,K}^2$ and λ from subsection 4.1.1 we arrive at:

$$\frac{\partial \sigma_{0,K}^2}{\partial \sigma_0^2} = 1 + \text{tr}(\mathbf{h}(x_0)\mathbf{h}(x_0)^T \mathbf{M}_B^{-1} \mathbf{M} \mathbf{M}_B^{-1}) \quad (19)$$

$$\frac{\partial \lambda}{\partial \sigma_0^2} = -\mathbf{H} \mathbf{M}_B^{-1} \mathbf{\Gamma}^{-1} \mathbf{M}_B^{-1} \mathbf{h}(x_0) \quad (20)$$

$$\begin{aligned} \frac{\partial \sigma_{0,K}^2}{\partial a_i^2} &= \frac{\sigma_0^4}{a_i^4} \text{tr}(\mathbf{h}(x_0)\mathbf{h}(x_0)^T \mathbf{M}_B^{-1} \mathbf{J}_i \mathbf{M}_B^{-1}) \\ \frac{\partial \lambda}{\partial a_i^2} &= \frac{\sigma_0^2}{a_i^4} \mathbf{H} \mathbf{M}_B^{-1} \mathbf{J}_i \mathbf{M}_B^{-1} \mathbf{h}(x_0) \end{aligned} \quad (21)$$

$$\frac{\partial \sigma_{0,K}^2}{\partial \alpha} = \sigma_0^2 \text{tr}(\mathbf{h}(x_0)\mathbf{h}(x_0)^T \mathbf{M}_B^{-1} \mathbf{J}_\alpha \mathbf{M}_B^{-1}) \quad (22)$$

$$\begin{aligned} \frac{\partial \sigma_{0,K}^2}{\partial C} &= \sigma_0^2 \text{tr}(\mathbf{h}(x_0)\mathbf{h}(x_0)^T \mathbf{M}_B^{-1} \mathbf{J}_C \mathbf{M}_B^{-1}) \\ \frac{\partial \lambda}{\partial \alpha} &= \mathbf{H} \mathbf{M}_B^{-1} \mathbf{J}_\alpha \mathbf{M}_B^{-1} \mathbf{h}(x_0) \end{aligned} \quad (23)$$

$$\frac{\partial \lambda}{\partial C} = \mathbf{H} \mathbf{M}_B^{-1} \mathbf{J}_C \mathbf{M}_B^{-1} \mathbf{h}(x_0), \quad (24)$$

where $\mathbf{M} = \mathbf{M}_B - \sigma_0^2 \mathbf{\Gamma}^{-1}$. Partial derivatives $\frac{\partial \sigma_{0,K}}{\partial \theta}$ are then given as

$$\frac{\partial \sigma_{0,K}}{\partial \theta} = \frac{\partial \sigma_{0,K}^2}{\partial \theta} / (2\sqrt{\sigma_{0,K}^2}). \quad (25)$$

4.1.4 Expression for the information matrix κ . The i, j -th element of the information matrix κ is defined in (10), where \mathbf{W} is defined in (14) and we must set

$$\mathbf{K} = \mathbf{H} \mathbf{\Gamma} \mathbf{H}^T + \sigma_0^2 \mathbf{I} - \mathbf{F} \mathbf{\Phi} \mathbf{F}^T. \quad (26)$$

In the semiparametric model θ_i and θ_j are either made of the parameters a_i, a_j, σ_0^2 ; for the parametric model θ_i and θ_j may be either made of the parameters α, C, σ_0^2 .

For the partial derivatives of \mathbf{K} we obtain along the

same lines of reasoning as in subsections 4.1.2 and 4.1.3:

$$\begin{aligned} \frac{\partial \mathbf{K}}{\partial \sigma_0^2} &= \mathbf{I} \\ \frac{\partial \mathbf{K}}{\partial a_i^2} &= \mathbf{H} \mathbf{L}_i \mathbf{H}^T \\ \frac{\partial \mathbf{K}}{\partial \alpha} &= \mathbf{H} \mathbf{L}_\alpha \mathbf{H}^T \\ \frac{\partial \mathbf{K}}{\partial C} &= \mathbf{H} \mathbf{L}_C \mathbf{H}^T, \end{aligned}$$

where

$$\begin{aligned} \mathbf{L}_i &= \sum_{m=0}^M d_m \sum_{k=1,2} \mathbf{E}_{m,i,k}, \\ \mathbf{L}_\alpha &= \sum_{i=1}^n \frac{\partial a_i^2}{\partial \alpha} \mathbf{L}_i, \\ \mathbf{L}_C &= \sum_{i=1}^n \frac{\partial a_i^2}{\partial C} \mathbf{L}_i. \end{aligned}$$

Inserting these expressions and the expression (14) for \mathbf{W} into the definition (10) of the Fisher information matrix we obtain, after some linear algebra, the following expressions for κ :

$$\kappa_{a_i^2, a_j^2} = \text{tr}(\mathbf{L}_j \mathbf{V} \mathbf{L}_i \mathbf{V}) \quad (27)$$

$$\kappa_{\sigma_0^2, \sigma_0^2} = \frac{n-m}{\sigma_0^4} + \text{tr}(\mathbf{\Gamma}^{-1} \mathbf{M}_B^{-1} \mathbf{\Gamma}^{-1} \mathbf{M}_B^{-1})$$

$$\kappa_{\sigma_0^2, a_i^2} = \text{tr}(\mathbf{\Gamma}^{-1} \mathbf{M}_B^{-1} \mathbf{V} \mathbf{L}_i) \quad (28)$$

$$\kappa_{\alpha, \alpha} = \text{tr}(\mathbf{L}_\alpha \mathbf{V} \mathbf{L}_\alpha \mathbf{V}) \quad (29)$$

$$\kappa_{C, C} = \text{tr}(\mathbf{L}_C \mathbf{V} \mathbf{L}_C \mathbf{V}) \quad (30)$$

$$\kappa_{\alpha, C} = \text{tr}(\mathbf{L}_C \mathbf{V} \mathbf{L}_\alpha \mathbf{V}) \quad (31)$$

$$\kappa_{\sigma_0^2, \alpha} = \text{tr}(\mathbf{\Gamma}^{-1} \mathbf{M}_B^{-1} \mathbf{V} \mathbf{L}_\alpha) \quad (32)$$

$$\kappa_{\sigma_0^2, C} = \text{tr}(\mathbf{\Gamma}^{-1} \mathbf{M}_B^{-1} \mathbf{V} \mathbf{L}_C), \quad (32)$$

where

$$\mathbf{V} = \mathbf{\Gamma}^{-1} - \sigma_0^2 \mathbf{\Gamma}^{-1} \mathbf{M}_B^{-1} \mathbf{\Gamma}^{-1},$$

n is the number of design locations and m is the dimension of the information matrix.

4.1.5 Expression for the Smith and Zhu (2004) design criterion dependent only on \mathbf{M}_B . We are now going to show that the Smith and Zhu [9] design criterion (9) is dependent on the spatial sampling design only via the Bayesian information matrix \mathbf{M}_B . For simplicity we consider here only the expression of this design criterion for the parametric model (13). By analogy, similar expressions may be derived also for the semiparametric model. Defining $\theta = (\sigma_0^2, \alpha, C)^T$ we have to derive expressions for

$$\text{tr}(\kappa^{-1} \left\{ \frac{\partial \lambda}{\partial \theta^T} \right\}^T \mathbf{K} \frac{\partial \lambda}{\partial \theta^T})$$

and

$$\left\{ \frac{\partial \sigma_{0,K}}{\partial \theta} \right\}^T \kappa^{-1} \frac{\partial \sigma_{0,K}}{\partial \theta}.$$

Expressions dependent only on \mathbf{M}_B for the 3×3 matrix κ , for the kriging variance $\sigma_{0,K}^2$ and all partial derivatives of $\sigma_{0,K}$ and λ have already been given in the last subsubsections.

Defining the 3-column matrix

$$\begin{aligned} \mathbf{R}_{\mathbf{x}_0} &= (-\mathbf{M}_B^{-1} \mathbf{\Gamma}^{-1} \mathbf{M}_B^{-1} \mathbf{h}(x_0), \\ &\mathbf{M}_B^{-1} \mathbf{J}_\alpha \mathbf{M}_B^{-1} \mathbf{h}(x_0), \mathbf{M}_B^{-1} \mathbf{J}_C \mathbf{M}_B^{-1} \mathbf{h}(x_0)) \end{aligned}$$

such that

$$\frac{\partial \lambda}{\partial \theta^T} = \mathbf{H} \mathbf{R}_{\mathbf{x}_0}$$

we obtain after some linear algebra

$$\begin{aligned} \text{tr}(\kappa^{-1} \left\{ \frac{\partial \lambda}{\partial \theta^T} \right\}^T \mathbf{K} \frac{\partial \lambda}{\partial \theta^T}) &= \\ &= \text{tr}(\kappa^{-1} \mathbf{R}_{\mathbf{x}_0}^T \{ \mathbf{M} \mathbf{U} \mathbf{M} + \sigma_0^2 \mathbf{M} \} \mathbf{R}_{\mathbf{x}_0}), \end{aligned} \quad (33)$$

where

$$\begin{aligned} \mathbf{M} &= \mathbf{M}_B - \sigma_0^2 \mathbf{\Gamma}^{-1} \\ \mathbf{U} &= \begin{pmatrix} \mathbf{0} & \mathbf{0} \\ \mathbf{0} & \mathbf{A} \end{pmatrix}. \end{aligned}$$

Obviously,

$$\left\{ \frac{\partial \sigma_{0,K}}{\partial \theta} \right\}^T \kappa^{-1} \frac{\partial \sigma_{0,K}}{\partial \theta} \quad (34)$$

is dependent on the spatial design only via the Bayesian information matrix \mathbf{M}_B , observing

expressions (27)-(32) for κ and the expressions (20)-(25) for the partial derivatives of $\sigma_{0,K}$.

We may now consider experimental design ideas and replace, in the above expressions for the Smith and Zhu [9] design criterion, the matrix \mathbf{M}_B everywhere by its continuous version $n\mathbf{M}_B(\xi)$, where n is the number of spatial samples in consideration and

$$\mathbf{M}_B(\xi) = \int_{\mathbf{X}} \mathbf{h}(x) \mathbf{h}(x)^T \xi(dx) + \frac{\sigma_0}{n} \mathbf{\Gamma}^{-1}$$

with $\xi(dx)$ a probability measure on the design space \mathbf{X} , is the so-called continuous Bayesian information matrix associated to the Bayesian spatial linear model (4). As already mentioned, the set of all such information matrices is convex and compact. This way the Smith and Zhu [9] design criterion becomes a continuous functional over the convex and compact set of all such continuous Bayesian information matrices $\mathbf{M}_B(\xi)$. Continuity and compactness are nice properties because they guarantee that actually a minimum among all such continuous information matrices exists for this design functional.

5 SPATIAL SAMPLING DESIGN FOR TRANS-GAUSSIAN KRIGING

In trans-Gaussian kriging the originally positive valued data $Z(x_i), i = 1, 2, \dots, n$ are transformed to Gaussianity by means of the Box-Cox-transformation

$$g_\lambda(z) = \begin{cases} \frac{z^\lambda - 1}{\lambda} & : \lambda \neq 0 \\ \log(z) & : \lambda = 0 \end{cases}.$$

Let $\mathbf{Z} = (Z(x_1), Z(x_2), \dots, Z(x_n))^T$ be the vector of original data and

$$\mathbf{Y} = (g_\lambda(Z(x_1)), g_\lambda(Z(x_2)), \dots, g_\lambda(Z(x_n)))^T$$

be the vector of transformed data. The predictive density for trans-Gaussian kriging at a location x_0 then may be written:

$$\varphi(g_\lambda(z); \hat{Y}_{OK}(x_0), \sigma_{OK}^2(x_0)) * z^{\lambda-1},$$

where $\varphi(\cdot; \hat{Y}_{OK}(x_0), \sigma_{OK}^2(x_0))$ is the Gaussian density with mean equal to the ordinary kriging predictor $\hat{Y}_{OK}(x_0)$ at x_0 and based on the

transformed variables \mathbf{Y} , and variance equal to the ordinary kriging variance $\sigma_{OK}^2(x_0)$. The expression $z^{\lambda-1}$ is the Jacobian of the Box-Cox transformation.

For spatial sampling design taking into account the REML estimation of the covariance parameters θ we can consider again the average of the lengths of estimated $(1 - \alpha)$ -predictive intervals. In order to make the lengths of estimated predictive intervals also dependent on REML-estimation of the covariance function, we can consider instead of the Gaussian density $\varphi(\cdot; \hat{Y}_{OK}(x_0), \sigma_{OK}^2(x_0))$ that unique Gaussian density whose $\alpha/2$ and $1 - \alpha/2$ quantiles are given by the endpoints of the following estimated $(1 - \alpha)$ predictive interval derived in [9] and having coverage probability bias 0 to order $O(n^{-1})$:

$$\begin{aligned} & \hat{Y}_{\hat{\theta}, OK}(x_0) \pm \\ & y_{1-\alpha/2} \sigma_{\hat{\theta}}(x_0) \{1 + \\ & \frac{1}{2\sigma_{\hat{\theta}}^2(x_0)} [\text{tr}(\kappa_{\hat{\theta}}^{-1} \{ \frac{\partial \lambda_{\hat{\theta}}(x_0)}{\partial \theta^T} \}^T \mathbf{K}_{\hat{\theta}} \frac{\partial \lambda_{\hat{\theta}}(x_0)}{\partial \theta^T}) + \\ & y_{1-\alpha/2}^2 \{ \frac{\partial \sigma_{\hat{\theta}}(x_0)}{\partial \theta} \}^T \kappa_{\hat{\theta}}^{-1} \frac{\partial \sigma_{\hat{\theta}}(x_0)}{\partial \theta} \} \}. \end{aligned} \quad (35)$$

Here, $\hat{\theta}$ is the REML estimate of the covariance parameters and all expressions are evaluated at this estimate, $y_{1-\alpha/2}$ is the $1 - \alpha/2$ quantile of the standard normal distribution.

Later, when calculating spatial sampling designs with the algorithms from the appendix and investigating new prospective design locations with no data available, we have to replace in the statistic $T_{\hat{\theta}}(\mathbf{Y}) = \hat{Y}_{\hat{\theta}, OK}(x_0)$ every variable $Y(x_i)$ for which we do not have a datum by its ordinary kriging predictor based on the available data.

The above estimated lower and upper quantiles $\hat{y}_{\alpha/2}$ and $\hat{y}_{1-\alpha/2}$ of the Gaussian estimated $1 - \alpha$ predictive intervals are transformed back to the original Z-scale by means of the inverse Box-Cox transformation $g_{\lambda}^{-1}(\cdot)$ to get estimated predictive intervals

$$[\hat{z}_{\alpha/2} := g_{\lambda}^{-1}(\hat{y}_{\alpha/2}), \hat{z}_{1-\alpha/2} := g_{\lambda}^{-1}(\hat{y}_{1-\alpha/2})]$$

for trans-Gaussian kriging.

Moreover, although we have spoken only about the coverage probability bias 0 to order $O(n^{-1})$

of the estimated predictive intervals $[\hat{y}_{\alpha/2}, \hat{y}_{1-\alpha/2}]$ for Gaussian random fields, coverage probability bias 0 is also true for the proposed estimated trans-Gaussian predictive intervals $[\hat{z}_{\alpha/2}, \hat{z}_{1-\alpha/2}]$ as long as we consider the transformation parameter λ to be fixed and not estimated. This can be easily seen from the fact that

$$\begin{aligned} P_{tG} &:= P_{tG}(Z_0 \leq \hat{z}_{1-\alpha/2} | \mathbf{Z}) = \\ &= P_{tG}(g_{\lambda}(Z_0) \leq g_{\lambda}(\hat{z}_{1-\alpha/2}) | \mathbf{Z}) = \\ &= P_G(Y_0 \leq \hat{y}_{1-\alpha/2} | \mathbf{Y}) =: P_G, \end{aligned}$$

where Z_0 and \mathbf{Z} are random variables from the true trans-Gaussian random field and Y_0 and \mathbf{Y} are random variables from the corresponding true Gaussian random field at locations $x_0, x_1, \dots, x_n \in \mathbf{X}$, and $g_{\lambda}(\cdot)$ is the Box-Cox transformation. Thus, the random variables P_{tG} and P_G coincide. They give the values of the true predictive trans-Gaussian and Gaussian distribution function at the estimated quantiles. For the Gaussian case we already know from the definition of $\hat{y}_{1-\alpha/2}$ that $\mathbf{E}\{P_G\} = 1 - \alpha/2$ to order $O(n^{-1})$ because of unbiasedness. Here, again, the expectation is taken with respect to the true Gaussian distribution of the data \mathbf{Y} . From the coincidence of the random variables P_{tG} and P_G we also have $\mathbf{E}\{P_{tG}\} = 1 - \alpha/2$ and the proposed estimated predictive intervals have thus coverage probability bias 0 also in the trans-Gaussian case.

In reality the transformation parameter λ itself is estimated, too, e.g., by maximum likelihood, is then plugged-in into the ordinary kriging predictor $\hat{Y}_{\hat{\theta}, OK}(x_0)$ of formula (35) by means of transforming the original data \mathbf{Z} with the estimated Box-Cox transformation, and is then used again to transform the Gaussian quantiles $\hat{y}_{\alpha/2}$ and $\hat{y}_{1-\alpha/2}$ by means of the inverse Box-Cox transformation to the original Z-scale. In a future paper we will take account of this additional uncertainty, assume that both λ and θ are estimated by means of maximum likelihood and will investigate estimated predictive intervals with coverage probability bias 0, too.

6 PROPERTIES OF THE SMITH AND ZHU (2004) DESIGN CRITERION AND A DETERMINISTIC OPTIMIZATION ALGORITHM

For the optimization of the Smith and Zhu [9] design criterion we make use of the same principal greedy design algorithms as described in the appendix. We must simply replace $\Psi(\xi)$ from the appendix by the Smith and Zhu [9] design functional or the design functional for the trans-Gaussian case, both given by expressions (19)-(35) and the inverse Box-Cox-transformation. From these formulas it is obvious that in the Gaussian case, where the criterion (9) must be optimized, the calculation of the integral over the design region \mathbf{X} appearing in (9) can be simplified. Because all expressions under the integral sign are specific linear combinations of the components of the matrix function $[\mathbf{h}(x_0)\mathbf{h}(x_0)^T]$ one just needs to compute the matrix $\mathbf{U} = \int_{\mathbf{X}} \mathbf{h}(x_0)\mathbf{h}(x_0)^T dx_0$ once, before applying the iterative design algorithms formulated in the appendix. One then gets the integral (9) just by inserting components $U_{i,j}$ from \mathbf{U} instead of $\mathbf{h}_i(x_0) * \mathbf{h}_j(x_0)$ in the expressions appearing in (9) and referenced above.

At the first sight no such computational simplification is possible for the trans-Gaussian case, since the components of $[\mathbf{h}(x_0)\mathbf{h}(x_0)^T]$ enter the Gaussian quantiles (35) nonlinearly through $1/\sigma_{\hat{\theta}}^2(x_0)$ and $\sigma_{\hat{\theta}}(x_0)$ and, moreover, these quantiles are transformed nonlinearly via the inverse Box-Cox transformation. The design functional in the trans-Gaussian case may be written as the difference of two expressions having the form

$$\int_{\mathbf{X}} \left\{ \begin{aligned} &\text{inv. Box-Cox transf. of} \{ \text{kriging predictor} + \\ &+ \sqrt{\text{linear combination 1 of functions} +} \\ &+ \frac{\text{linear combination 2 of functions}}{\sqrt{\text{linear combination 1 of functions}}} \} dx_0 \end{aligned} \right.$$

The functions referred to in the linear combinations are just the components of the matrix function $\mathbf{h}(x_0)\mathbf{h}(x_0)^T$. Thus, if one could show that integrals of the above form can be expressed just by the integrals of the component functions, then one could compute the above mentioned matrix \mathbf{U} just before applying the design algorithms from

the appendix and the computational complexity during optimization would decrease a lot. Up to date we could not show that the above mentioned simplification is possible. Therefore, in our implementation of the design algorithms given in the appendix we have to compute an integral in every step of the optimization algorithms. This is computationally quite demanding as we will see in the following section, where we apply our ideas.

The proof of convexity properties of the Smith and Zhu [9] design functional and the design functional for the trans-Gaussian case is a further topic for future research.

7 NETWORK DESIGN WITH RAINFALL DATA

Applications and numerical examples for the I-optimality design criterium of the appendix have already been given in Spöck and Pilz [10]. There the so-called Gomel and Jura data sets have been considered. All the following computations are done with the MATLAB and Octave toolbox spatDesign:

www.uni-klu.ac.at/guspoeck/spatDesignMatlab.zip
www.uni-klu.ac.at/guspoeck/spatDesignOctave.zip,

which is freely available from the first author.

7.1 DATA SET AND PREPARATORY CALCULATIONS

The data set considered here is a rainfall data set from Upper Austria, see Mateu and Müller [5]. The monitoring network comprises 36 locations. Average monthly rainfall has been measured at each location, starting in January 1994 and ending in December 2009. In Fig. 1 we see that there are obviously areas in the design region that look very empty, having no sampling locations. Next let us calculate, for each station, the mean rainfall over the years, as well as the residual rainfall, for each of the 12 months, Fig. 2. Hereafter, we calculate for each station the mean of standardized rain residuals, the empirical semivariogram corresponding to these means and a fitted exponential semivariogram to the means of original rain residuals, Fig. 3. The fact that

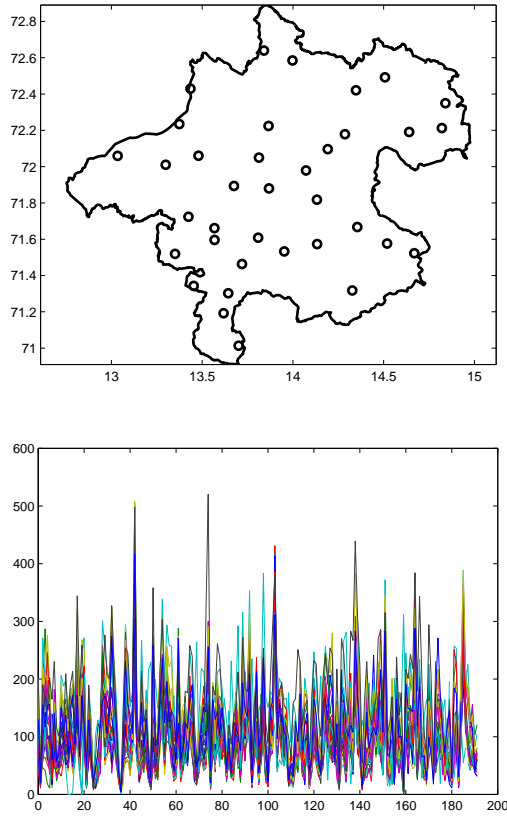


Figure 1. Above: The 36 sampling locations of the Upper Austria rainfall data set. Below: The 36 time series of average monthly rainfall at each station.

the standardized semivariograms are almost the same for all months means that the space-time random field is separable and that we can use one and the same semivariogram (the grey one at the Bottom of Fig. 3) for doing spatial sampling design for each month. As the next step we calculate the polar spectral distribution function, Fig. 4, corresponding to the covariance function in Fig. 4. Obviously, this spectral distribution function almost attains its maximum of 1735.2 at frequency $w = 47$. We select frequencies $w_i, i = 1, 2, \dots, 34$, calculate an approximation to the spectral distribution function via a step function (the steps are the a_i^2 from (12,13)) and check whether this approximation to the spectral distribution function provides a good fit to the original covariance function, Fig. 4. A look at the approximating covariance function in Fig. 4. shows that the difference between the true covariance function and the approximating

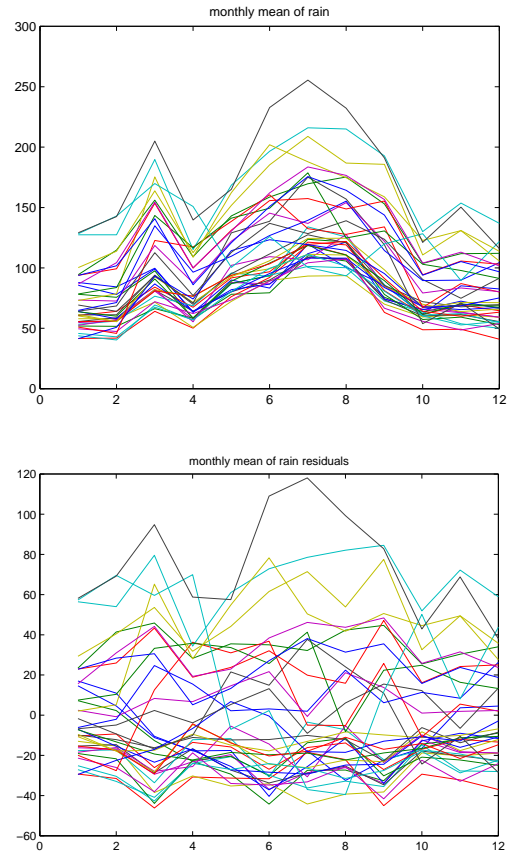


Figure 2. Above: The average monthly rainfall over the years at each of the 36 stations, for each of the 12 months. Below: The residual rainfall at each of the 36 stations, for each of the 12 months.

covariance function at the origin is 20. This is small scale variation that the approximating covariance function does not take into account. Later in spatial sampling design we will add this value of 20 to the nugget effect 106.8 of the true covariance function. Thus, $20 + 106.8$ is the variance of the uncorrelated error process $\epsilon_0(x)$ in our approximating BSLM (4).

We now have all quantities that we need in order to do spatial sampling design on the basis of our approximating Bayesian spatial linear model, corresponding to the assumption of Gaussianity of observations.

7.2 OPTIMAL DESIGN FOR GAUSSIAN KRIGING

We consider to add 14 additional sampling locations from the complete design region X to the

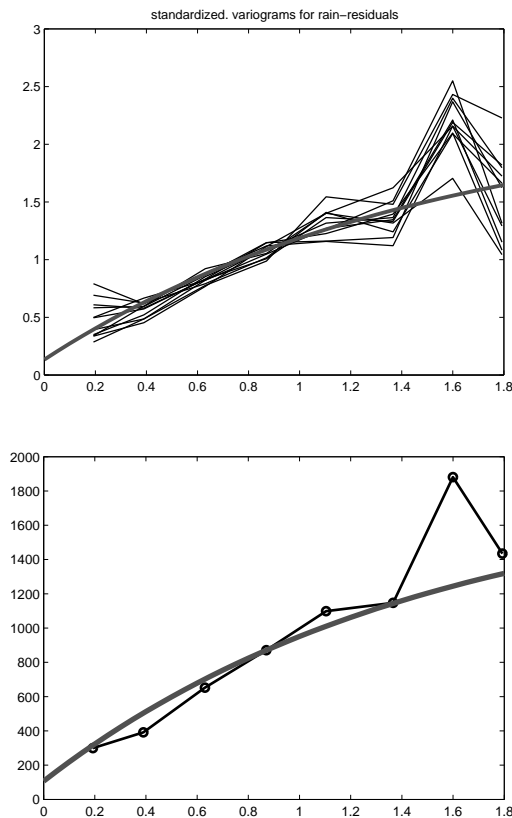


Figure 3. Above: Empirical semivariograms of the standardized rain residuals for all of the 12 months and a fitted exponential semivariogram (grey). Below: Empirical semivariogram for the means of original rain residuals and a fitted exponential semivariogram (grey).

available grid of 36 sampling locations. We design for the random field of means of the original rain residuals with corresponding covariance function given in Fig. 4 and being proportional to the individual covariance functions of the monthly rain residuals. Because of this proportionality, designs calculated with the mentioned covariance function would be optimal also for the individual monthly residual rainfall fields. Fig. 5. shows the optimal 8 and 14 point designs. Obviously, certain locations have been selected with multiplicities larger than 1. The reason is that the Smith and Zhu design criterion does not only take account of best prediction but also of covariance estimation; in order to get the nugget effect and the behaviour of the covariance function close to its origin well estimated locations are needed in the optimal design which are close to each other. Fig. 6 plots the decrease of the average of the lengths of the

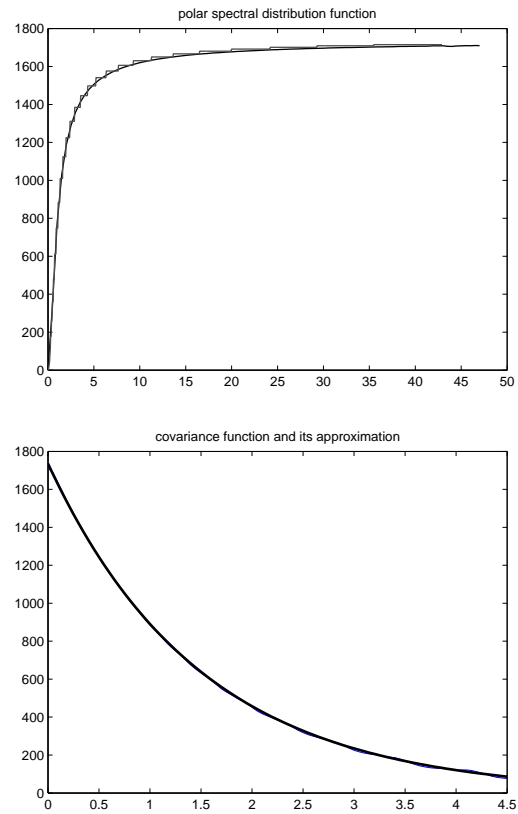


Figure 4. Above: Polar spectral distribution function and its approximation (grey). Below: True covariance function (black) and its worst approximation (grey).

95% predictive intervals when adding up to 14 design locations in an optimal way.

7.3 OPTIMAL DESIGN FOR TRANS-GAUSSIAN KRIGING

In the above example we have assumed the data to be Gaussian and have used ordinary kriging for prediction, although, as is visible from Fig. 7, the data are not Gaussian. Thus, we will consider now the assumption that the standardized rainfall residuals can be transformed to Gaussianity by means of a Box-Cox transformation. Since the Box-Cox transformation works only for positive valued data we have to add a positive offset to the 12 monthly sets of standardized rainfall residuals. To identify the appropriate offset and optimal Box-Cox transformation parameter λ_0 we perform a sequence of Lilliefors tests for Gaussianity on the transformed standardized rainfall residuals. We

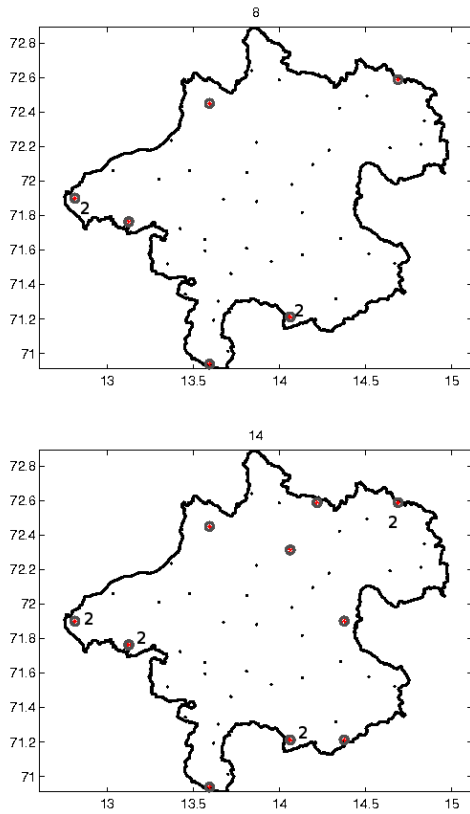


Figure 5. Above: Optimal 8 point design for Gaussian kriging. Below: Optimal 14 point design for Gaussian kriging. Certain locations have been selected with multiplicities larger than 1.

then retain that offset and that corresponding Box-Cox transformation parameter λ_0 , where the sum of the 12 p-values from the Lilliefors tests attains its maximum. Fig. 8 gives the corresponding surfaces of the sum of p-values and number of rejected hypotheses for Gaussianity at the 10% significance level. According to these figures the optimal parameters are chosen as: offset=53, $\lambda_0 = -0.25$. Obviously, for these parameters only one hypothesis of Gaussianity is rejected at the 10% significance level.

When designing for trans-Gaussian kriging we have the problem that the designs and the ordinary kriging predictor $\hat{Y}_{\hat{\theta}, OK}(x_0)$ therein are also, dependent via formula (35), on the actual data. Since we want to find only one unique design for all 12 months, we have to agglomerate the monthly data somehow and have to design for these agglomerated data. We proceed as in the Gaussian case and consider the random field of

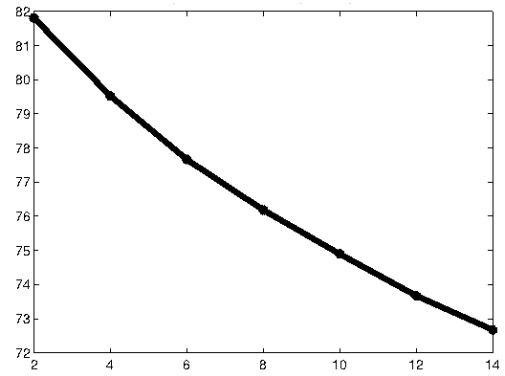


Figure 6. Average of the lengths of estimated 95% predictive intervals, when adding up to 14 design locations.

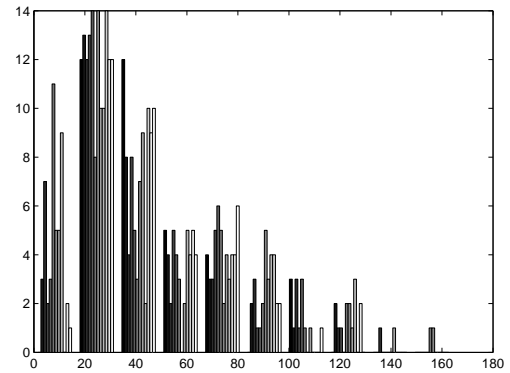


Figure 7. The 12 histograms of the rainfall residuals+53.

the means of standardized rain residuals for spatial sampling design. Let $R(x, i)$ be the original rainfall residual plus 53 at location $x \in \mathbf{X}$ and at month $i = 1, 2, \dots, 12$ and let $\hat{\sigma}_i^2$ be the usual empirical estimate of the variance of the rain residuals for the i -th month. Then standardization is performed in the following way:

$$Z(x, i) = R(x, i) \sqrt{\frac{\sum_{j=1}^{12} \hat{\sigma}_j^2}{12 \hat{\sigma}_i^2}} \quad (36)$$

In the following we discard that the standardization and $\hat{\sigma}_i^2$ actually are estimates and assume them to be fixed and not random. According to our exploratory analysis the random variables $Z(x, i)$ all come from trans-Gaussian random fields with the same Gaussian covariance function and Box-Cox transformation parameter $\lambda_0 =$

-0.25 but possibly different means. Consequently, $Y(x, i) = g_{\lambda_0}(Z(x, i))$, $i = 1, 2, \dots, 12$, with $g_{\lambda_0}(\cdot)$ denoting the Box-Cox transformation, come from Gaussian random fields with the same covariance functions but possibly different means. Assuming independence of all random fields at different months, the mean $M(x) = \frac{1}{12} \sum_{i=1}^{12} Y(x, i)$ also comes from a Gaussian random field with covariance function as given above but divided by 12. As a consequence, $g_{\lambda_0}^{-1}(M(x)) = g_{\lambda_0}^{-1}(\frac{1}{12} \sum_{i=1}^{12} g_{\lambda_0}(Z(x, i)))$ comes from a trans-Gaussian random field with Box-Cox parameter $\lambda_0 = -0.25$ and Gaussian covariance function divided by 12. It may be shown directly that

$$g_{\lambda_0}^{-1}(M(x)) = \frac{(\frac{1}{12} \sum_{i=1}^{12} Z(x, i)^{\lambda_0})^{1/\lambda_0}}{\frac{1}{12} \sum_{i=1}^{12} Z(x, i)} \frac{1}{12} \sum_{i=1}^{12} Z(x, i) \quad (37)$$

We have validated by means of simulations that for $\lambda_0 = -0.25$ the standard deviation of the expression

$$\frac{(\frac{1}{12} \sum_{i=1}^{12} Z(x, i)^{\lambda_0})^{1/\lambda_0}}{\frac{1}{12} \sum_{i=1}^{12} Z(x, i)}$$

is quite small compared to the values of $\frac{1}{12} \sum_{i=1}^{12} Z(x, i)$. Hence we may assume the above expression to be constant with value $d > 0$, the simulated mean of above expression. Because all considered random fields are stationary, the factor d is unique to all locations $x \in \mathbf{X}$. An alternative choice for d would be

$$d = \frac{\text{stdev}(g_{\lambda_0}^{-1}(M(x)))}{\text{stdev}(\frac{1}{12} \sum_{i=1}^{12} Z(x, i))} = \frac{\text{stdev}(g_{\lambda_0}^{-1}(M(x)))}{\frac{1}{12} \sqrt{\sum_{i=1}^{12} \hat{\sigma}_i^2}}$$

with $\text{stdev}(\cdot)$ denoting standard deviation, thus making the variances to the left and right in the approximation to expression (37) equal. Thus the distribution of $\frac{1}{12} \sum_{i=1}^{12} Z(x, i)$ is quite well approximated by the distribution of $\frac{1}{d} g_{\lambda_0}^{-1}(M(x))$. It can be shown that scaling up trans-Gaussian random variables by a factor $c > 0$ results again in a trans-Gaussian random field, but with the corresponding Gaussian random field having as covariance function the original covariance

function multiplied by $c^{2\lambda}$ and having as mean the original Gaussian mean multiplied by c^λ and then linearly shifted by $\frac{c^\lambda - 1}{\lambda}$. According to this result the distribution of $\frac{1}{d} g_{\lambda_0}^{-1}(M(x))$ is trans-Gaussian, too, with transformation parameter λ_0 and above mentioned unique Gaussian covariance function of the random fields $\{Z(x, i); x \in \mathbf{X}\}$, $i = 1, 2, \dots, 12$ multiplied by $\frac{1}{12}(\frac{1}{d})^{2\lambda_0}$. The above approximation is slightly biased with respect to both, the mean and the covariance of the Gaussian random variables $M(x)$ and the approximately Gaussian random variables $g_{\lambda_0}(d \frac{1}{12} \sum_{i=1}^{12} Z(x, i))$.

In our approach to spatial sampling design we can therefore assume that the random field of the means of standardized rain residuals can be approximated by a trans-Gaussian random field with Box-Cox transformation parameter $\lambda_0 = -0.25$ calculated from the 12 monthly trans-Gaussian random fields of standardized monthly rain residuals and corresponding Gaussian covariance function multiplied by $\frac{1}{12}(\frac{1}{d})^{2\lambda_0}$. Furthermore, we note that $\frac{1}{12} \sum_{i=1}^{12} R(x, i) = \frac{1}{12} \sum_{i=1}^{12} Z(x, i)$. We thus run our optimal design algorithms from the appendix for the agglomerated random field $\{\frac{1}{12} \sum_{i=1}^{12} R(x, i); x \in \mathbf{X}\}$, the random field of mean original raw rainfall residuals. Fig. 9 shows empirical semivariogram estimates of the Box-Cox transformed standardized rain residuals and a fitted exponential semivariogram function.

We go on to calculate the spectral distribution function corresponding to the covariance function of the Box-Cox transformed standardized rain residuals multiplied by $\frac{1}{12}(\frac{1}{d})^{2\lambda_0}$, its step-wise approximation and the worst approximating covariance function. We note that, close to the origin $h = 0$, the difference between the true covariance function and its approximation is 0.001. Finally, Fig. 10 visualizes optimal 8- and 14-point designs for trans-Gaussian kriging of $\{\frac{1}{12} \sum_{i=1}^{12} R(x, i); x \in \mathbf{X}\}$. Fig. 11 gives the lengths of estimated 95% predictive intervals. Obviously, the designs for trans-Gaussian kriging in Fig. 10 are completely different from the designs for Gaussian kriging in Fig. 5. Whereas the designs in Fig. 5 are much more space-filling the design locations in Fig. 10 have been selected in areas that have high mean value of residual rainfall. This fact becomes more transparent when we compare

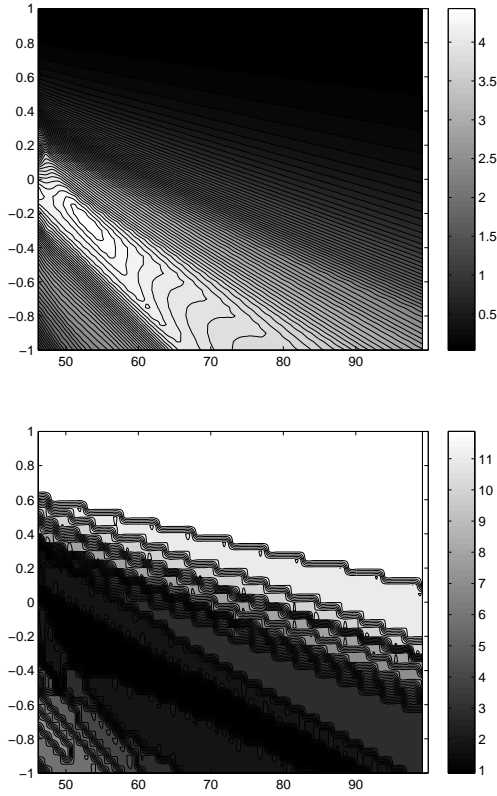


Figure 8. Above: Sum of the p-values, depending on the transformation parameter λ and the offset. Below: Number of rejected hypotheses of Gaussianity at 10% significance level, depending on the transformation parameter λ and the offset.

Fig. 10 to Fig. 12, where the predictive median of mean residual rainfall from the estimated predictive distributions of trans-Gaussian kriging is visualized. Obviously, in areas with high mean residual rainfall the average length of estimated 95% predictive intervals can be most decreased. This fact results from a fundamental difference between designs for Gaussian random fields and trans-Gaussian ones: Designs for trans-Gaussian kriging have stronger dependence on the data values themselves through the ordinary kriging predictor in formula (35) and the inverse Box-Cox transformation of the corresponding estimated Gaussian predictive quantiles.

Predictive maps for the original rainfall field at each month can be obtained by means of applying (trans-) Gaussian kriging also to the means of original rainfall values visible in Fig. 2 and then adding these predictive maps for the mean rainfall to appropriately scaled, cp. (36), predictions for the

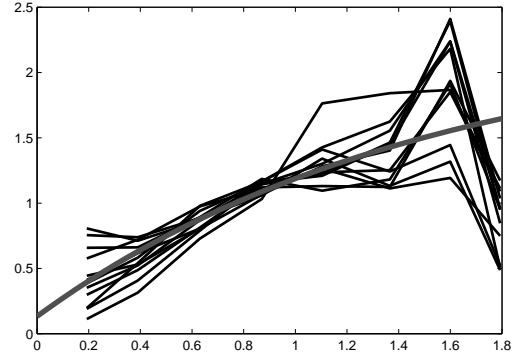


Figure 9. Empirical semivariograms of the Box-Cox transformed standardized rain residuals for all of the 12 months and a fitted exponential semivariogram (grey). The same Box-Cox parameter $\lambda = -0.25$ is used for the calculation of all variograms.

mean rainfall residuals.

According to (37), we have

$$\begin{aligned} g_{\lambda_0}^{-1}(M(x)) &\approx \\ &\approx d \frac{1}{12} \sum_{i=1}^{12} R(x, i) = \\ &= d \frac{\frac{1}{12} \sum_{i=1}^{12} R(x, i)}{R(x, j)} R(x, j) \end{aligned} \quad (38)$$

By means of simulations we could once again show that for our $\lambda_0 = -0.25$ the variance of the quotient in (38) is quite small. Thus the trans-Gaussian random variables $g_{\lambda_0}^{-1}(M(x))$, $R(x, j)$, $j = 1, 2, \dots, 12$ and the approximately trans-Gaussian random variable $\frac{1}{12} \sum_{i=1}^{12} R(x, i)$ are approximately proportional to each other, with proportionality factors unique for all $x \in \mathbf{X}$ because of stationarity of the considered random fields. Moreover, we note that the above approximations are quite good because all random fields corresponding to above approximations have correct Gaussian correlation functions. Bias is introduced in the above approximations mainly in the mean of the corresponding Gaussian variables. Because the unscaled rain residuals $R(x, j)$ are approximately proportional to $\frac{1}{12} \sum_{i=1}^{12} R(x, i)$ and $g_{\lambda_0}^{-1}(M(x))$ and because the estimated predictive quantiles for random variables $cZ := c * (Z(x_1), Z(x_2), \dots, Z(x_n))^T$ are c times the estimated predictive quantiles for the random

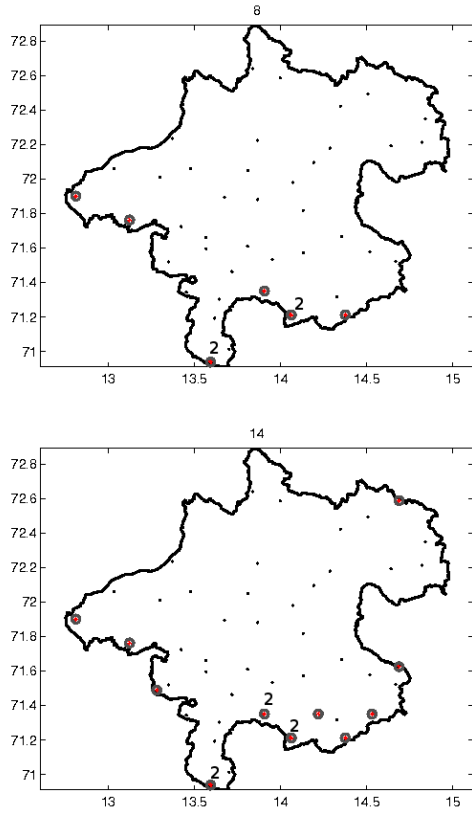


Figure 10. Above: Optimal 8 point design for trans-Gaussian kriging. Below: Optimal 14 point design for trans-Gaussian kriging. Certain locations have been selected with multiplicities larger than 1.

variables $Z := (Z(x_1), Z(x_2), \dots, Z(x_n))^T$, our approximately optimal designs calculated for the random variables $\frac{1}{12} \sum_{i=1}^{12} R(x, i)$ are approximately optimal also for the raw rain residuals $R(x, j)$ at all months $j = 1, 2, \dots, 12$. This can be seen easily from the fact that when using the trans-Gaussian random variables cZ in (35) the proportionality constant for the covariance function $c^{2\lambda_0}$ cancels to c^{λ_0} and that the new kriging predictor is c^{λ_0} times the one based on Z plus the constant $\frac{c^{\lambda_0}-1}{\lambda_0}$, observing that kriging weights sum-up to 1. Applying the inverse Box-Cox transformation to the estimated quantile given in (35)

$$\hat{y}_{1-\alpha/2, cZ} = c^{\lambda_0} Y_{OK, Z} + \frac{c^{\lambda_0}-1}{\lambda_0} + c^{\lambda_0} z_{1-\alpha/2} \sigma_{est, Z},$$

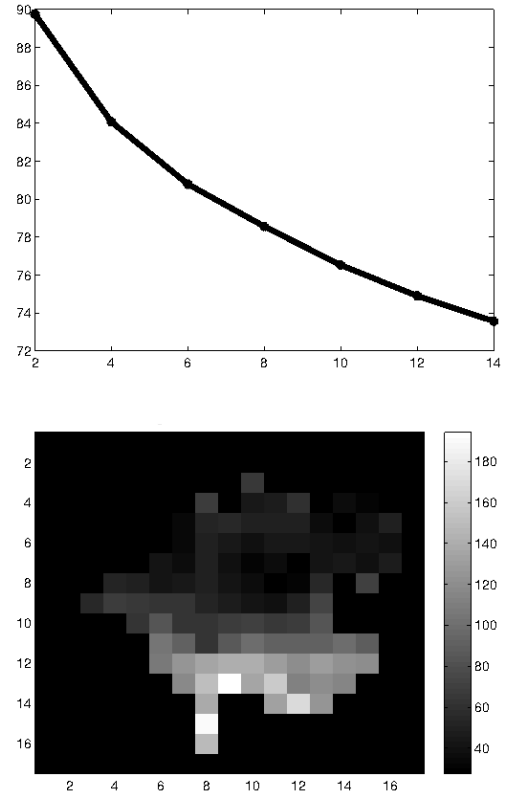


Figure 11. Above: Decrease of the average of the lengths of estimated 95% predictive intervals, when adding up to 14 design locations. Below: Lengths of estimated 95% predictive intervals corresponding to the optimal 14 point design.

we get

$$\begin{aligned} & (\hat{y}_{1-\alpha/2, cZ} \lambda_0 + 1)^{1/\lambda_0} = \\ & = (c^{\lambda_0} (Y_{OK, Z} + z_{1-\alpha/2} \sigma_{est, Z}) \lambda_0 + c^{\lambda_0})^{1/\lambda_0} \\ & = c (\hat{y}_{1-\alpha/2, Z} \lambda_0 + 1)^{1/\lambda_0} \end{aligned}$$

Therefore, the 12 different design functionals are just rescaled by different proportionality factors and are otherwise approximately equivalent, with the exception that they are based on different data. Clearly, data at different times are not truly proportional, only approximately so (in distributional law). True equivalence holds if the unstandardized residuals are truly proportional to each other and to a unique trans-Gaussian variable $V(x)$, with the same Gaussian correlation function.

One could calculate also estimated expected lengths of estimated predictive intervals by means

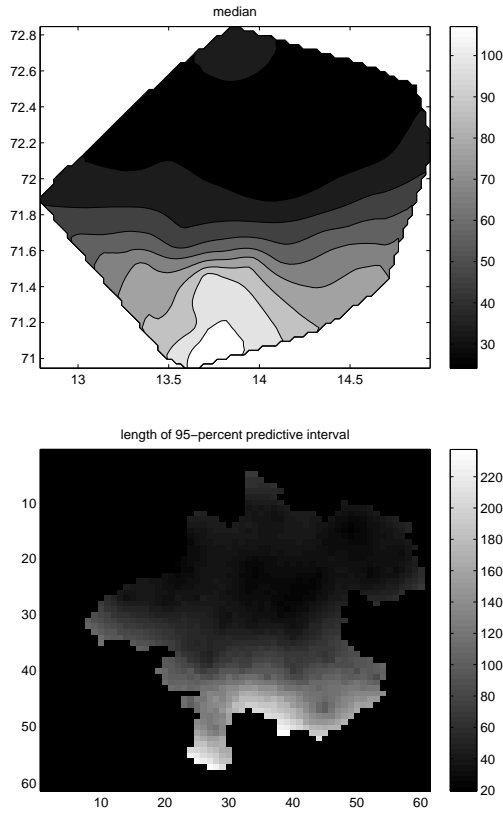


Figure 12. Above: The predictive median of the mean residual rainfall field+53 calculated from the predictive distributions of trans-Gaussian kriging applied to the 36 means of rainfall residuals+53. Below: Lengths of estimated 95% predictive intervals corresponding to the trans-Gaussian kriging from the upper figure.

of taking either the expectations of the ordinary kriging predictors in (35), which are all unique because of stationarity, plus/minus the expectation (or not) of the additional Gaussian-quantile times the standard deviation term, and then applying the inverse Box-Cox transformation on the expected Gaussian quantiles (35), or by means of taking expectations of the inverse Box-Cox transformed Gaussian quantiles. Then we get design criteria that are independent of the actual data values, at least with the exception that the true mean and true covariance function of the corresponding Gaussian random field must be estimated somehow. Up to date we could not show that these two proposed approaches are equivalent, although we know that the first one is maybe more practical and mathematically easier, whereas the second one would be statistically and mathematically correct. We will follow up these approaches in a future

paper. These approaches would be especially useful and necessary, when one has no data available and one desires to plan a design for a trans-Gaussian random field without having data from the scratch.

A similar approach as above also applies to stationary random fields $Z(x, i)$ that are correlated in space and time and whose Gaussian correlation function can be assumed to be separable, i.e., $C(\Delta x, \Delta i) = C_{\mathbf{X}}(\Delta x) * C_{\mathbf{T}}(\Delta i)$, if we assume the Gaussian time-correlation function to be fixed and not estimated and only the Gaussian spatial covariance function to be estimated by REML. As before, the trans-Gaussian $R(x, i)$ are assumed to have same Gaussian correlation functions but possibly different trans-Gaussian variances $\hat{\sigma}_i^2$. Then the same standardization may be applied as above in (36), and the trans-Gaussian $Z(x, i)$ are again assumed to have the same Gaussian covariance function. The only difference to the time-uncorrelated case is that now $\frac{1}{d} \frac{1}{12} \sum_{i=1}^{12} R(x, i)$ and $\frac{1}{d} \frac{1}{12} \sum_{i=1}^{12} Z(x, i)$ do not have the same variance. We thus calculate our designs for $\frac{1}{d} \frac{1}{12} \sum_{i=1}^{12} Z(x, i)$. Let σ^2 be the variance of the Gaussian variables $Y(x, i) = g_{\lambda_0}(Z(x, i))$. From the separability of the random field $\{Y(x, i), x \in \mathbf{X}, i = 1, 2, \dots, 12\}$ we conclude that the average $M(x) = \frac{1}{12} \sum_{i=1}^{12} Y(x, i)$ has covariance

$$\begin{aligned} \text{cov}(M(x_1), M(x_2)) &= \\ &= \left\{ \frac{1}{12} \sum_{i,j=1}^{12} C_{\mathbf{T}}(|i - j|) \right\} \frac{\sigma^2}{12} C_{\mathbf{X}}(x_1 - x_2). \end{aligned}$$

This is the multiple of $1/12$ times the spatial covariance function of the $Y(x, i)$ times the constant, $\left\{ \frac{1}{12} \sum_{i,j=1}^{12} C_{\mathbf{T}}(|i - j|) \right\}$. Thus, the same approach to optimal design may be applied as already discussed before. In (35) the ordinary kriging predictor based on the data $M(x)$ does not change in comparison to the uncorrelated case, because it is dependent only on the spatial correlation function, but what changes is the right-hand side of (35); the original estimated standard deviation term from the time-uncorrelated case is now multiplied by $\sqrt{\frac{1}{12} \sum_{i,j=1}^{12} C_{\mathbf{T}}(|i - j|)}$, due to time-correlation.

Another approach to design would be to time-decorrelate the $Y(x, i)$ by means of multiplying for each location $x \in \mathbf{X}$ the vector $(Y(x, 1), \dots, Y(x, 12))$ with the matrix-root of the inverse Gaussian time-correlation matrix, to average the resulting vector and to base the sampling design

on these time-averages of decorrelated Gaussian standardized rain residuals. Because this time-decorrelation does not change the Gaussian spatial covariance function of the time-decorrelated Gaussian standardized residuals in comparison to the uncorrelated case, an approach similar to before results for design, with the exception that now the ordinary kriging predictor in (35) is different from the original one in the uncorrelated case; However, the estimated standard deviation term in the right-hand side of (35) remains the same as in the uncorrelated case, because the time-decorrelation has not changed the spatial covariance function.

It is an open question whether both proposed approaches are equivalent. We will follow-up both of the above approaches and investigate this question in one of our next papers.

Actually, in our example, trans-Gaussian kriging and optimal design could have been performed also on the original, raw data, instead of the residual rainfall data. But then, as we have found out, the Box-Cox transformation parameters for each month would not have been the same and our approach of calculating a unique design for all months would not have been possible. Instead it would have been necessary to calculate individual designs for each of the 12 months and then combine them in some way to form a single usable design.

7.4 COMPUTATION

Whereas the computations of the designs for the I-optimality criterion in Spöck and Pilz [10] took only 6 hours on a 3.06 Ghz CPU in MATLAB the computations with the Smith and Zhu [9] design criterion and trans-Gaussian kriging took 7 days on the same CPU and a NVIDIA GTX 580 graphics card acting as multi-coprocessor with CUDA support (http://www.nvidia.de/page/tesla_computing_solutions.html).

The reason for this long computation time is that the averaging over the design area X must be done for the I-optimality criterion only once by means of calculating the matrix U in Eq. (7) before the actual design algorithm starts. On the other hand, when using the trans-Gaussian Smith-Zhu design criterion, it is clear from the derivations in Section 6 that the averaging over the design region X must take place in every step when a new design location

is tested for being added or being removed from the design. Although we made use of the freely available GPUMat toolbox (<http://gp-you.org>) to parallelize matrix multiplications on the GTX 580 GPU, the computations took so much time. As we have tested, without this implementation on the GPU the computations would take 110 times longer. One disadvantage of the GPUMat toolbox is that it can work only with one single GPU but our mainboard can deal with up to 6 GPUs. In future we will investigate whether the MATLAB parallelization toolbox and JACKET (<http://www.accelereyes.com>) can further speed up the computations on multi-GPUs.

8 CONCLUSION

The preceding sections demonstrate that design functionals have a convenient and mathematically tractable structure and there is no need for stochastic search algorithms in order to optimize them. The trace functional criterion is shown to be a convex functional similar to design functionals from the theory of optimal experimental design for linear regression models. Powerful tools from this theory can be used to get this criterion optimized. The Smith and Zhu design functional is shown to be continuously extendable to the compact set of continuous information matrices. To show convexity properties of this design functional remains a topic for future research. Designs with the Smith and Zhu criterion differ from designs with the trace functional. Because the Smith and Zhu design criterion takes the uncertainty of the covariance function into account, resulting designs with this criterion must have sampling locations very close to each other as well as space-filling locations. Designs resulting from optimization of the trace functional only show quite regular space filling locations. Designs for trans-Gaussian kriging via minimizing the average of the lengths of estimated predictive intervals also are strongly dependent on the data values themselves in sharp contrast to designs for Gaussian kriging without REML correction, which, if the covariance function can be assumed to be certain, are completely independent of the data. Furthermore, we remark that a similar approach for spatial sampling design of non-stationary random fields is under development (cp. also Spöck and Pilz [11]) and will soon become freely available

in the spatDesign toolbox of the first author, see Spöck [12].

9 APPENDIX

9.1 ITERATION PROCEDURES FOR DETERMINING EXACT DESIGNS

We are now going to formulate iteration procedures for the construction of approximately optimal exact designs. Contrary to the construction of optimal discrete designs, here we cannot prove convergence of the exact designs to the functional value $\Psi(d^*)$ of an optimal exact design d^* ; we can only guarantee stepwise improvement of a given exact starting design, i.e. the sequence of functional values $\Psi(d_{n,s})$ decreases monotonically with increasing iteration index s . The algorithm is an exchange algorithm improving n -point designs and starts with a given initial design.

9.1.1 Exchange algorithm: Step 1. Use some initial design $d_{n,1} = \{x_{1,1}, \dots, x_{n,1}\} \in \mathbf{X}^n$ of size n .

Step 2. Beginning with $s = 1$, form the design $d_{n+1,s} = d_{n,s} + (x_{n+1,s})$ by adding the point

$$x_{n+1,s} = \arg \min_{x \in \mathbf{X}} \Psi(\mathbf{M}_B(d_{n,s} + (x)))$$

to $d_{n,s}$.

Then form $d_{n,s}^j = d_{n+1,s} - (x_{j,s})$, $j = 1, 2, \dots, n+1$ and delete that point $x_{j^*,s}$ from $d_{n+1,s}$ for which

$$\Psi(\mathbf{M}_B(d_{n,s}^j)) = \min_{j \in \{1, \dots, n+1\}} \Psi(\mathbf{M}_B(d_{n,s}^j)).$$

Step 3. Repeat Step 2 until the point to be deleted is equivalent to the point to be added.

For the design functional (8), Step 2 is determined as follows:

$$x_{n+1,s} = \arg \max_{x \in \mathbf{X}} \frac{\mathbf{h}(x)^T \mathbf{M}_B(d_{n,s})^{-1} \mathbf{U}}{n + \mathbf{h}(x)^T \mathbf{M}_B(d_{n,s})^{-1} \mathbf{h}(x)}$$

$$\frac{\mathbf{M}_B(d_{n,s})^{-1} \mathbf{h}(x)}{\mathbf{M}_B(d_{n+1,s})^{-1} \mathbf{h}(x_{j,s})},$$

$$j^* = \arg \min_{1 \leq j \leq n+1} \frac{\mathbf{h}(x_{j,s})^T \mathbf{Q}_B(d_{n+1,s}) \mathbf{h}(x_{j,s})}{n + 1 - \mathbf{h}(x_{j,s})^T \mathbf{M}_B(d_{n+1,s})^{-1} \mathbf{h}(x_{j,s})},$$

where

$$\mathbf{Q}_B(d_{n+1,s}) = \mathbf{M}_B(d_{n+1,s})^{-1} \mathbf{U} \mathbf{M}_B(d_{n+1,s})^{-1}.$$

For the Smith and Zhu design criterion no such simplification exists and the complete design functional (9), (35) must be recalculated in every step.

9.1.2 Generation of an initial design. The starting design is taken as a one-point design which minimizes the design functional among all designs of size $n = 1$. Note that such a design exists since the Bayesian information matrix is positive definite even for designs of size $n = 1$.

Step 1. Choose $x_1 \in \mathbf{X}$ such that $x_1 = \arg \min_{x \in \mathbf{X}} \Psi(\mathbf{M}_B((x)))$, and set $d_1 = (x_1)$.

Step 2. Beginning with $i = 1$, find x_{i+1} such that $x_{i+1} = \arg \min_{x \in \mathbf{X}} \Psi(\mathbf{M}_B(d_i + (x)))$ and form $d_{i+1} = d_i + (x_{i+1})$. Continue with i replaced by $i + 1$ until $i + 1 = n$.

Step 3. If $i + 1 = n$ then stop and take $d_{n,1} = \{x_1, \dots, x_n\}$ as an initial design.

It is a good idea to combine the initial design algorithm 9.1.2 and the exchange algorithm 9.1.1.

9.1.3 Reduction of experimental designs. Often it is desired to reduce a given experimental design $d = \{x_1, x_2, \dots, x_n\}$ to one including only $m < n$ design points from d :

Step 1. Delete that design point x_{j^*} from d for which

$$x_{j^*} = \arg \min_{x_j \in d} \Psi(\mathbf{M}_B(d - (x_j))), \text{ and set } d := d - (x_{j^*}).$$

Step 2. Iterate Step 1 until the design d contains only m design points.

Also, this algorithm may be combined with an improvement step similar to the exchange algorithm 9.1.1. In algorithm 9.1.1 the calculation of $x_{n+1,s}$ has merely to be replaced by

$$x_{n+1,s} = \arg \min_{x \in d - d_{n,s}} \Psi(\mathbf{M}_B(d_{n,s} + (x))),$$

where d is the initial design that has to be reduced. This improved algorithm has the advantage that design points once deleted can reenter the design in the exchange step.

9.1.4 Determining the inverse of the information matrix. Obviously, the calculation of exact designs requires in every step the calculation of the inverses of the information matrices $\mathbf{M}_B(d_{n,s})$ and $\mathbf{M}_B(d_{n+1,s})$. We saw that these information matrices can have a quite high dimension of about 4000×4000 . So, how can one invert such large matrices in affordable time? A first artificial, inverse information matrix in spatial sampling design can always be one with block-diagonal structure corresponding to 0 selected design points, having one very small block, being the a priori covariance matrix for deterministic trend functions, and having one further block, being just a diagonal matrix of very high dimension (about 4000 diagonal elements, being the variances of the stochastic amplitudes resulting from a harmonic decomposition of the random field into sine-cosine-Bessel surface harmonics). So, no inversion is needed at a first step. The inversion of all other information matrices becomes easy, and there is computationally no need to make explicit use of numerical matrix inversion algorithms, when one considers equations (13.26) and (13.28) in [8]:

$$\mathbf{M}_B(d_{n,s} + (x))^{-1} = \frac{n+1}{n} \left\{ \mathbf{M}_B(d_{n,s})^{-1} - \frac{\mathbf{M}_B(d_{n,s})^{-1} \mathbf{h}(x) \mathbf{h}(x)^T}{n + \mathbf{h}(x)^T \mathbf{M}_B(d_{n,s})^{-1} \mathbf{h}(x)} \right\},$$

$$\mathbf{M}_B(d_{n,s}^j)^{-1} = \frac{n}{n+1} \left\{ \mathbf{M}_B(d_{n+1,s})^{-1} + \frac{\mathbf{M}_B(d_{n+1,s})^{-1} \mathbf{h}(x_{j,s}) \mathbf{h}(x_{j,s})^T}{n+1 - \mathbf{h}(x_{j,s})^T \mathbf{M}_B(d_{n+1,s})^{-1} \mathbf{h}(x_{j,s})} \right\}$$

Obviously, only matrix- and vector multiplications are needed in these update formulae.

REFERENCES

- [1] Abt, M., (1999), Estimating the prediction mean squared error in Gaussian stochastic processes with exponential correlation structure, *Scandinavian Journal of Statistics*, 26, 563-578.
- [2] Diggle, P. and Lophaven, S., (2006), Bayesian Geostatistical Design, *Scandinavian Journal of Statistics*, 33, 53-64.
- [3] Fedorov, V., (1996), Design of spatial experiments: Model fitting and prediction. In S. Ghosh and C.R. Rao (Eds.), *Handbook of Statistics*, Vol. 13, 515-553, Elsevier, Amsterdam.
- [4] Harville, D.A. and Jeske, D.R., (1992), Mean squared error of estimation or prediction under a general linear model, *Journal of the American Statistical Association*, 87, 724-731.
- [5] Mateu, J. and Müller, W.G., (2012), *Spatio-temporal Design: Advances in Efficient Data Acquisition*, Wiley, New York.
- [6] Omre, H., (1987), Bayesian kriging - merging observations and qualified guess in kriging, *Mathematical Geology*, 19, 25-39.
- [7] Omre, H. and Halvorsen, K., (1989), The Bayesian bridge between simple and universal kriging, *Mathematical Geology*, 21, 767-786.
- [8] Pilz, J., (1991), *Bayesian Estimation and Experimental Design in Linear Regression Models*, Wiley, New York.
- [9] Smith, R.L. and Zhu, Z., (2004), *Asymptotic Theory for Kriging with Estimated Parameters and its Application to Network Design*, Technical Report, University of North Carolina.
- [10] Spöck, G. and Pilz, J., (2010), Spatial sampling design and covariance-robust minimax prediction based on convex design ideas, *Stochastic Environmental Research and Risk Assessment*, 24, 463-482.
- [11] Spöck, G. and Pilz, J., (2008), Non-stationary spatial modeling using harmonic analysis, in J.M. Ortiz and X. Emery (ed.), *Proceedings of the Eight International Geostatistics Congress, Gecamin, Chile*, 389-398.
- [12] Spöck, G., (2011), *spatDesign V.2.1.0: Matlab/Octave spatial sampling design toolbox*, <http://wwwu.uni-klu.ac.at/guspoeck/spatDesignMatlab.zip>, <http://wwwu.uni-klu.ac.at/guspoeck/spatDesignOctave.zip>.
- [13] Yaglom, A.M., (1987), *Correlation Theory of Stationary and Related Random Functions*, Springer-Verlag, New York.
- [14] Zhu, Z. and Stein, M.L., (2006), Spatial sampling design for prediction with estimated parameters, *Journal of Agricultural, Biological and Environmental Statistics*, 11, 24-44.
- [15] Zimmerman, D.L., (2006), Optimal network design for spatial prediction, covariance

Authors Index

Blanco, J. M.	11
Brus, J.	19
Burian, J.	19
Castañeda, H. M.	70
Danko, M.	43
Halmova, D.	53
Káposztásová, D.	61, 65
Karkova, M.	47
Kilianová, H.	39
Kucarova, K.	53
Lee, H.	43
Machar, I.	39
Maldonado, J. L.	70
Markovič, G.	65
Miklanek, P.	34, 43
Mitkova, V. B.	34
Pechanec, V.	39
Pekar, J.	53
Pekárová, P.	34, 43, 53
Peña, F.	11
Pilz, J.	79
Poor, P.	47
Prochazkova, D.	27
Remaki, L.	11
Rysulová, M.	61
Sandoval, R. F.	70
Simon, M.	47
Sobotová, L.	47
Sokáč, M.	57
Spöck, G.	79
Stastny, S.	19
Velísková, Y.	57
Vranayová, Z.	61, 65